Universidade de Aveiro
2023

Mafalda Sofia
Mendonça de Castro

The impact of *Leishmania* infection on the migratory behaviour of host macrophages

Universidade de Aveiro
2023

Mafalda Sofia Mendonça de Castro

O impacto da infeção por *Leishmania* no comportamento migratório dos macrófagos do hospedeiro

Dissertação apresentada à Universidade de Aveiro para cumprimento dos requisitos necessários à obtenção do grau de Mestre em Biomedicina Molecular, realizada sob a orientação científica da Doutora Ana Tomás, Líder do grupo Parasitologia Molecular do Instituto de Investigação e Inovação em Saúde da Universidade do Porto, e Professora Associada no Instituto de Ciências Biomédicas Abel Salazar da Universidade do Porto, e da Doutora Ana Margarida Sousa, Investigadora Principal no Instituto de Biomedicina da Universidade de Aveiro, e Professora Auxiliar no Departamento de Ciências Médicas da Universidade de Aveiro.

This work was funded by National Funds through FCT – Fundação para a Ciência e a Tecnologia, I.P., under the project PTDC/BIA-MIC/5343/2020.
Mafalda Sofia Mendonça de Castro was a recipient of the fellowship Fellow_BI/FCT_Proj2020/i3S/12080609/2022 in the context of the project.

“Science is, in itself, revolutionary because it does not settle with what is known, with what peers and politicians claim to be known, or even with stablished knowledge.”

– Maria Ângela Brito de Sousa

o júri

presidente

Doutor Marco Aurélio Gouveia Alves
Equiparado a Investigador Principal da Universidade de Aveiro

vogais

Doutora Ângela Margarida Amorim Costa
Investigadora Júnior da Universidade do Porto - Instituto de Investigação e Inovação em Saúde

Professora Doutora Ana Maria Luís Ramos Tomás
Professora Associada da Universidade do Porto - Instituto de Ciências Biomédicas de Abel Salazar
Investigadora Principal da Universidade do Porto - Instituto de Investigação e Inovação em Saúde

agradecimentos

À Professora Doutora Ana Tomás, agradeço desde já pela oportunidade de trabalhar consigo e de confiar em mim para ter um papel nos seus projetos. Agradeço por toda a paciência, simpatia, disponibilidade contínua ao longo de todo o projeto e sobretudo por tudo o que me ensinou.

À Mestre Filipa Dias, obrigada pela paciência milagrosa que sempre mantiveste enquanto eu questionava tudo deste universo. Obrigada por tirares sempre tempo para garantir que eu verdadeiramente compreendia tudo, por tudo que me ensinaste e por todo o apoio, dentro e fora do laboratório. Já podemos ser amigas.

Às minhas colegas de laboratório que se tornaram rapidamente amigas, Dr the Lion, Teresa e Margarida, por estarem sempre lá para mim e por tornarem o dia a dia mais divertido nas pausas para café e discutir os outfits da red carpet. Obrigada por tudo que me ensinaram e por me terem integrado verdadeiramente na equipa. Levo um bocadinho de todas vocês para o resto da minha vida.

Aos i3s buddies, Vítor e Carolina, que me seguiram do mestrado até ao i3s. Obrigada por me fazerem companhia durante este ano, pelos finos depois do trabalho acompanhados com fofoca, por estarem lá para me ouvirem e por confiarem em mim quando eu mais duvidava.

À minha família, especialmente aos meus pais e irmão, por sempre me incentivarem a fazer o meu melhor sem negligenciar o meu bem-estar. Obrigada por tudo o que me ensinaram e fizeram que me permitiu ser quem sou e estar onde estou. Um carinho especial aos meus avós que tanto fizeram por mim e sempre foram como uns segundos pais.

Aos meus amigos, Ana, Guilherme, Hugo, Teresa e Tiago, que já me acompanham desde 2017 e agora não têm outra hipótese se não me aturar para o resto da vida. Obrigada pelo apoio, pela amizade e por manterem a minha sanidade mental. Por muitos mais anos juntos pelo mundo todo.

À Cris, que, apesar da distância, nunca deixou de ser um raio de sol na minha vida. Obrigada pela pessoa incrível que és, por estares sempre pronta para me ouvir e dar os melhores conselhos.

Por fim, mas de uma importância incomparável, ao Afonso, que me tem acompanhado ao longo de vários anos nos bons e maus momentos. Obrigada por nunca (ou quase nunca) perderes a paciência comigo e por me ouvires, acreditares em mim e me motivares a fazer sempre mais. Obrigada por estares sempre do meu lado e seres um fonte constante de felicidade na minha vida.

palavras-chave

Leishmania; macrófagos; migração; via PI3K/AKT/RTK; inibidores de migração.

resumo

A leishmaniose, uma doença tropical negligenciada prevalente, afeta milhões de pessoas em todo o mundo e é transmitida pela picada de uma mosca da areia infetada com parasitas do género *Leishmania*. Embora existam tratamentos para a Leishmaniose, estes não são específicos para parasitas de *Leishmania*, estão frequentemente associados a efeitos secundários significativos e permanecem inacessíveis em muitas regiões endémicas. A doença apresenta uma variedade de formas clínicas, desde lesões cutâneas até infeções viscerais possivelmente fatais. As espécies de *Leishmania* estão ligadas a diferentes tropismos da doença, mas os mecanismos específicos responsáveis por essas variações permanecem desconhecidos. Pesquisas sugerem que os macrófagos desempenham um papel fundamental na disseminação da doença. Para estudar o impacto da *Leishmania* na migração de macrófagos, é crucial estabelecer boas taxas de infeção. Exploramos métodos de enriquecimento e deteção de parasitas. Nem as técnicas baseadas em PNA nem as baseadas em Ficoll melhoraram significativamente as taxas de infeção no nosso modelo *in vitro*. Pelo contrário, a pré-marcação de promastigotas com CFSE provou ser um método confiável para deteção da infeção. Para estudar os padrões de migração dos macrófagos, recorreu-se a diferentes ensaios de migração celular. Ensaios “wound healing” revelaram inconsistências que podem ser atribuídas a limitações do modelo experimental. Alternativamente, ensaios “random single cell” sem estímulos permitiram a monitorização precisa e individual dos macrófagos individualmente. No entanto, este método também não mostrou padrões consistentes na migração de macrófagos dependentes da infeção por *Leishmania*. Para além disso, Dasatinib e Wortmannin, dois conhecidos inibidores da migração noutros tipos de células, foram testados para determinar o seu efeito em macrófagos, o que representava um aspeto previamente inexplorado fora do nosso grupo de investigação. Contudo, estas não demonstraram efeitos significativos nos nossos ensaios. Diferenças no tipo de célula e no desenho do ensaio podem explicar essas inconsistências. A análise da morfologia celular sugere que a polarização de macrófagos pode influenciar os padrões de migração, sendo por isso necessária investigação adicional para compreender os mecanismos subjacentes. Em conclusão, o nosso estudo destaca a complexidade das interações entre a *Leishmania* e os macrófagos, e salienta a necessidade de realizar mais estudos para elucidar a complexa dinâmica entre o hospedeiro e os parasitas no contexto da Leishmaniose e da biologia de macrófagos.

keywords

Leishmania; macrophages; migration; PI3K/AKT/RTK pathway; migration inhibitors.

abstract

Leishmaniasis, a prevalent neglected tropical disease, impacts millions of people worldwide and is transmitted through the bite of a sandfly infected with *Leishmania* parasites. While treatments for Leishmaniasis exist, they are not *Leishmania*-specific, are often associated with significant side effects, and remain inaccessible in many endemic regions. The disease presents a range of clinical forms, spanning from cutaneous lesions to severe visceral infections. *Leishmania* species are linked to distinct disease tropisms, but the precise mechanisms responsible for these variations remains unknown. Research suggests that macrophages play a pivotal role in the disease's dissemination. To study *Leishmania*'s impact on macrophage migration, it is crucial to have good infection rates stablished. We explored both parasite enrichment and detection methods. Neither the PNA nor Ficoll-based techniques significantly improved infection rates in our *in vitro* model. Instead, pre-labelling promastigotes with CFSE proved a reliable infection detection method. To study the macrophages migration patterns, different cell migration assays were employed. Wound healing assays revealed inconsistencies attributed to limitations within the assay model. Alternatively, a stimuli-free random cell migration assays enabled precise tracking of individual macrophages. Nevertheless, this method also showed no consistent patterns in the macrophage's migration dependent of *Leishmania* infection. Moreover, Dasatinib and Wortmannin, known inhibitors of migration in other cell types, were also tested for their effect on macrophages, an aspect that had not been previously explored beyond our research group. However, they exhibited no significant effects in our assays. Differences in cell type and assay design may account for these inconsistencies. Analysis of cell morphology suggested that macrophage polarization could influence migration patterns and further investigation is required to understand the underlying mechanisms. In conclusion, this research underscores the complexities of *Leishmania*-macrophage interactions and emphasizes the need for further studies to elucidate the intricate host-parasite dynamics in the context of Leishmaniasis and macrophage biology.

List of contents

Introduction 1
1. Leishmaniasis 1
    1.1. Leishmaniasis epidemiology 1
    1.2. Taxonomy 1
    1.3. Life Cycle 3
    1.3.1. Vector 3
    1.3.2. Mammals 4
    1.4. Clinical manifestations and diagnosis 5
    1.5. Prevention and treatment 7
    1.6. Shifting drug targets 8
2. Macrophages 9
    2.1. Macrophage biology and functions 9
    2.2. Macrophage polarization and migration 9
3. Macrophage-parasite interaction 10
    3.1. Recognition and uptake of *Leishmania* parasites by macrophages 10
    3.2. Mechanisms of *Leishmania* to escape death and to alter macrophage migration 10
    3.3. General function of the PI3K/RTK/AKT pathway 11
    3.4. PI3K and RTK pathway inhibitors 12
4. *In vitro* methods to measure macrophage migration 14
    4.1. Bone marrow derived macrophages (BMDMs) 14
    4.2. BMDMs' infection and metacyclic selection methods 15
    4.3. Wound healing migration assays 17
    4.4. Random single cell migration assays 20
    4.5. Transwell migration assays 21
    4.6. Microfluidic devices for chemotactic migration assays 22

Aims of the study 24

Materials and Methods 25

Results 32
1. Optimization of macrophage infection by *L. infantum* and *L. donovani* 32
    1.1. Peanut agglutinin (PNA) metacyclic selection 32
    1.2. The Ficoll density gradient metacyclic selection 35
    1.3. Optimization of parasite detection through CFSE staining 37

2. Migration inhibitors' cytotoxicity assays 38
3. Migration assays 39
3.1. Wound healing assays 39
3.1.1. Testing Dasatinib effect on BMDMs migration 41
3.1.2. Testing Wortmannin effect on BMDMs migration 42
3.2. Random single cell migration assays 43
3.2.1. Automatic tracking using the Harmony software 44
3.2.2. MTrackJ manual tracking 46
3.2.3. Chemical inhibitor assays 48
3.3. Macrophage morphology and migration 51
Discussion 56
1. Metacyclic selection and detection of infection 56
2. Inhibitors' cytotoxicity assessment 59
3. Migration assays 60
4. Effect of morphology on BMDM migration 63
Conclusion 64
References 66
Supplementary Data 74

List of Figures

Figure 1. Life cycle of *Leishmania* parasites in the vector 4
Figure 2. Clinical presentations of leishmaniasis 6
Figure 3. Biosynthesis of PIP, PIP2 and PIP3 through phosphorylation 12
Figure 4. The PI3K/RTK/AKT signalling pathway and the drugs' site of action 13
Figure 5. Schematic representation of the mechanisms behind microfluidic devices 23
Figure 6. PNA-selected parasites did not result in significantly higher infection rates than their non-selected counterparts 34
Figure 7. Parasites selected by the Ficoll gradient method did not yield higer infection rates than their non-selected counterparts 36
Figure 8. Parasite staining with 10 μM revealed to be ideal for image acquisition 37
Figure 9. At the concentrations to be employed in the migration assays, Dasatinib and Wortmannin are not cytotoxic to the BMDMs 38
Figure 10. The gap closure analysis is more reliable in the first 5 hours of the assay 39
Figure 11. Wound healing migration assays revealed no differences in relative migration rates across all conditions 40
Figure 12. Dasatinib did not significantly impair macrophage migration or infection rates, independently of *Leishmania* species 41
Figure 13. Wortmannin did not significantly impair macrophage migration or infection rates, independently of *Leishmania* species 42
Figure 14. The speed of the individual macrophage remained constant independently of the duration of the analysis 43
Figure 15. Automatic tracking of individual cell's random migration revealed naïve macrophages migrate slightly more than *Leishmania*-infected macrophages 45
Figure 16. Manual tracking of individual cell's random migration revealed no consistent pattern of macrophages migration 47
Figure 17. Dasatinib and Wortmannin did not impact BMDM infection rates in the manual RSC migration assays, independently of *Leishmania* species 49
Figure 18. Automatic and manual tracking of individual cell's random migration showed no consistent impact of the drugs on the macrophage's migration 50
Figure 19. Around one quarter of all detected BMDMs displayed a rounder shape and lack of extensions, associated with less motility 51

Figure 20. Round BMDMs exhibit diminished motility relative to non-round counterparts, with naïve (N) non-round cells showcasing faster and more extensive migration than *L. infantum* (L.i.), *L. major* (*L.m.*) and *L. donovani* (*L. d.*) infected-BMDMs 52
Figure 21. The exclusion of data associated with round BMDMs from the MTrackJ results revealed no consistent pattern of macrophages migration..... 53
Figure 22. The exclusion of data associated with round BMDMs from the Harmony results revealed that Dasatinib only had a slight effect on the accumulated distance and speed of all BMDMs regardless of infection status, while Wortmannin showed no effect..... 54
Figure 23. The exclusion of data associated with round BMDMs from the MTrackJ Dasatinib and Wortmannin had no consistent effect migration regardless of infection status..... 55

List of Tables

Table 1. Species of *Leishmania* that cause human disease and respective classification..... 2
Table 2. Summary of the cell-removing methods 18
Table 3. PNA negative selection failed in the enrichment of parasites with morphologies associated with metacyclic forms. 33
Table 4. The Ficoll gradient method failed in the enrichment of parasites with morphologies associated with metacyclic forms. 35
Table 5. Mean values of accumulated distance, displacement, and speed of the round BMDMs retrieved after Harmony analysis. 53

List of Abbreviations

AM	Alveolar Macrophages
BMDM	Bone Marrow Derived Macrophages
cDMEM	Complete Dulbecco's Modified Eagle Medium
CFSE	Carboxyfluorescein Succinimidyl Ester
CL	Cutaneous Leishmaniasis
CR	Complement Receptors
DC	Dendritic Cells
DCL	Diffuse Cutaneous Leishmaniasis
DMEM	Dulbecco's Modified Eagle Medium
DMSO	Dimethyl sulfoxide
ECM	Extracellular Matrix
FSC	Forward Scatter
GPCR	G Protein-coupled Receptor
HASP	Hydrophilic Acylated Surface Protein
HEPES	4-(2-hydroxyethyl)-1-piperazineethanesulphonic acid
HSC	Hematopoietic Stem Cells
iDMEM	Incomplete Dulbecco's Modified Eagle Medium
iFBS	Heat-inactivated Fetal Bovine Serum
IFN-	Interferon-gamma
IL	Interleukin
L. amazonensis	*Leishmania amazonensis*
L. braziliensis	*Leishmania braziliensis*
L. donovani	*Leishmania donovani*
L. infantum	*Leishmania infantum*
L. lainsoni	*Leishmania lainsoni*
L. major	*Leishmania major*
L. mexicana	*Leishmania mexicana*
L.d.	*Leishmania donovani*
L.i.	*Leishmania infantum*
L.m.	*Leishmania major*
LAMP	Loop-mediated Isothermal Amplification
LCL	Localized Cutaneous Leishmaniasis
LPG	Lipophosphoglycan
mAb	Monoclonal Antibodies

M-CSF	Murine Macrophage Colony-stimulating Factor
ML	Mucocutaneous Leishmaniasis
MM	Metacyclic Morphology
MOI	Multiplicity of Infection
MR	Mannose-fucose Receptor
N	Naïve
NTD	Neglected Tropical Diseases
NW	New World
OW	Old World
p.i.	Post-infection
PI3K	Phosphatidylinositol 3 kinase
PIP	Phosphatidylinositol-4-phosphate
PIP2	Phosphatidylinositol 4,5-phosphate
PIP3	Phosphatidylinositol 3,4,5-phosphate
PKB	Protein Kinase B
PKLD	Post-kala-azar Dermal Leishmaniasis.
PM	Peritoneal Macrophages
PNA	Peanut Agglutinin
PNA-	PNA Negative Fraction
PNA+	PNA Positive Fraction
PV	Parasitophorous Vacuole
RSC	Random Single Cell
RT	Room Temperature
RTK	Receptor Tyrosine Kinase
SSC	Side Scatter
TGF-β	Transforming Growth Factor-beta
TNF-α	Tumor Necrosis Factor-alpha
VL	Visceral Leishmaniasis
WH	Wound Healing

Introduction

1. Leishmaniasis

1.1. Leishmaniasis epidemiology

Leishmaniases are a group of diseases caused by at least 20 species of parasitic protozoa of the genus *Leishmania* [5]. These are transmitted between mammalian hosts by the bite of female sandflies, mainly of the genera *Phlebotomus* (Old World) and *Lutzomyia* (New World) [6]. It is one of the most prominent neglected tropical diseases (NTDs), estimated to affect around 700 000 to 1 million people annually, and its visceral manifestation is reported to lead to up to 70 000 deaths per year [7-9]. According to the Global Health Observatory, in 2022, cutaneous leishmaniasis (CL) was documented as endemic in 87 countries, while visceral leishmaniasis (VL) was reported as endemic in 79 countries [10]. Despite having the third highest mortality rate among all NTDs, the morbidity resulting from this disease is frequently misunderstood and downplayed by both clinicians and scientists [11]. Several factors contribute to this underestimation and to the continued spread of these infections. These factors include the strong association of the disease with low socioeconomic conditions, malnutrition, human migration driven by conflicts and political instability, and environmental and climate changes [7, 11].

1.2. Taxonomy

Leishmania parasites are classified within the Protista kingdom, *Trypanosomatidae* family, *Leishmaniinae* subfamily, and *Leishmania* genus [12]. There are approximately 53 described *Leishmania* species, with 31 of them known to be parasitic in mammals, and over 20 pathogenic to humans [12].

Based on DNA sequence-based phylogenetic analyses, *Leishmania* parasites can be further categorized into different subgenera, including *Leishmania*, *Viannia*, *Sauroleishmania*, and more recently, *Mundinia* [13, 14] (**Table1**). Parasites in the subgenus *Sauroleishmania* infect reptiles, while those in the remaining subgenera primarily infect humans and other mammals [15].

Alternatively, the species can be classified based on the regions of the world where they are prevalent. Old World (OW) leishmaniasis is found in the Eastern Hemisphere and is endemic in regions across Asia, Africa, and southern Europe. On the other hand, New World (NW) leishmaniasis is endemic in the Western Hemisphere, extending from south-central Texas to Central and South America [16].

Table 1. Species of *Leishmania* that cause human disease and respective classification[12, 15-18].

Subgenus	Species	New World or Old World	Disease
Leishmania	*Leishmania donovani*	OW	VL, PKLD, ML (rare)
Leishmania	*Leishmania infantum* / *Leishmania chagasi*	OW	VL, PKLD, ML (rare)
Leishmania	*Leishmania tropica*	OW	CL, ML (rare), VL (rare)
Leishmania	*Leishmania major*	OW	CL, ML (rare)
Leishmania	*Leishmania aethiopica*	OW	CL, DCL
Leishmania	*Leishmania mexicana*	NW	CL, DCL (rare)
Leishmania	*Leishmania amazonensis*	NW	CL, DCL, ML, VL (rare), PKLD (rare)
Leishmania	*Leishmania venezuelensis*	NW	CL, DCL (rare)
Leishmania	*Leishmania waltoni*	NW	DCL
Viannia	*Leishmania braziliensis*	NW	CL, ML, VL
Viannia	*Leishmania guyanensis*	NW	CL, ML
Viannia	*Leishmania panamensis*	NW	CL, ML
Viannia	*Leishmania peruviana*	NW	CL
Viannia	*Leishmania lindenbergi*	NW	CL
Viannia	*Leishmania naiff*	NW	CL
Viannia	*Leishmania shaw*	NW	CL
Viannia	*Leishmania lainsoni*	NW	CL
Mundinia	*Leishmania chancei*	OW	CL
Mundinia	*Leishmania martiniquensis*	NW, OW	CL, VL
Mundinia	*Leishmania orientalis*	OW	CL
Mundinia	*"Leishmania siamensis"* [1]	NW, OW	CL, VL
Unclear	*Leishmania colombiensis*	NW	CL, VL

[1] "*Leishmania siamensis*" is between quotation marks as it is a *nomem nudum*, indicating that it has not been described in accordance with Article 13 of the International Code of Zoological Nomenclature and, therefore, it does not hold taxonomic validity.

CL: Cutaneous Leishmaniasis.

DCL: Diffuse Cutaneous Leishmaniasis.

ML: Mucocutaneous Leishmaniasis.

NW: New World.

OW: Old World.

PKLD: Post-kala-azar Dermal Leishmaniasis.

VL: Visceral Leishmaniasis.

1.3. Life Cycle

1.3.1. Vector

Leishmania spp. is an intracellular protozoan parasite with a digenetic and complex life cycle that involves both a mammalian host and an insect vector [19]. *Leishmania* exhibits two primary morphologies: the extracellular promastigote form with 5-14 μm in length and 1.5-3.5 μm in width, found in the sandfly, and the intracellular spheric amastigote form, with 2-4 μm in diameter, present in the mammalian host [19, 20].

The life cycle starts when the sandfly takes a blood meal from an infected mammal. This blood contains amastigotes which are released into the sandfly's abdominal midgut enclosed by the peritrophic matrix [19, 21]. These amastigotes subsequently undergo differentiation into procyclic promastigotes, which represent one of *Leishmania*'s proliferative forms [21]. During this transition, a long and motile flagellum extends from the flagellar pocket located at the anterior tip of the parasite, enabling mobility [22]. Next, the procyclic promastigotes transform into nectomonad promastigotes, which escape the peritrophic matrix and adhere to the microvilli in the midgut. They subsequently migrate to the thoracic midgut and the stomodeal valve, where they further differentiate into leptomonad promastigotes [19]. At this stage, the leptomonad promastigotes differentiate into metacyclic promastigotes, which are the mammalian infective stage of *Leishmania* [19]. This stage is distinguished by its morphology, featuring an elongated flagellum and a significantly reduced cell body, both of which contribute to enhanced motility [22].

For decades, the accepted understanding of the *Leishmania* life cycle was based on single blood meal experiments, with metacyclic promastigotes considered the final stage [23]. However, recent studies with sandfly models that take multiple blood meals, which is the most likely scenario in nature, have unveiled the remarkable plasticity of metacyclic promastigotes [23]. These studies have shown that multiple blood meals stimulate the proliferation of leptomonad promastigotes [21]. Additionally, they trigger a process known as "reverse metacyclogenesis", causing metacyclic promastigotes to differentiate into retroleptomonad forms, which can rapidly divide [21]. Afterwards, the retroleptomonad and leptomonad promastigotes differentiate into metacyclic promastigotes, increasing the infectiousness of the vector. This cycle of metacyclic promastigote amplification through retroleptomonad division is reinitiated when the sandfly takes subsequent blood meals [21, 23] (**Figure 1**).

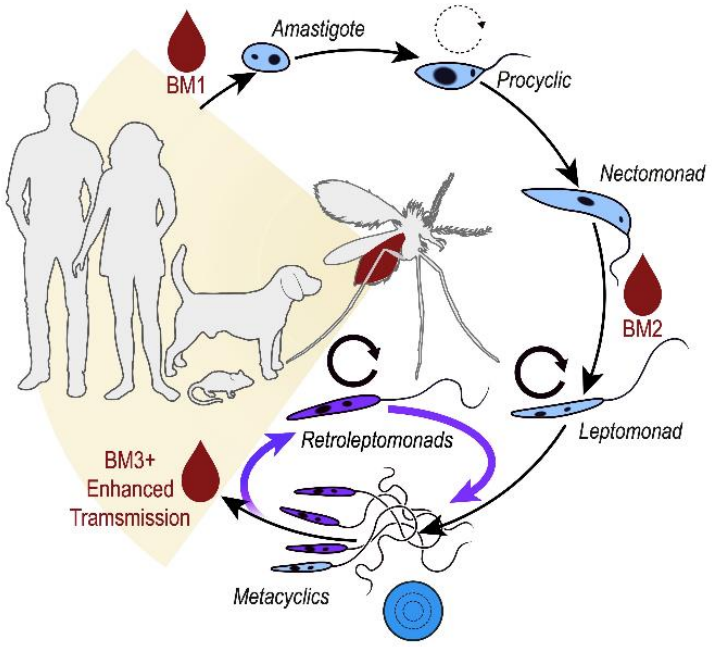

Figure 1. Life cycle of *Leishmania* parasites in the vector. Recent research has described a new process known as "reverse metacyclogenesis", where metacyclic parasites differentiate from their non-replicative form to a highly multiplicative retroleptomonad form, resulting in better infection. Adapted from Serafim, T. (2018) [23].

1.3.2. Mammals

When a sandfly infected with *Leishmania* takes a blood meal, metacyclic promastigotes are deposited at the site of the bite [19]. This injury triggers the recruitment of immune cells to the affected site, such as neutrophils, monocytes, and macrophages. It is within the macrophages that the promastigotes change forms into intracellular amastigotes in the parasitophorous vacuole (PV). Here, the parasites employ strategies to resist degradation and successfully establish themselves by regulating the maturation of the PV [24-26]. There are two types of PVs, depending on the number of parasites that it carries. Type I vacuoles are smaller and surround only one parasite. *Leishmania* species commonly associated with these vacuoles include *Leishmania major* (*L. major*), *Leishmania donovani* (*L. donovani*), and *Leishmania infantum* (*L. infantum*) [25, 27]. On the other hand, type II vacuoles are significantly larger and carry multiple parasites, such as *Leishmania mexicana* (*L. mexicana*) and *Leishmania amazonensis* (*L. amazonensis*) [25].

During the amastigote transition, the flagellum undergoes a reduction in length, to the extent that it barely protrudes from the tip of the flagellar pocket. This arrangement has been proposed as a potential mechanism for aiding in the delivery of parasite components to the infected macrophage or

for receiving signals from the host [22]. Moreover, by hiding its flagellum, the cell surface to volume ratio of the parasite significantly decreases, and thus less of the cell is exposed to the challenging environment surrounding it [19]. Amastigotes can multiply within the macrophage until i) the cell lyses and releases parasites back into blood or other interstitial space where they may infect other cells or ii) they are transferred between cells [28]. Additionally, amastigotes are characterized by their smaller size and reduced metabolic load. These characteristics are believed to have evolved under the selective pressure to avoid overwhelming the host's immune system. By not doing so, the host can survive for a longer period, allowing the parasite to proliferate for an extended duration and increasing the chances of parasite transmission to a sandfly [19].

Alternatively, if the parasites are unable to overcome the host's immune response, their growth is constrained, and the infection is controlled.

1.4. Clinical manifestations and diagnosis

The clinical manifestations of leishmaniasis are diverse and multifactorial, influenced by various factors such as the infecting species, the host's immunological status, the vectors' biology, and environmental conditions [6]. These manifestations encompass a wide spectrum of forms, from CL, which represents around 90% of the leishmaniasis outcomes, to mucocutaneous infections (ML) and the most severe form, VL [6, 29].

CL can be further divided into localized cutaneous (LCL) and diffuse cutaneous disease (DCL) [8]. LCL typically begins as a papule at the site of the sandfly bite, which develops into a pustule that eventually breaks open, forming a rounded ulcer (**Figure 2A**) [9]. Although it may be itchy, pain is usually not associated with these lesions, although they can take up to two decades to heal [6, 8, 9]. In some instances, the initial lesion may not ulcerate but instead develop a vegetating appearance that typically self-heals in less than a year and a half [9]. When the initial nodule progresses to multiple non-ulcerating papules and nodules involving the entire cutaneous surface, it is classified as DCL (**Figure 2B**) [6, 8]. ML usually originates in the nasal mucosa and subsequently spreads to affect the oral and pharynx mucosa, the larynx, the nose and lips (**Figure 2C**) [9]. This spread is believed to occur through either hematogenous or lymphatic dissemination and often arises two years to decades after the resolution of cutaneous lesions [6, 8]. Additionally, it appears to be more common among immunocompromised individuals [6, 8]. All CLs can result in scarring and disfigurement, leading to social and psychological consequences due to the changes in appearance and associated stigma [6]

VL, also known as kala-azar, affects the visceral organs and is characterized by persistent and irregular fever, splenomegaly, pancytopenia, hepatomegaly, hypergammaglobulinemia, and

weight loss (**Figure 2D**) [6, 29]. If not treated, this leishmaniasis form can be fatal within two years due to secondary bacterial infections or severe anaemia [6]. The incubation period ranges three to eight months and it the most commonly affects immunocompromised and undernourished individuals, as well as preschool children [9]. Following treatment for the visceral disease, cutaneous symptoms may emerge as a papular rash on the face and upper extremities, clinically referred to as "post-kala-azar dermal leishmaniasis" (PKLD) [8].

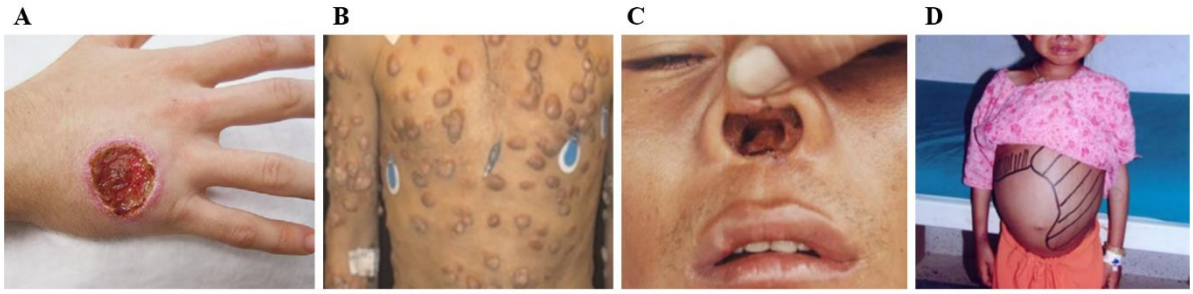

Figure 2. Clinical presentations of leishmaniasis. **A)** LCL: Ulcer on the right hand of a patient due to *Leishmania panamensis* (*L. panamensis*) infection. Adapted from Knapp, A. (2020) [1]; **B)** DCL: Patient's thorax showing polypoid nodules due to *L. mexicana* infection. Adapted from Ordaz-Farias, A (2013) [2]; **C)** ML: Lesions in nasal mucosal tissue, septal perforation and swelling of upper lip due to *Leishmania braziliensis* (*L. braziliensis*) infection. Adapted from Calvopina, M (2006) [3]; **D)** VL: Abdominal distension due to visceral infection by *L. donovani*. Adapted from Joshi, S. (2006) [4].

Since the initial symptoms of this disease can resemble those of various infectious diseases, a definitive diagnosis typically requires the microscopic observation of amastigotes in scrapings of cutaneous or mucosal ulcer tissues, or by analysing aspirations of infected organs [6, 9, 20]. Alternatively, parasitemia in the form of free parasites or those residing within macrophages can be detected in blood samples through blood smears, although the sensitivity is lower [6, 9]. Several serological assays are available, but interpreting the diagnosis based on antibody detection can be challenging. Antibodies often remain detectable for an extended period after recovery, and they may also be present in a considerable number of asymptomatically infected individuals. Additionally, some immunocompromised patients do not produce detectable antibodies. Consequently, it's crucial to evaluate these serological results in conjunction with the patient's clinical history [6]. Molecular methods, such as polymerase chain reaction and loop-mediated isothermal amplification (LAMP) of DNA fragments specific to some *Leishmania* species have also been developed. However, they come with drawbacks such as high cost, the need for skilled experts to interpret results, and, in the case of LAMP, issues related to secondary structures and required temperature ranges [20].

1.5. Prevention and treatment

Currently, the main prevention strategies rely on vector control, including indoor residual spraying, long-lasting insecticidal nets, and environmental management [6]. However, concerns have arisen due to insecticide resistance and the fact that disease vectors also feed outdoors [6, 30]. In contrast to most parasitic infections, patients who recover from leishmaniasis develop protective immunity against reinfection. This opens the possibility of preventing the disease through vaccination [31]. As of today, there are no licensed vaccines available for human leishmaniasis [6, 31]. However, as dogs are one of the main reservoirs, their vaccination with one of the four vaccines available and use of insecticide dog collars have shown promise in reducing the disease burden [30, 31]. Patients with untreated leishmaniasis are also parasites' reservoirs. Due to the stigma associated with the disease, many patients choose not to report their condition and the disease may remain in small communities [6]. Thus, it is essential to stablish a good community perception of the disease and promote healthcare-seeking behaviour to further prevent the transmission of leishmaniasis [30].

The primary approach for treating and preventing the spread of the disease relies heavily on chemotherapy [31, 32]. The first-line treatment involves pentavalent antimonial drugs, with alternatives like amphotericin B, pentamidine isethionate, miltefosine, paromomycin, and antifungal azoles available [31-33]. However, these drugs come with various drawbacks, including high toxicity, lack of specificity for *Leishmania*, multiple side effects, and emerging drug resistance [30-32]. Moreover, their cost, limited availability, need for non-oral administration and lengthy regimens pose challenges, particularly in low and middle-income regions with limited healthcare facilities where this disease is endemic [30, 32]. In addition, the response of the parasite to these drugs can vary significantly depending on the *Leishmania* species and geographical area, leading to relapses and the potential appearance of post-kala-azar dermal leishmaniasis even months after therapy ends [34].

Efforts are ongoing to develop new drug candidates, both novel and repurposed therapies, which are in pre-clinical trials phase and not yet approved for general use [32]. To address issues of toxicity, tolerability, and drug resistance, combination therapies may be administered, with current combinations involving amphotericin B with miltefosine or paromomycin, paromomycin with miltefosine, or sodium stibogluconate [32, 35]. Nevertheless, concerns related to drug availability, uncertain toxicity, and resistance to drug combinations persist [35].

Various forms of thermotherapies and cryotherapies are also used to treat leishmaniasis. Thermotherapies involve the use of machines that deliver heat in the form of infrared light, lasers, hot water soaks, or radiofrequencies directly applied to the lesions to slow parasite growth and eliminate them [32]. Cryotherapy, on the other hand, utilizes liquid nitrogen and carbon dioxide

solids to directly target infected tissue [32]. It is important to note that these therapies only work on CL and are associated with pain, scaring and risk of secondary infections [31, 32].

1.6. Shifting drug targets

Leishmania's ability to rapidly evolve drug-resistant phenotypes, facilitated by its genome plasticity, has prompted experts to consider a promising alternative: shifting the drug target from the parasite to the mammal host [34, 36]. *Leishmania* parasites employ various mechanisms to reduce the effectiveness of the host's immune system and other functions [37]. A deeper understanding of how *Leishmania* interferes with macrophage functions may reveal potential target molecules involved in essential biochemical and metabolic pathways crucial for parasite viability or infectivity.

While host-directed therapies may raise concerns about toxicity, it is worth noting that many host functions are already the targets of successful therapies for many diseases, including cancer or autoimmunity. Some of these therapies have already been repurposed and successfully applied on various infectious diseases [34]. Drug repurposing or repositioning, can be defined as “the process of finding new uses outside the scope of the original medical indication for existing drug” [38], and some of the advantages of this process include faster development times, reduced risks and lower costs [39]. Therefore, the repurposing of existing host-directed therapies represents an interesting and promising approach to address some of the existing problems with leishmaniasis treatments.

2. Macrophages

2.1. Macrophage biology and functions

The human body's immune response relies on immune cells, the majority of which originate from hematopoietic stem cells (HSCs) found in the bone marrow. Immune cells are broadly categorized into two groups based on their common precursors: myeloid cells, which encompass phagocytes and most dendritic cells (DCs), and lymphoid cells. Phagocytes, such as neutrophils and monocytes, are specialized cells primarily responsible for engulfing and eliminating microbes and clearing damaged tissues. Monocytes, in particular, undergo further differentiation into macrophages, which play a crucial role in these processes [40]. Additionally, these cells play non-immune roles in processes like development and homeostasis [41, 42].

2.2. Macrophage polarization and migration

Macrophages play a central role in immune responses, and one of their key attributes is their plasticity. In their quiescent state, they are referred to as M0 macrophages. Depending on the signals they receive, these cells can adopt different phenotypes: classically activated pro-inflammatory M1 macrophages or alternatively activated anti-inflammatory M2 macrophages [43]. The Th1 lymphocyte profile promotes the differentiation of macrophages into M1. These M1 macrophages are characterized by their heightened secretion of pro-inflammatory cytokines, such as tumor necrosis factor-alpha (TNF-α), and interleukin (IL)-6. They also exhibit increased mitochondrial metabolism and generate reactive oxygen species. All these features contribute to the destruction of *Leishmania* parasites [43, 44]. Conversely, Th2 lymphocytes induce M0 differentiation into M2. These macrophages are recognized by their elevated expression of anti-inflammatory cytokines, like IL-10 and transforming growth factor-beta (TGF-β), and play important roles in processes like wound healing and chronic inflammation [44]. It is thought that the M2 phenotype creates an environment rich in essential metabolites that support the survival of parasites [43].

Cells exhibit two distinct migration modes: the mesenchymal, often referred to as the "path-generating" mode, and the amoeboid, known as the "path-finding" mode [45]. Mesenchymal migration is typically associated with dense matrices. In this mode, elongated cells tightly adhere to the surrounding extracellular matrix (ECM), utilize podosomes, and employ proteases to degrade the ECM, thereby creating pathways for movement [45, 46]. In contrast, during amoeboid migration, cells are highly deformable and present weak adhesion to the ECM and reduced or absent proteolytic activity, making it a faster mode of migration [45]. In the case of infection, macrophages can employ both the amoeboid and mesenchymal migration modes, adapting their migration strategy as needed [46].

3. Macrophage-parasite interaction

3.1. Recognition and uptake of *Leishmania* parasites by macrophages

The injury caused by the sandfly's bite and its saliva leads to the development of an acute inflammatory response, responsible for the recruitment of immune cells to the site [19, 21]. The first responding cells are neutrophils and monocytes that migrate to the wound within minutes of the injury. In mice models, these cells have been shown to be crucial for the dissemination of the *L. major* and *L. donovani* parasites [47, 48]. However, the macrophages are the main host cells for *Leishmania* parasites [43, 44]. Evidence suggests that the initial contact between the parasite and the macrophage occurs through the tip of the parasite's flagellum, as this extension serves as a guide at the front part of the parasite during its movement [19]. The host cells' uptake of *Leishmania* promastigotes follows a classical receptor-mediated process that initiates phagocytosis [49]. Several surface molecules on macrophages have been implicated in the interaction with the *Leishmania* parasites, including complement receptors 1 and 3, the fibronectin receptor, and the mannose-fucose receptor (MR). However, some studies have speculated that certain species of promastigotes tend to evade binding to the MR during their invasion of macrophages, as this binding has been shown to promote inflammatory responses, thus increasing intracellular survival [49, 50].

Neutrophils are the initial cells to be recruited to the site of infection and are highly effective in capturing parasites [49]. Research has indicated that, in addition to direct phagocytosis, parasites can clandestinely enter macrophages by exploiting these infected neutrophils as "Trojan horses," thus evading cellular activation [49, 51].

3.2. Mechanisms of *Leishmania* to escape death and to alter macrophage migration

Many immune cells have been found to carry *Leishmania* parasites, such as neutrophiles and dendritic cells, however, a strong body of evidence pinpoints macrophages as the parasites' final niche for replication and long-term survival [28].

Leishmania, like many successful pathogens, has evolved strategies to elude the host's immune mechanisms, enabling it to survive within the host [37]. Some studies have revealed that *Leishmania* parasites can prevent the activation of the immune complement system by preventing the insertion of C5–C9 membrane attack complex and by phosphorylating the C3, C5, and C9 proteins [52]. They have also been described to inhibit the activation of Toll-Like Receptor pathways and manipulate T Cell responses by shifting T cell polarization towards a more susceptible Th2 phenotype [53-55]. Other paths that *Leishmania* employs for immune evasion include avoiding the harsh environment of the phagolysosome by delaying or inhibiting endosomal maturation [56, 57],

interfering with the antigen presentation capacity of macrophages by sequestering or hindering the loading of antigens onto MHC class II molecules. Furthermore, they modify macrophage signalling and modulate the release of cytokines and chemokines, inducing the production of key cytokines like IL-10, which is crucial for their survival and disease progression [37, 58-60].

Several studies have demonstrated that these parasites influence other macrophages functions, particularly with respect to migration. However, how these interactions translate into the migration dynamics of infected macrophages remains an open question, as different articles suggest different outcomes. While some researchers propose that *Leishmania* infection could enhance macrophage motility by many mechanisms including increasing the phosphatidylinositol 3 kinase (PI3K)γ activity [61], decreasing macrophages' adhesion to tissues [62, 63] or increasing their secretion of matrix metalloproteinases [64], others argue the opposite, suggesting that *Leishmania* infection leads to a decrease in macrophage motility [62, 65-67].

3.3. General function of the PI3K/RTK/AKT pathway

PI3K signalling is known to play a role in the host's response to *Leishmania* infections [68]. The inositol head group plays an especially important role in signal transduction. There are three classes of enzymes known as PI3K that phosphorylate the position 3 of the inositol ring. Class I enzymes are primarily located on the plasma membrane and are responsible for phosphorylating phosphatidylinositol 4,5-phosphate (PIP2) to form phosphatidylinositol 3,4,5-phosphate (PIP3) (**Figure 3**) [69]. The Class I enzymes can activate protein kinase B (PKB), also known as AKT, which plays a critical role in several cellular functions, including cell survival, proliferation, differentiation, and intracellular trafficking [70]. Class I enzymes are further divided into two subclasses, which differ in their overall structure and the stimuli that activate them: class Ia and class Ib [68]. The Class Ia enzymes include PI3Kα, PI3Kβ, and PI3Kδ (**Figure 4**). Class I catalytic PI3K subunits are activated by extracellular stimuli through two major modes, namely, receptor tyrosine kinases (RTKs) and G protein-coupled receptors (GPCRs) [71]. In contrast, the class Ib kinase PI3Kγ is primarily activated by GPCRs [68]. Class II enzymes phosphorylate phosphatidylinositol-4-phosphate (PIP) into PIP2 (**Figure 3**) and are the least understood enzymes among the three classes. Class III enzymes phosphorylate an unphosphorylated inositol ring at the 3 position, turning it into PIP (**Figure 3**) [68]. When it comes to *Leishmania* infections, research has predominantly focused on the contributions of Class I PI3 kinases [68]. For instance, studies have shown that inactivating PI3Kδ led to limited infection in the spleen and liver by *L. donovani* [72]. Additionally, a study with *L. mexicana* has shown that PI3Kγ inhibition or deletion resulted in decreased infection due to impaired parasite phagocytosis by macrophages and neutrophils [73].

Various stimuli, including growth factors, cytokines, and hormones, have been reported to activate PI3K. These stimuli bind to the corresponding extracellular region of RTKs, leading to the autophosphorylation of tyrosine residues in its cytoplasmic region, linker molecule and 85SH2 [74]. The interaction between the domain and the phospho-Tyr residue on the RTK complex facilitates the recruitment of PI3K to RTKs, ultimately leading to the activation of PI3K [74].

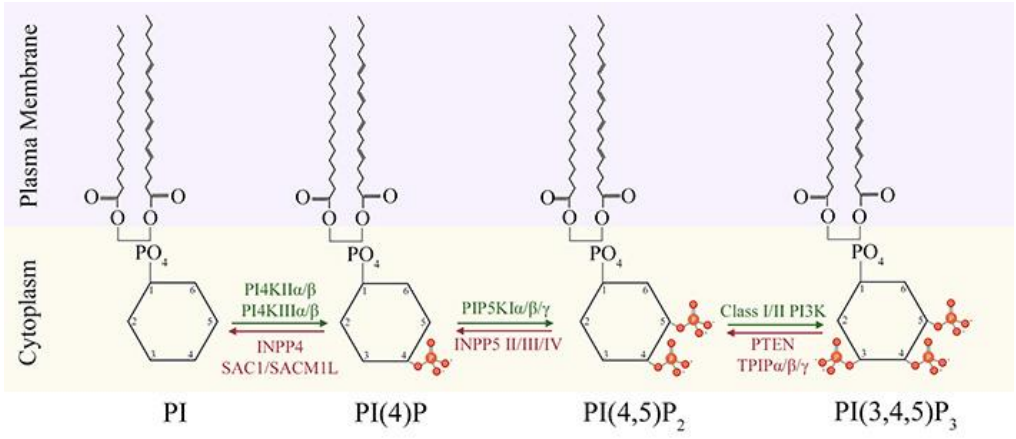

Figure 3. Biosynthesis of PIP, PIP2 and PIP3 through phosphorylation. In the interface between the cytoplasm and the plasma membrane, PI3K enzymes phosphorylate the position 3 of the inositol ring of PIP2, resulting in PIP3. Adapted from Tariq, K (2021)[75].

3.4. PI3K and RTK pathway inhibitors

The PI3K signalling pathway is recognized as a significant player in cancer evolution and, as a result, a range of PI3K inhibitors has been clinically developed [76]. In the early stages of many diseases, particularly cancer, the understanding of the structure and isoforms of the PI3K protein is limited. Consequently, most of the inhibitors developed targeted all four isoforms of Class I PI3K, earning them the designation "pan-inhibitors" [76]. The first established PI3K inhibitors were Wortmannin and LY294002 [77]. Wortmannin is a natural mold metabolite with anti-inflammatory properties that irreversibly inhibits the PI3K pathway, whereas LY294002 is a synthetic PI3K inhibitor with reversible effects [77]. Other pan-PI3K inhibitors include Copanlisib and Buparlisib [76]. In addition to pan-inhibitors, there are inhibitors specific to each isoform of PI3K. These include Alpelisib for PI3Kα, AZD8186 and GSK2636771 for PI3Kβ, Idelalisib, Duvelisib, and Umbralisib for PI3Kδ, and IPI 549, AS-604850, and AS-605240 for PI3Kγ inhibitors [76, 78].

RTKs also are pivotal regulatory signalling proteins that govern the growth and metastasis of cancer cells. Over the last two decades, numerous molecules targeting RTKs have been employed in oncology as either first- or second-line therapies for various types of cancer [79]. These inhibitors

are categorized into different classes based on their mechanisms of action. Type-I inhibitors are ATP-competitive and bind to active conformations (e.g., Dasatinib, Brigatinib and Dacomitinib) while type-II inhibitors bind near the ATP site of inactive kinases, maintaining their inactivity (e.g., Nilotinib, Lapatinib and Lenvatinib). Type-III inhibitors are highly selective and work through allosteric binding to sites distant from the ATP site (e.g., Binimetinib, Cobimetinib and Trametinib). Type-IV inhibitors reversibly target substrate-binding sites and are still in development. Lastly, type-V inhibitors form covalent bonds with their targets (e.g., Acalabrutinib, Ibrutinib and Neratinib) [79].

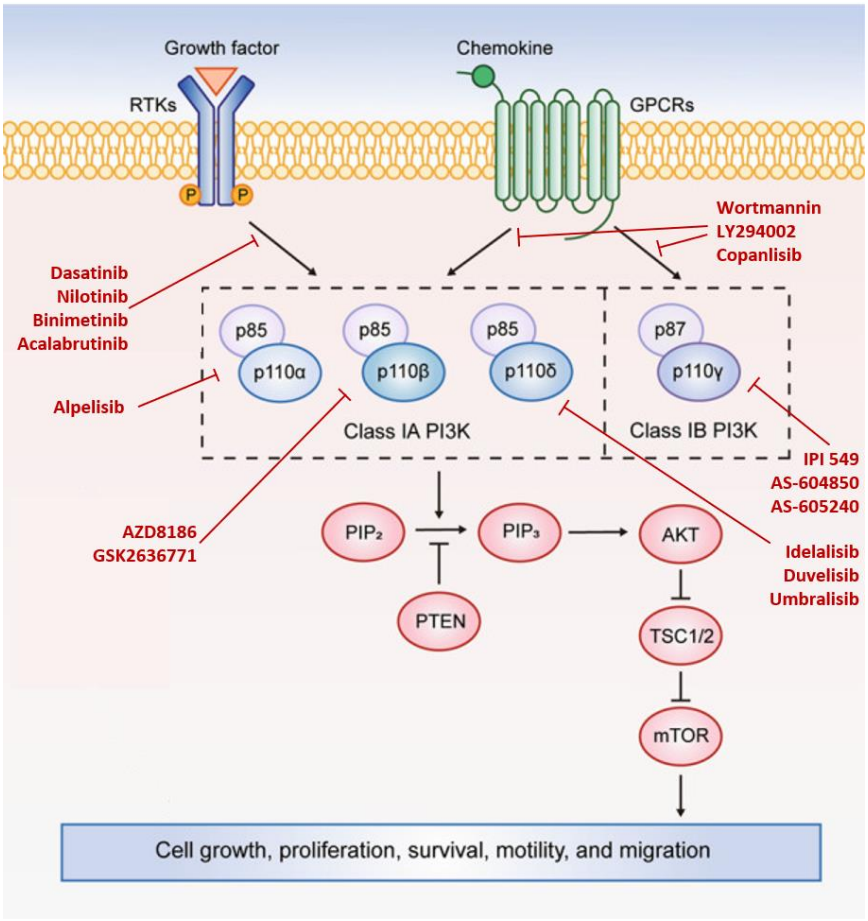

Figure 4. The PI3K/RTK/AKT signalling pathway and the drugs' site of action. Class Ia PI3Ks can be activated by RTKs and other adapter proteins, while class Ib PI3K is exclusively activated by GPCRs. PI3K activation leads to phosphorylation of PIP2 into PIP3, which activates the AKT/mTOR pathway. These activation can be blocked by both RTK and PI3K inhibitors, which may impair the growth, proliferation, survival, motility and migration of cells. Adapted from Sun, P. (2020)[80].

4. *In vitro* methods to measure macrophage migration

4.1. Bone marrow derived macrophages (BMDMs)

Macrophages have a plethora of functions within the immune system, making them a prime focus in the study of several pathologies. *In vitro* models for these studies often rely on BMDMs and other primary cell sources such as peritoneal macrophages (PM) and alveolar macrophages (AM), each with its own advantages and limitations [81]. For instance, while PM and AM can be readily harvested from the mouse, the yield is low, and the cells could already be stimulated by interactions with other immune cells or external factors [81]. In contrast, BMDMs are fully differentiated *in vitro* from bone marrow HSCs and are naïve (M0) regardless of the mice's health conditions [81, 82], while experimentally inducible into M1 or M2 phenotypes [83]. BMDMs can also be obtained in high yields, with a single mouse providing a substantial quantity of homogeneous cells that can remain for up to three weeks without significant cell death or morphological changes, minimizing the number of sacrificed animals [81, 82]. Because these cells can be cultivated in culture dishes and even cryopreserved for extended periods without significant changes, they are recognized as a cost-effective and ethically preferable option [81]. Furthermore, these macrophages can be directly isolated from transgenic mice or, with modern technologies like lentiviral transfection, genetically altered [84].

Due to the limited proliferative capacity of differentiated primary macrophages and associated animal ethical concerns, many researchers have turned to immortalized macrophage-like myeloid cell lines, including J774A.1, RAW264.7, P388D1, and PU5-1.8 [81, 85]. However, these cell lines often diverge from primary macrophages as the continual subculture of these cell lines exerts selective pressure, leading to the loss of genes that are not essential for proliferation but are critical for macrophage immune functions [81]. Consequently, cell lines exhibit differences from primary macrophages in functions such as phagocytic activity, cytokine production, and the regulation of oxidative burst, besides being less suitable for microscopy [84]. Depending on the cellular and molecular processes under investigation these cell lines may prove inadequate tools to understand biological phenomena. As such, BMDMs, due to their remarkable homogeneity, transfection capabilities, proliferation potential, extended lifespan, ease of handling, cost-effectiveness, and ethical advantages, have been recognized as crucial models for investigating macrophage biology, in specific macrophage-pathogen interactions and macrophage migration [81, 84, 86].

4.2. BMDMs' infection and metacyclic selection methods

In vitro protocols for the infection of BMDMs with *Leishmania* present a wide range of variations depending on the parasite species, strain, life stage, culture conditions and the objectives of the assay. For example, several parasite-to-macrophage ratios [or multiplicity of infection (MOI)] have been described, spanning from 5:1 to 20:1, along with varying incubation periods, typically between 3 to 72 hours [61, 66, 87, 88]. Regarding infections with promastigotes, specialized protocols have been developed to isolate metacyclic forms to enhance infection rates in a consistent manner.

It has been documented that the leishmanial virulence towards their hosts, mammalian and sandfly vector, is due to glycoconjugates, and it is widely reported that the majority of *Leishmania* species express a glycolipid known as lipophosphoglycan (LPG) [89]. However, during metacyclogenesis, these glycan residues are capped with arabinose, effectively concealing them [90, 91]. The peanut agglutinin (PNA), a lectin derived from peanuts, can selectively bind to the galactose residues present in LPG, enabling the separation of metacyclic promastigotes from LPG- promastigotes [91]. This separation can be achieved through incubation followed by centrifugation, which results in non-agglutinated metacyclic promastigotes remaining in the supernatant, while the PNA-agglutinated forms are found in the pellet [92]. Importantly, the agglutination can be easily reversed through dilution of the suspension [89].

This method has been well-documented to work effectively with *Leishmania* species like *L. major*, *L. infantum*, and *Leishmania orientalis* (*L. orientalis*), leading to improved infection rates, a higher number of amastigotes per infected cell, and parasites that closely resemble metacyclic forms [89, 91-94]. However, for *L. donovani*, the results are not as clear-cut, with success depending on the number of passages in axenic culture, where fewer than 5 passages yield more consistent results, while from 5 to 10 passages, outcomes vary [95, 96]. Other LPG-dependent methods are available for purifying metacyclic promastigotes of *Leishmania*. For instance, the monoclonal antibody 3F12, which binds to arabinose-capped metacyclic-specific LPG in *L. major* [97]. In the case of *L. braziliensis*, two alternative methods are used: Bauhinia purpurea lectin, which recognizes β-gal(1→3)-galNAC and separates non-metacyclic promastigotes, and lentil lectin, which targets D-Mannose-terminal glycoconjugates, allowing for positive selection of metacyclic promastigotes [98, 99].

The LPG-based methods or purifying metacyclic *Leishmania* parasites have been noted for their inconsistency across different *Leishmania* species. To address this challenge, alternative LPG-independent methods have been developed, focusing on the density characteristics of the parasites [100]. As previously described, the infective metacyclic stage of all *Leishmania* species exhibits distinct morphological features, characterized by a short, narrow body and a long flagellum [22].

This distinction raised the question of whether metacyclic forms exhibit different sedimentation properties under specific conditions [100]. Building on this premise, the Ficoll gradient method was introduced [100]. Ficoll, a commonly used density medium, is known for its high molecular weight and is typically used for isolating peripheral blood mononuclear cells from other blood components through centrifugation [101]. To separate metacyclic promastigotes, a Ficoll gradient method is employed, which involves the preparation of two distinct Ficoll solutions with varying concentrations. These solutions are layered within a conical tube, with the denser Ficoll solution at the bottom, followed by the less concentrated Ficoll solution, and these are then topped with a suspension of parasites in medium [100]. Following centrifugation, a layer containing the metacyclic promastigotes forms between the upper medium and the Ficoll layers. This metacyclic-enriched layer is subsequently aspirated and separated from the other parasite forms [100].

This method has proven effective in obtaining enriched cultures of metacyclic promastigotes, featuring their distinctive morphology, and leading to increased infection rates [100, 102]. It is now established as a reliable metacyclic isolation technique, widely applied to numerous *Leishmania* species, including but not limited to *L. mexicana*, *L. major*, *L. donovani*, *L. infantum*, *L. amazonensis*, and *Leishmania lainsoni* (*L. lainsoni*) [103-108]. However, due to variations in the size, shape, and density of *Leishmania* parasites, it is essential to determine the most effective Ficoll concentrations for each specific parasite species [100].

4.3. Wound healing migration assays

One widely used *in vitro* technique applied in the study of collective cell migration in 2D is the wound healing (WH) assay [109-111]. This assay involves creating a cell-free area within a confluent cell monolayer, which then stimulates collective cell migration into the cleared area, allowing for the measurement of the collective cell speed through the gap closure rate [109, 111]. This method is very versatile and can be used for a variety of studies, spanning from medium to high throughput applications [111]. Important factors to consider include the initial cell density, incubation period, frequency of media changes, the passage number of cells, and the choice of substrate for cell plating [109-111]. Ensuring that the assay consistently initiates after the monolayer reaches confluence is essential as the results may vary according to the maturity of monolayer [111].

Throughout the course of the assay, cells migrate into the gap and can sometimes proliferate. Therefore, in relevant cases, it becomes essential to hinder cell proliferation to prevent any interference with the measurement of migration. This can be achieved through different methods, such as utilizing drugs like actinomycin C13 and implementing serum starvation [111]. However, the dosage of these methods must be carefully controlled to prevent apoptosis or other toxic effects that could impact cell migration [111].

A cell-free gap in the monolayer can be created with two different methods: cell-removing methods and cell-excluding methods [110]. In the cell-removing methods, cells are initially seeded and later removed. In contrast, cell-excluding methods involve the placement of a barrier first, and only after the cells are seeded, resulting in a cell-free area upon its removal, except for liquid barriers. In assays employing liquid barriers, no barrier is pre-applied to the plate, but rather the cells are separated when seeded within a liquid medium. The cell-removing methods are described on **Table 2**.

Table 2. Summary of the cell-removing methods [109, 110, 112-117].

Method	Mechanism	Advantages	Disadvantages
Cell-removing methods			
Scratch assay	Gap created manually using tools like a pipette tip, needle, or similar sharp instruments.	• Most commonly used. • Cost-effective easy to use. • Requiring minimal modifications to routine cell culture conditions.	• Challenging in making consistent and reproducible gaps. • Excessive pressure during scratching can potentially damage the extracellular matrix.
Stamp wounds	Stamps is pressed into the cell layer using weights and, after their removal, an area filled with cell debris is left behind. Afterwards, the surrounding cells migrate towards this area.	• Maintains matrix integrity.	• The dead or damaged cells in the region to where the cells migrate towards can alter the migration patterns.
Electrical Removal	A dense cell population is established over an electrode-containing substrate. A high-voltage pulses induce electroporation and cell death, creating a void over the electrode.	• Automated void creation, reducing irregularities compared to manual scratching.	• Changes in adhesion and cell density can alter the outcome.
Chemical Removal	Use of a chemical substances, such as trypsin, that, within microfluidic devices, creates voids and nests of cells.	• Uniform and predictable matrix in the cell-free void.	• Requires expertise for microfluidic experiments. • Associated challenges include air bubbles, cell clumping, and fluidic system management.
Cell excluding methods			
Solid Barriers			
Stoppers	Stoppers are implemented with friction and compression to secure themselves into the bottom of a dish.	• Can seal against wet and protein-coated surfaces. • Requires fewer seeded cells.	• Manual insertion is required, which can disrupt matrix proteins or result in an incomplete seal.
Adhesion Stencils	Stencils that rely on auto adhesion rather than gravity.	• Auto adhesion provides a tight seal against the matrix. • Low equipment and expertise required.	• Manual insertion and removal which damage cells or substrates. • Require a dry, hydrophobic surface for effective adhesion.

Magnetic Attraction	Stencils create a seal by using magnetic attraction to magnets positioned beneath the plate.	• Seal successfully on a big range of substrates including wet surfaces. • Minimal damage to the matrix • High reproducibility.	• Manual removal can potentially damage cells or substrates.
Gel Barriers (Degradable Gel Droplets)	Gels are applied to the plate and dried or polymerized. Afterwards, the gel is dissolved, enabling migration into the cleared area.	• The gel dissolves by applying a solution, eliminating the human error associated with manual removal.	• Limited investigation possibilities of the cell-matrix interactions due to the drying or polymerization process. • The gel's thinner edges dissolve faster, leading to irregularities.
Liquid Barriers			
Immiscible Solutions	Cells are placed in one part of an immiscible or two-phase solution, enabling them to adhere to the substrate in that specific area and not the other.	• Allow patterning of cells on delicate matrices. • Avoid substrate damage inherent in solid barriers.	• Necessity of employing solutions that are not typically used in cell culture, which could impact cell behaviour, migration, or even alter the conditions of the matrix.
Laminar Flow in Microfluidics	Employment of solutions to pattern cells through laminar flow within microfluidic devices.	• Removes the risk of substrate damage • Enables dynamic control of medium conditions • Allows the creation of gradients.	• Lack of surface tension or physical force to prevent immediate cell migration after adhesion.
Air Interface as a Barrier (Droplets and Microfluidics)	Cells droplets are applied into a dry substrate, where the air interface acts as a natural barrier due to the surface tension. After cell adhesion, more medium is introduced rehydrate the dry surface surrounding the droplets.	• Simplicity and ease of patterning cells • Delicate materials.	• Variability in cell patterning • Requirement for cells to adhere quickly • Need for temporary drying of the matrix • Limited compatibility with elastic surfaces in microfluidics.

Once a cell-free area is established, images of the gap are captured over time using either a manual or automatic microscope, employing various techniques such as fluorescence, brightfield, or phase-contrast microscopy [111, 118]. These images not only offer data about the migration rate, but also valuable insights into cell morphology and protein localization [118].

Overall, the WH assays are regarded as simple, reliable, and versatile methods for studying cell migration. Moreover, these assays do not require the use of specific chemoattractant or gradient chambers, as the cell-free area itself generates a strong directional migratory response, even in cell types that typically exhibit weaker responses in migration assays [118].

4.4. Random single cell migration assays

In order to study the factors influencing cell movement, a variety of 2D and 3D cell migration assays have been developed. Migration assays in 2D, particularly, have been favoured for their simplicity and are primarily used to study mesenchymal migration [119]. Among these, the random single cell (RSC) migration assay stands out as the most straightforward. Single-cell migration plays a crucial role in enabling cells to move within and between different tissue compartments, which is particularly significant in the context of inflammation-induced migration of leukocytes [120]. The RSC migration assay focuses on single-cell movement, allowing cells to migrate freely in the absence of specific stimuli, making it ideal for studying the basal migration characteristics of cells [119]. RSC assays involve seeding cells in plates under the conditions of interest and monitoring their migration over time, all without external stimulation. This simplicity makes it a valuable tool for investigating various parameters that influence cell migration, including the cell culture medium, substrate properties, and cell density [119, 120].

RSC assays demand single cell tracking and trajectory analysis using software tools like MTrackJ from ImageJ [119]. These tools can track cell movements over time and retrieve their coordinates, allowing for the study of migration patterns, displacement, and cell speed under basal conditions [119, 121]. For example, when studying the trajectories of single cells and small cell groups restricted within circular regions, researchers have observed that specific cell types display a characteristic known as "persistence" in their movements, i.e., these cells tend to continue moving in their current direction rather than changing course [120].

However, obtaining reliable and efficient data in this context comes with its challenges, since cell segmentation and tracking rely heavily on algorithmic and automated analyses and requires some expertise [121]. Manual tracking of individual cells is also an option but it is labour intense and prone to operator bias and error [121]. Additionally, it's important to note that this type of migration assay, while useful for studying the fundamental migration behaviour of individual cells, may not fully represent the conditions of cells within tissues where collective migration plays a significant role.[119-121].

4.5. Transwell migration assays

A widely used method for studying directed cell migration involves the use of transwell inserts. This technique, also known as Boyden chamber assay, allows for the analysis of migration in both 2D and 3D settings [122]. Transwell migration assays (2D) enable the analysis of the chemotactic capability of cells toward a chemoattractant, and transwell invasion assays (3D) evaluate both chemotaxis and cell invasion through a matrix. These assays are designed to evaluate the ability of individual cells to directionally respond to a variety of chemoattractants, including chemokines and growth factors, helping to characterize the key regulators of cell migration [123] .

In this method, two chambers filled with culture medium are separated by a porous membrane. Cells are seeded on this membrane, and typically, a chemoattractant is introduced into the lower chamber to stimulate cell migration [124]. To assess the cells' invasion abilities, a matrix material like Matrigel can be applied on top of the transwell membrane, and then cells are placed on the matrix layer [123, 124]. It is crucial that the chemoattractant solution makes contact with the upper well's membrane to establish a chemotactic gradient [123]. After incubation, adherent cells will attach to the underside of the membrane, while non-adherent cells will drop into the lower chamber. The quantification of migrated cells can be performed using a hemocytometer or flow cytometer [123].

The appropriate incubation time and the specific pore size of the transwell membrane depend on the cell type and chemoattractant used. For instance, if cells are very small, they might pass through the pores due to gravity, bypassing the need for migration facilitation. Conversely, if the cells are too large, they might not fit through the pores [123, 125, 126]. Furthermore, transwell assays do not provide a complete understanding of the migration dynamic of individual cells as they can only offer an endpoint readout for the total number of cells that migrated [126]. The gradients formed are also poorly defined, which may lead to increased variability between assays [127]. Lastly, the removal of non-invading cells remaining on the upper side of the transwell insert is typically done with a cotton swab before staining the invasive cells on the membrane's bottom. This process is often challenging, lacks quantifiability, is prone to human error, and can lead to variable results [125].

4.6. Microfluidic devices for chemotactic migration assays

Over the years, numerous microfluidic devices have been developed, with each new one designed to address the challenges and limitations of its predecessors. Despite their variations, they all share a common framework, which involves the observation of cell migration within a central channel or bridge connecting two or three reservoirs [128]. One reservoir contains the chemoattractant, while the other(s) contain the culture medium [128]. The most commonly mentioned microfluidic devices are the Zigmond chamber, the Dunn chamber, and, more recently, the µ-Slide Chemotaxis chamber (**Figure 5**) [127, 129]. These chambers offer well-defined linear gradients and provide researchers with enhanced control over experimental setups [122, 127]. Moreover, they allow for either an endpoint and continuous analysis of migration, which can be monitored using brightfield, phase-contrast, or fluorescence microscopy [122]. In comparison to traditional transwell assays, microfluidic chambers require minimal sample volumes and enable precise control of the microenvironment [122]. However, they typically lack the ability to distinguish individual cells and do not allow cell retrieval after migration. An additional drawback of microfluidic chambers is that they can be more time- and cost-intensive than simpler methods such as RSC and WH migration assays [122].

The earliest microfluidic device to be developed was the Zigmond chamber, which marked a significant advancement in the rapid evaluation of cell orientation within specified concentrations. It enabled a comprehensive analysis of cell behaviour and morphology throughout the initiation, execution, and reversal phases of chemotactic responses [128]. Afterwards, the Dunn chamber was introduced, offering improved optical clarity, dimensional precision, and long-term stability compared to its predecessor [130]. More recently, the µ-Slide Chemotaxis chamber became commercially available. Unlike the previous two chambers that required cleaning, sterilization, and assembly, the µ-Slide's disposable nature addresses these concerns, ensuring maximum reproducibility [127]. This modern microfluidic device was designed to enhance microscopy quality, provide well-defined linear concentration gradients, support extended assay durations, and enable the observation of slowly migrating cells through time lapse microscopy [127].

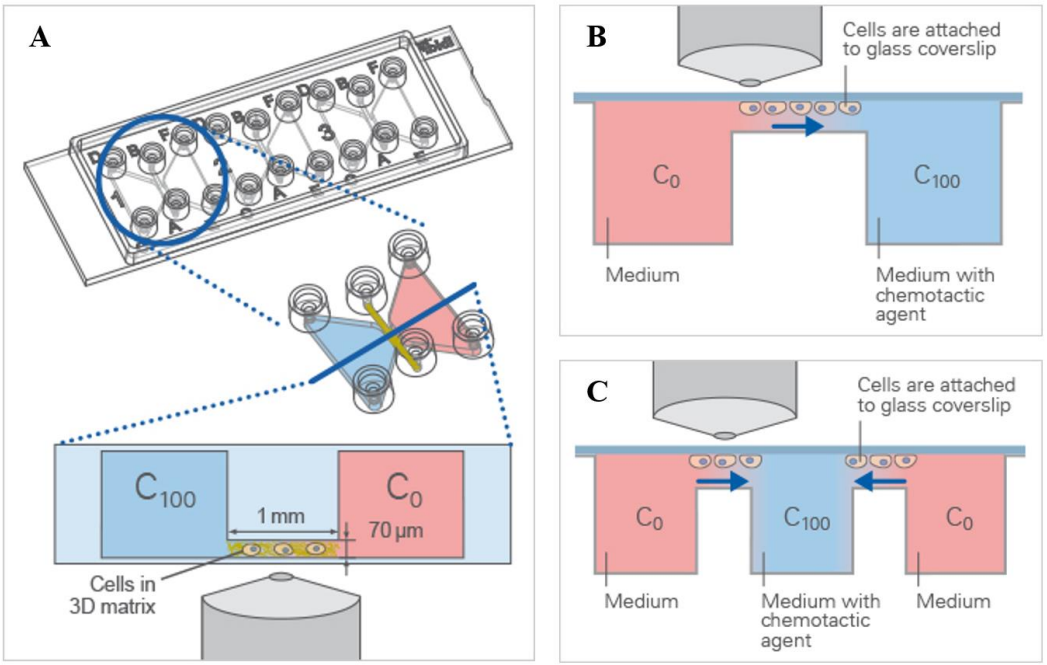

Figure 5. Schematic representation of the mechanisms behind microfluidic devices. A) µ-Slide Chemotaxis chamber; **B)** Zigmond chamber; **C)** Dunn chamber. Adapted from Ibidi (2023) [129].

Aims of the study

The primary objective of this study was to determine the impact of *Leishmania* infection on the migration of macrophages, their host cells. This research builds upon prior studies conducted within the Molecular Parasitology Group with the ultimate aim of understanding why some species of *Leishmania* remain in the skin while others disseminate to internal organs. Towards our end, the following objectives were defined:

1. Establish protocols for i) robust infection rates by *Leishmania* parasites, and for ii) distinguishing infected cells from non-infected ones, two requirements for implementing of migration assays.
2. Compare the migration patterns of infected and non-infected macrophages in distinct *in vitro* migration assays.
3. Study the effect of different migration inhibitors for their capacity to impact *Leishmani*a-infected macrophages.

The findings of this thesis are anticipated to contribute to a deeper understanding of the impact of *Leishmania* infection on the behaviour of macrophages.

Materials and Methods

Ethics statement

In this study, experiments with male BALB/c mice were conducted in conformance with the procedures approved by the Local Animal Ethics Committee of i3S and licensed by DGAV (Direção Geral de Alimentação e Veterinária, Govt. of Portugal). Animal handling and care were performed in accordance with the European Legislation (directive 2010/63/EU, revising directive 86/609/EEC) and the corresponding national authorities (DGAV, directive 113/2013 from 7th of August). To ensure ethical treatment, mice were euthanized using an overdose of isoflurane inhalation, followed by cervical dislocation to confirm death.

Culture Media

In all assays performed, Dulbecco's Modified Eagle's Medium (DMEM) (Gibco™, Thermo Fisher Scientific, MA, USA) was consistently used for both macrophages and parasites. During washing procedures, incomplete DMEM (iDMEM) was employed, i.e., DMEM supplemented with 1% (v/v) nonessential amino acids, 50 U/mL penicillin, and 50 µg/mL streptomycin (all the compounds are from Gibco™, Thermo Fisher Scientific, MA, USA). However, cells were cultured in iDMEM supplemented with 10% (v/v) heat-inactivated fetal bovine serum (iFBS), resulting in complete DMEM (cDMEM). Additionally, for *Leishmania* cultures, cDMEM was supplemented with 25 mM HEPES (Sigma-Aldrich, MO, USA), adjusted to a pH of 6.8.

BMDM cell culture

Hematopoietic cells were recovered from the bone marrow of 1 to 2 months old BALB/c mice under aseptic conditions. Femurs and tibias were collected and flushed with iDMEM using 25-gauge needles. After collection, the cells were centrifuged at 200 g at 4ºC for 10 minutes (Centrifuge 5810 R, Eppendorf, DE) and then re-suspended in cDMEM and plated in a 10-cm Petri dish (Nunclon, cell culture treated, VWR, Ref. 734-2043). Cells were incubated in a humidified 5% CO_2 atmosphere at 37ºC (Binder, DE) for a minimum of 4 hours before non-adherent cells were recovered into a 50 mL conical tube by washing twice with 10 ml pre-warmed iDMEM medium. Afterwards, the cells were centrifuged at 200 g, at 4ºC for 10 minutes, the supernatant discarded, and the pellet resuspended in cDMEM. Cells were counted using a haemocytometer (Bright-Line®, Reichert, NY, USA) and 0.4% Trypan Blue Solution (Gibco™, Thermo Fisher Scientific, MA, USA) to assess cell viability.

Cells were seeded in a 96-well plate (Thermo Fisher Scientific, MA, USA) at a density of $5x10^4$ cells per well for the WH assays and $2x10^4$ cells per well for the random single cell assays. Differentiation into macrophages was induced by supplementing the culture medium with 30 ng/mL of murine macrophage colony-stimulating factor (M-CSF) (PeproTech, NJ, USA) for 8 days, with medium change on day 3 and 6.

Leishmania cell culture

In the context of this work, three species of *Leishmania* were used – *L. major* strain MHOM/SA/85/JISH118, *L. infantum* strain MHOM MA67ITMAP263 and *L. donovani*, strain MHOM/IN/82/Patra1. *L. donovani* was generously provided by Doctor Ricardo Silvestre from the Life and Health Sciences Research Institute (ICVS/3B's, Minho, Portugal). All *Leishmania* promastigotes were cultured at 26°C in cDMEM supplemented with 25 mM 4-(2-hydroxyethyl)-1-piperazineethanesulphonic acid (HEPES) (Sigma-Aldrich, MO, USA), pH 6.8 with a starting inoculum of $2x10^6$ parasites/mL for *L. major* or $1x10^6$ parasites/mL for *L. infantum and L. donovani*. Parasite were counted in a haemocytometer, after dilution with 0.25% glutaraldehyde (Merck KGaA, DE).

To prevent the loss of infectivity due to the extended time in culture, aliquots of low-passaged parasites stored in liquid nitrogen, after being retrieved from spleens of experimentally infected animals, were periodically thawed. Upon defrosting parasites were cultured overnight in a $25cm^2$ flask at 27°C in Schneider medium (Sigma-Aldrich, MO, USA). The next day, parasites were centrifuged at 2000 g, room temperature (RT), for 10-minutes and cultured in cDMEM pH 6.8 at 27°C. Virulent parasites were maintained in culture for a maximum of seven passages before being replaced with fresh aliquots.

Selection of Metacyclic Promastigotes

Metacyclic promastigotes were isolated by two methods: PNA negative selection and the Ficoll gradient.

For the PNA negative selection method, stationary phase parasites were centrifugated (Centrifuge 5418, Eppendorf, DE) at 2000g, RT, for 10 minutes and resuspended in a 100 µl/mL PNA solution (Merck KGaA, DE). The parasites suspension was incubated at 26°C for 30 minutes with gentle shaking every 10 minutes. Afterwards, cells were centrifugated at 200g for 5 minutes, RT to form a pellet constituted by PNA-positive (PNA^+) promastigotes while PNA-negative (PNA^-) promastigotes (metacyclic) remained in the supernatant. The PNA^- fraction was collected into a new conical tube.

Regarding the Ficoll gradient, a 15mL conical tube was layered with two Ficoll (Merck KGaA, DE) solutions prepared with a half-and-half mixture of Medium 199 (Gibco™, Thermo Fisher Scientific, MA, USA) and 1x PBS: 20% (v/v) on the bottom and 10% (v/v) on top. In parallel, stationary phase parasites were centrifuged at 775 g, RT, for 10 minutes and resuspended in iDMEM. The parasite suspension was placed on top of the Ficoll gradient, and the tube was centrifuged at 365g, RT, for 10 minutes. The fraction between 0-10% Ficoll was harvested into a new conical tube to retrieve the metacyclic promastigotes, which were further centrifugated at 2110 rpm, RT, for 15 minutes and resuspended in cDMEM.

Following both protocols, the parasites within the recovered fractions were counted using a haemocytometer and photographed with an Olympus CX33 upright microscope with a 40x objective connected to a digital camera (ACCU-SCOPE AU-600-HD, Olympus Corporation, JPN). Parasites were also distinguished based on their morphology and metacyclic promastigotes were identified by featuring a slim body with a length of less than 12.5 µm and a flagellum that is at least twice the size of the body [92, 100, 131].

Parasite Staining

Under the scope of this project, a protocol for parasite staining with a fluorescent dye, carboxyfluorescein succinimidyl ester (CFSE), was established. Stationary phase parasites were centrifugated for 2000 g, RT, for 10 minutes, and the pellet resuspended in 12mL 1xPBS (Merck KGaA, DE). After a second centrifugation, the pellet was resuspended in 1mL of 10µM CellTrace™ CFSE solution (Excitation/Emission [Ex/Em]: 492/517nm) (Thermo Fisher Scientific, MA, USA) and incubated for 15 minutes at 37°C with occasional shaking. Afterwards, the parasites were subjected to two additional rounds of centrifugation, as detailed above and finally resuspended in cDMEM for further applications. To assess the morphology of the parasites and the durability of the staining, we examined the parasites at various time points after the staining process using the Axio Imager Z1 microscope (Zeiss Group, DE). Images were taken with an 40x amplification with aid of the 38 HE filter set (Excitation: BP 470/40; Beam Splitter: FT 495; Emission: BP 525/50).

BMDMs infection with *Leishmania* promastigotes

Infection of BMDMs was conducted with *Leishmania* promastigotes prepared by different protocols: i) stationary phase cultures, ii) metacyclic enriched fractions obtained from PNA negative selection or Ficoll gradient or iii) CFSE labelled promastigotes.

BMDMS at day 8 of differentiation were co-incubated with promastigotes at different parasite-to-macrophage ratios, or multiplicity of infection (MOI) of 10:1 for *L. infantum* and *L. donovani* or 5:1 for *L. major*. Upon 3 hours of contact, the non-phagocytosed promastigotes were washed away with iDMEM. Cells were incubated with cDMEM supplemented with 15 ng/mL M-CSF (5% CO_2, 37 °C) until needed.

Detection of infection

Following the infection protocol described above, cells were fixed immediately (0 hours) or at 18 hours post-infection [p.i.]) with 4% paraformaldehyde (Sigma-Aldrich, MO, USA) for 15 minutes. The cells were permeabilized with 0.1% (v/v) Triton X-100 (Sigma-Aldrich, MO, USA) for 20 minutes, and stained with 0.1 µg/ml DAPI (Ex/Em: 364/454nm) (Sigma-Aldrich, MO, USA) and 0.01 µg/ml HCS CellMask Deep Red stain (Ex/Em: 588/612nm) (Invitrogen, Thermo Fisher Scientific, MA, USA) for 30 minutes. Images from 9 fields were acquired with the Operetta® CLSTM microscope under a 20× water objective (PerkinElmer, MA, USA). Images were analysed using the HarmonyTM 5.1 software which enables automatic calculation of the infection parameters. To streamline this process, two analysis sequences were developed to accommodate for CFSE labelled or unlabelled parasites. Both sequences followed a very similar basis, diverging in the parasites' detection method. Briefly, DAPI and HCS CellMask Deep Red allowed for segmentation of the cells' nuclei and cytoplasm, respectively.

Afterwards, the morphological proprieties of each nucleus and cytoplasm were calculated, ensuring the selection of cells with viable conformations by excluding cells with unconventional morphologies or in contact with the borders of the frame. Additionally, nuclei inferior to 30 μm^2 were not considered for the segmentation of the macrophages since these dimensions included signal from the parasites. Parasite detection was performed within the cells' cytoplasm by i) identifying nuclei <30 μm^2 when unlabelled parasites were used or by ii) identifying objects segmented with the CFSE signal when parasites were labelled. Finally, the number of infected and non-infected cells was calculated, along with the number of parasites per infected cell.

Inhibitors

In the context of this project, two chemical inhibitors were used: Wortmannin (Sigma-Aldrich, MO, USA) and Dasatinib (Santa Cruz Biotechnology, TX, USA). All inhibitors arrived in powder form and were posteriorly dissolved in Dimethyl sulfoxide (DMSO) (D4540, Sigma-Aldrich, MO, USA) according to manufacturer's instructions.

Cytotoxicity assays

To assess whether the inhibitors' concentrations being used had any cytotoxic effects on the BMDMs, various concentrations were tested. BMDMs were differentiated as previously described and, on day 8, several concentrations of each drug (Wortmannin and Dasatinib) were added to different wells in triplicates, both ranging from 195 to 50 000µM.

To evaluate the BMDMs viability, 20µL of 0.32 mg/mL Resazurin Sodium Salt (Sigma-Aldrich, MO, USA) was added to each well, allowing the measurement of the metabolic activity of the BMDMs. Following a 24-hour incubation period, cell viability was quantified on a plate reader (Synergy Mx microplate reader, BioTek Instruments, Winooski, VT, USA) by fluorimetry, using the following settings: excitation, 540/25 nm; emission: 620/40 nm. The data obtained was converted to "% Survival" by first subtracting experimental values from the average of a control with only with media, and then converting these values into percentage proportions of a cell-only control.

Wound Healing Assay

In vitro WH assays were performed in 96-well plates (Thermo Fisher Scientific, MA, USA) with 5×10^4 BMDMs seeded per well. On the eighth day of macrophage differentiation cells were infected as previously described. After washing the non-phagocytosed promastigotes, all the confluent BMDM monolayers were disturbed by creating a cell-free straight-line area ("wound") with a 200µl micropipette tip (Thermo Fisher Scientific, MA, USA). Upon removing cell debris with 2-3 gentle washings with DMEM, BMDMs were replenished with fresh cDMEM supplemented with 15 ng/mL M-CSF and, where applicable, with chemical inhibitors. Collective macrophage migration was monitored by acquiring images every 20 minutes for a period of 18 hours with the Operetta® CLS™ microscope with a 10× air objective, under a controlled environment (5% CO_2, 37°C). To obtain time-lapses of each well, the TIFF files acquired were stitched using the Operetta Importer plugin (BIOP package) from the Fiji 2.9.0/1.54f software (ImageJ, National Institutes of Health). Subsequently, the evolution of the gap of each well was analysed in Fiji with a custom-made macro "Woundhealing_TimeSegmentation" designed by the i3S Scientific Platform Advanced Light Microscopy (**Supplementary Material 1**). The typical image analysis workflow was followed: i)

image preprocessing (background subtraction, Gaussian plus Variance filtering); ii) thresholding segmentation to identify the cell-free area; iii) measurement of the cell free area.

By plotting the wound area as a function of time, the resulting slope provided an estimate of the gap closure rate, quantifying the speed at which the cell-free area was closing. To account for the intrinsic variability of the assay, migration rates were normalized for the untreated naïve cells of each experiment (negative control).

Random Single Cell Migration

For the random single cell migration assays, BMDMs were plated at lower densities, with $2x10^4$ cells per well in 96 well plates. Afterwards, the plate was directly transferred to the Operetta® CLS™ microscope. The images were acquired every 3 minutes with a 10× air objective under a controlled environment (5% CO_2, 37°C) and time-lapse TIFF files were obtained as previously described.

Single cell tracking of uninfected and infected macrophages was performed by two different methods: i) a high throughput Harmony™ analysis sequence developed by our group and ii) a semi-automatic analysis using the MTrackJ plugin from Fiji [132]. Upon implementation, the Harmony™ software analysis sequence allowed for the automatic tracking of each cell. Briefly, individual BMDMs were segmented from the digital phase-contrast images. Cells with unusual morphological properties and those in contact with the borders of the frame at any time point were excluded. Each of the resulting cells was tracked, and their track and kinetic proprieties were calculated. Alternatively, the MTrackJ plugin enables the manual tracking of the cells. At the first time point, 10 infected and 10 non-infected macrophages were randomly selected per well. After manually indicating the cells' movements through the assay, we obtained the data pertaining to each individual track.

The resulting tracks were further analysed using Excel (Microsoft® Office), allowing data filtering. During the Harmony analysis, tracks with a starting or ending type labelled as "split" or "merged" were excluded, as these represented cells that the software had difficulty detecting accurately. Moreover, for the macrophage morphology analysis, cells which displayed roundness values over 0.92 were excluded.

In the case of the MTrackJ analysis, only the BMDMs that remained within the image field for the entire duration of the assay were taken into account. After processing the data, the speed, displacement and accumulated distance travelled by each track were obtained. It was also possible to retrieve the x and y coordinates of the individual cells. By setting the initial cell position as x=0 and y=0, we were able to build rose plot graphs for visualization of the migration paths of individual

macrophages, distinguished by a unique track identification number (ID) and infection status (Condition). The rose plots were built in the RStudio software (PBC, MA, USA) with the ggplot2 package (tidyverse collection, created by Hadley Wickham [133]) using the following code:

```
ggplot (data = dataRP, mapping = aes(x = X, y = Y, group = ID, col = Condition)) + geom_path() + geom_point() + scale_color_manual (values = c("#col1", "#col2", "#col3", "#col4")) + coord_cartesian (xlim = c(A, B), ylim = c(C, D))
```

In this code, A, B, C, D, X, Y, ID, Condition, "#col1", "#col2", "#col3" and "#col4" are all variables. A and B represent the values limiting the x axis of the Rose plot, while C and D symbolize the limits of the y axis. To better visualise the results, a colour was associated to each track, being #col1, 2, 3 and 4 representative of where the colour codes are added.

Statistical Analysis

All the statistical analysis were performed in GraphPad Prism software v8.0.2 (GraphPad Software, MA, USA). The significance was defined as $P \leq 0.05$. Data normality was checked using the Shapiro-Wilk test. In instances where the data exhibited a parametric distribution, comparisons with the one experiment group were made by the one-way analysis of variance (ANOVA) with Turkey's multiple comparisons test, while the Sidak's multiple comparison test was employed when comparing across multiple conditions. In case the data followed a non-parametric distribution, the Kruskal-Wallis' test was employed for comparisons among all experimental groups. To identify outliers, the ROUT method was used with a Q=1%.

Results

1. Optimization of macrophage infection by *L. infantum* and *L. donovani*

To analyse the consequence of *Leishmania* infection in macrophage migration, it was important to secure a high percentage of infected macrophages. Thus, the first objective of this thesis was to optimize *Leishmania* infection rates in BMDMs by isolating metacyclic promastigotes, the parasite's infective form, from *in vitro* promastigote cultures. Two methods, PNA negative selection and Ficoll gradient, were used for this purpose.

L. infantum and *L. donovani* promastigote cultures were first grown for 5 to 13 days as, in this time window, they are expected to have transitioned into the stationary growth phase and, hence, be enriched in metacyclic forms. Parasites from those different timings were then subjected to the PNA and Ficoll protocols as described in the Method section. To evaluate the success of the procedures, the isolated parasites' morphology was analysed in images acquired through upright microscopy. Promastigotes with a slim body with less than 12.5 µm in length and a flagellum twice the size of the body were recognized as metacyclic. Moreover, the isolated "metacyclic parasites" were also co-incubated with BMDMs and the resulting infections compared with those of non-selected parasites. Macrophages were also infected with unselected *L. major*, acting as an infection control, since it delivers high infection rates in our model.

1.1. Peanut agglutinin (PNA) metacyclic selection

As outlined previously, the PNA lectin was shown to enable metacyclic promastigote selection in certain *Leishmania* species by selectivity agglutinating non-metacyclic parasites from metacyclic forms which remain unbound in a PNA negative fraction (PNA-)[89, 91].

As shown on **Table 3**, for both *L. infantum* and *L. donovani*, the 5-day cultures yielded the highest number of PNA^- parasites, although microscopic evaluation revealed that less than 10% of these parasites exhibited the morphology associated with metacyclic forms (**Supplementary Figure 1**). The PNA^- fraction obtained from cultures with 12 days delivered the highest percentage of parasites with metacyclic morphology (% MM), with 39.5% for *L. infantum* and 26.9% for *L. donovani.* However, the correspondent PNA^+ fraction, while resulting in somewhat lower % MM, with 22.1% for *L. infantum* and 23.0% for *L. donovani*, contained the highest total number of metacyclic parasites. In fact, for every time point tested, the PNA^+ fraction contained around to 3-7 times more parasites than the PNA^- fraction. Thus, while the PNA^- fraction was enriched in parasites with metacyclic morphology, the majority of total metacyclic forms were found in the PNA^+ fraction.

In fact, on the days that yielded a higher number of parasites with a metacyclic morphology, day 9 and 12, only 26.5-28.4% and 14.9-30.0% of them were found in the PNA$^-$ fraction for *L. infantum* and *L. donovani,* respectively. When considering both fractions together, day 12 also corresponded to the time point with the highest % MM in the culture, amounting to 25.0% for *L. infantum* and 23.5% for *L. donovani* (**Table 3**).

Table 3. PNA negative selection failed in the enrichment of parasites with morphologies associated with metacyclic forms.

Species	*L. infantum*				*L. donovani*			
Days in culture	5	7	9	12	5	7	9	12
% MM in culture	4.36	11.7	14.9	25.0	3.33	1.57	5.7	23.5
PNA-	1.85×10^6	9.73×10^5	1.75×10^6	1.37×10^6	2.05×10^6	1.94×10^6	1.43×10^6	1.28×10^6
% MM (PNA-)	7.0	16.7	21.2	39.5	5.4	9.1	11.3	26.9
PNA+	8.55×10^6	6.53×10^6	7.00×10^6	6.80×10^6	6.31×10^6	9.30×10^6	8.00×10^6	8.57×10^6
% MM (PNA+)	3.8	11.0	13.3	22.1	2.7	0.0	4.7	23.0
% MM (PNA-) in all MM	28.4	18.4	28.4	26.5	39.5	-	30.0	14.9

% MM in culture: Percentage of parasites with metacyclic-associated morphology in the initial culture.

PNA-: Number parasites retrieved from the PNA negative fraction.

PNA+: Number parasites retrieved from the PNA positive fraction.

% MM (PNA-): Percentage of parasites with metacyclic-associated morphology in the photos acquired of the PNA- fraction.

% MM (PNA+): Percentage of parasites with metacyclic-associated morphology in the photos acquired of the PNA+ fraction.

% MM (PNA-) in all MM: Percentage of parasites with metacyclic-associated morphology present in the PNA- fraction, considering all the parasites with metacyclic morphology captured.

BMDMs were infected with PNA$^-$ parasites, to test if co-incubation with this enriched fraction resulted in a higher percentage of infected macrophages when compared with non-selected promastigote cultures. Given that higher % MM were obtained from days 9 and 12 cultures, BMDMs were infected with parasites selected and non-selected from cultures with 9, 11, 12 and 13 days for 3 hours. In these experiments, naïve BMDMs were included as a negative control of infection, with the detection protocol delivering 5.5% of cells with false positive signal, and a positive control of infection with *L. major* returning an infection rate of 59.6%.

We found that in both *L. infantum* and *L. donovani,* BMDMs infections with PNA$^-$ and unselected promastigotes resulted in similar infection rates, all of which were considerably low in comparison with the infection rates obtained for *L. major* (**Figure 6**). Except for parasites cultured for 11 days, *L. infantum* selected parasites hinted at a trend for relatively higher infections, yet not statistically significant, rising from 16.1% to 17.9% for day 9, and from 31.4% to 43.6% for day 12 (**Figure 6**). On the other hand, *L. donovani* PNA$^-$ parasites performed less effectively than their non-selected counterparts, with infection rates decreasing from 41.5% to 25.0% and from 32.6% to 27.8% on days 9 and 12, respectively (**Figure 6**).

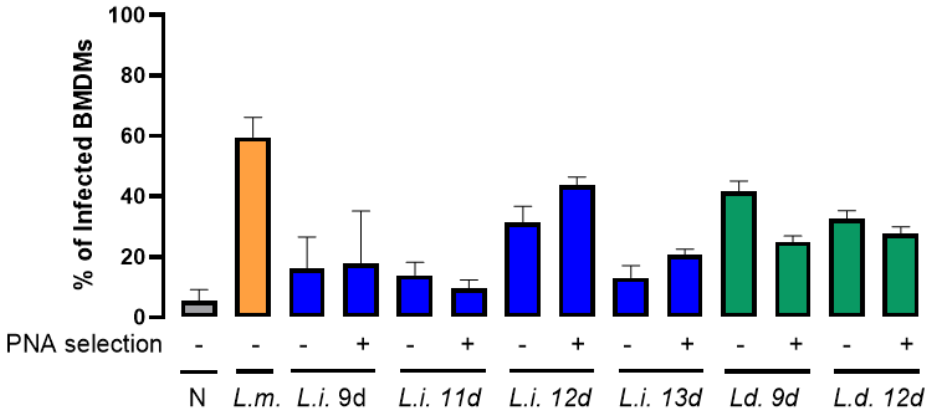

Figure 6. PNA-selected parasites did not result in significantly higher infection rates than their non-selected counterparts. BMDM were incubated with PNA-selected and non-selected *L. infantum* (*L.i.*) *and L. donovani* (*L.d.*) promastigotes that had been cultured for different periods, specifically 9, 12 and 13 days. Naïve (N) macrophages and *L. major* (*L.m.*)-infected macrophages were also analysed in the same assay as negative a positive controls of infection, respectively. Parasites were in contact with the BMDMs for 3 h, after which time non-phagocytosed organisms were washed away. At 18 h p.i., cells were fixed for the estimation of infection rates by DAPI detection. Values represent means and standard deviations of two independent experiments, each performed in triplicate.

1.2. The Ficoll density gradient metacyclic selection

While Ficoll is typically employed as a density gradient medium for isolating eukaryotic cells, organelles, and bacteria, it has also been documented as an alternative method for the selective enrichment of infective *Leishmania* metacyclic promastigotes across all the *Leishmania* species used in this thesis [90, 100, 102, 103, 134, 135].

Application of the Ficoll density gradient to *L. infantum* cultures (days 5, 7, 9 and 12) resulted in parasite recoveries ranging from 70.9% to 91.5% of the initial parasites in culture (**Table 4**). However, less than 50% of these promastigotes displayed metacyclic morphology (**Supplementary Figure 2**).

As for *L. donovani*, Ficoll separation recovered fewer than 50% of the parasites present at days 5 to 9, but with minus than 20% exhibiting the morphology associated with metacyclic forms, indicating that these fractions were not enriched in these forms. We could not separate metacyclic parasites from 12 days culture, as all the initial parasites were present in the layer between the upper medium and the Ficoll layers where the metacyclic promastigotes are supposed to remain.

All Ficoll-selected parasites resulted in lower infection rates compared to their non-selected equivalents, albeit with varying degrees of decrease. In this assay, *L. donovani* parasites that had been cultured for 12 days and were not subjected to selection exhibited infection rates that were most closely aligned with those of *L. major*, standing at 70.8% and 79.1%, respectively (**Figure 7**).

Table 4. The Ficoll gradient method failed in the enrichment of parasites with morphologies associated with metacyclic forms.

Species	*L. infantum*				*L. donovani*			
Days in culture	5	7	9	12	5	7	9	12
% Ficoll	70.9	73.5	91.5	72.5	48.1	41.5	39.5	100.0
PA	51	49	77	75	40	24	52	101
MM	9	11	29	34	6	2	10	30
% MM	17.6	22.4	37.7	45.3	15.0	8.3	19.2	29.7

% Ficoll: percentage of the initial macrophages that were retrieved after the Ficoll gradient selection.

PA: Number of parasites analysed on the acquired photos.

MM: Number of parasites with a metacyclic-associated morphology.

% MM: Percentage of parasites retrieved after the Ficoll gradient selection with metacyclic-associated morphology.

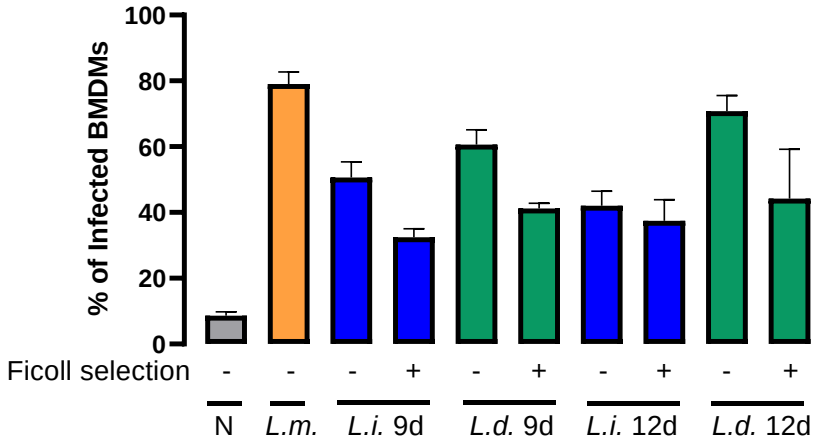

Figure 7. Parasites selected by the Ficoll gradient method did not yield higer infection rates than their non-selected counterparts. BMDM were incubated with Ficoll-selected and non-selected *L. infantum* (*L.i*) *and L. donovani* (*L.d*) promastigotes that were kept in culture for different periods, specifically 9 and 12 days. Naïve (N) macrophages and *L. major* (*L..m.*)-infected macrophages were also analysed in the same assay as negative a positive controls, respectively. The parasites were in contact with the BMDMs for 3 h, after which time non-phagocytosed parasites were washed away. At 18 h p.i., cells were fixed for the estimation of infection rates. Values represent means and standard deviations of one experiment performed in triplicate.

1.3. Optimization of parasite detection through CFSE staining

Some of the assays planned for this work entailed analysis of migration at the level of the infected cell. For this, we set up a method to follow such cells during the timespan of the experiments.

To distinguish infected BMDMs from bystanders (BMDM that contacted *Leishmania* but remained uninfected), we labelled parasites with CFSE previous to infection using a protocol developed by us, based on the literature [136-138]. To implement this methodology, stationary phase promastigotes previously stained with CFSE concentrations of 5 and 10 µM were imaged at 0- and 18-hours post-staining with a fluorescence microscope. This allowed us to assess the staining's intensity and durability throughout the migration assays. Both conditions resulted in successful and stable parasite staining for at least 18 hours However, image acquisition was facilitated when parasites were stained with 10 µM CFSE because shorter exposure times were required, which is also important to avoid phototoxicity (**Figure 14**). While setting up the staining, we observed that smaller, rounder parasites displayed higher signal intensity than those with the longer and straighter morphology typically associated with *Leishmania* promastigotes. The reason for this is unclear at this moment. We investigated whether CFSE staining had any impact on the viability of parasites by closely following the CFSE stained parasites' morphology and behaviour over 72 hours.

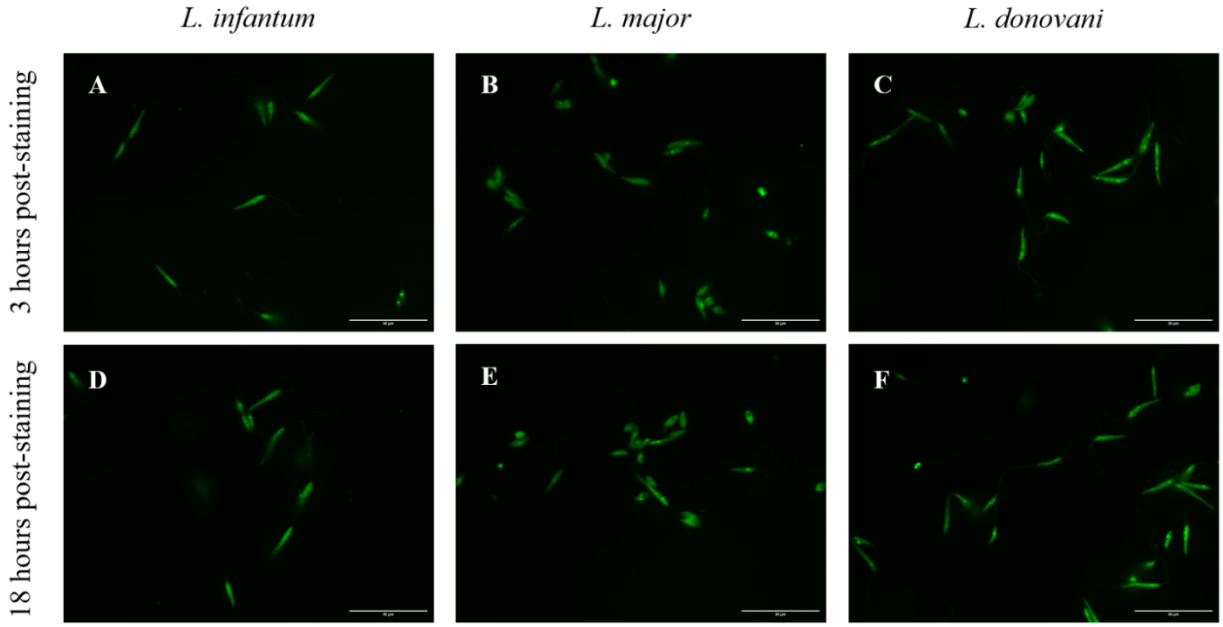

Figure 8. Parasite staining with 10 µM revealed to be ideal for image acquisition. Parasites were stained with 10 µM of CFSE and analysed at different times post-staining using the Zeiss Axio Imager Z1 microscope. Images were taken with an 40x amplification, the 38 HE filter set (Excitation: BP 470/40; Beam Splitter: FT 495; Emission: BP 525/50). All parasites were easily detected with exposure times of 850ms, at 3 hours post-staining **A)** *L. infantum*, **B)** *L. major*, and **C)** *L. donovani*; and at 18 hours post-staining **D)** *L. infantum*, **E)** *L. major*, and **F)** *L. donovani*. The scale represents 30µm.

2. Migration inhibitors' cytotoxicity assays

The study of the impact of Dasatinib and Wortmannin on the migration of *Leishmania*-infected macrophages migration was one of our main goals. However, to achieve this, it is crucial to determine the concentrations at which these drugs adversely affect the macrophage's viability. Given the lack of available information regarding the cytotoxic concentrations of these drugs on BMDMs, we chose to assess the effects of concentrations significantly higher than those intended for use in the migration assays.

Macrophages were exposed to drug concentrations ranging from 195 nM to $5x10^4$ nM for 24 hours. Following this exposure, the metabolic activity of the cells was assessed by measuring the reduction of resazurin. The cytotoxicity of the solvent, DMSO, was also assessed up to $7.05x10^8$ nM.

Our data indicate that the survival of BMDMs at a concentration of 1500 nM Desatinib approaches 50% (**Figure 9A**). However, the relative survival rate of macrophages exposed to Wortmannin did not appear to be affected by any of the tested concentrations (**Figure 9B**). In terms of DMSO, macrophages only seem to be affected at concentrations of $3.52x10^8$ nM and higher (**Figure 9C**).

Overall, we only observed an impact on cell viability at concentrations that were several orders of magnitude higher than those we aimed to employ in the migration assays, i.e., 100 or 200 nM Dasatinib and 200 or 400 nM Wortmannin. Since these drugs were dissolved in DMSO, the resulting drug solutions contained 2.82×10^5 nM and 2.4×10^5 nM of DMSO, respectively.

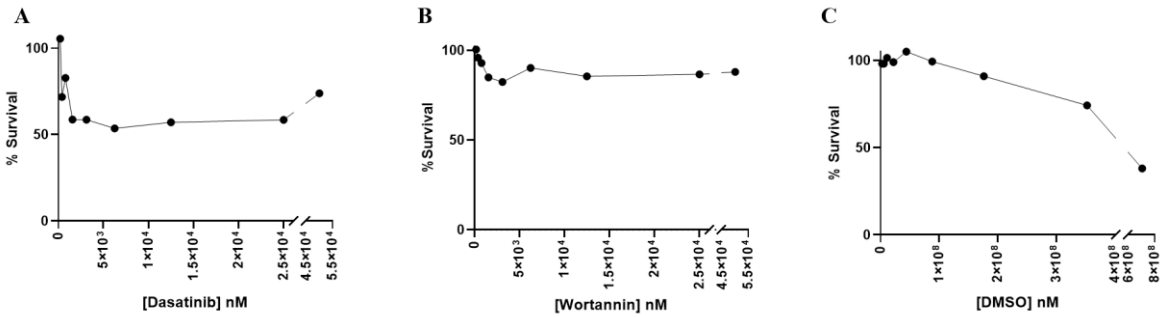

Figure 9. At the concentrations to be employed in the migration assays, Dasatinib and Wortmannin are not cytotoxic to the BMDMs. Relative cell viability of BMDMs exposed for 24h to **A)** Dasatinib (195 nM to $5x10^4$ nM) and **B)** Wortmannin (195 nM to $5x10^4$ nM); **C)** Cytotoxicity of the drug solvent, DMSO, to BMDM at concentrations ranging from 2.75×10^6 nM to 7.05×10^8 nM. All data were normalized to the viability value of untreated control measured 24 h after exposer. The x scale represents is a logarithmic scale.

3. Migration assays

3.1. Wound healing assays

The impact of *Leishmania* infection on macrophage migration was evaluated resorting to WH assays, where collective cell migration towards closure of a cell free area, the "wound", was monitored every 20 mins, for approximately 18 hours. The dynamics of wound-closure were analysed by plotting the cell free area over time and retrieving the value of the slope as an expression of cell velocity, or the relative gap closure rate. While analysing our data, we observed that cell velocity was not constant along the duration of the assays. Rather, it was higher in the first hours, and diminished gradually as the wounds closed, reaching values proximate to zero at the end of the assay (**Figure 10A**). Similarly, the correlation coefficients of the slopes were high in the first part of the assays (**Figure 10B**), indicating data consistency, contrary to what was found when the whole assay was considered (**Figure 10A**).

To account for such discrepancies, gap closures of the assays performed in the context of this thesis were calculated from the first 5 hours of migration. At this timing, wounds are always far from resolved. This facilitates the comparison between assays as these contain wound areas inevitably distinct due to being performed manually, which could interfere with the migration rates.

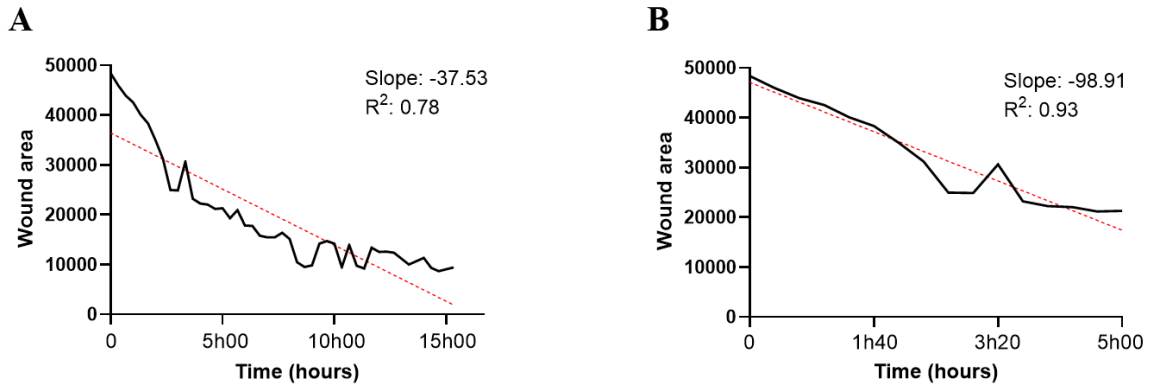

Figure 10. The gap closure analysis is more reliable in the first 5 hours of the assay. A) Example of a plotting graph which reveals the inconsistent dynamics of wound-closure during an 18 hours-assay (R^2: 0.78); **B)** The plotting graph of the same assay but only considering the first 5 hours shows a more constant variation (R^2: 0.93).

In wound healing analysis, data from each experiment were normalized according to naïve macrophage relative gap closure, to account for any intrinsic variability. Consequently, the relative migration rate for the naïve macrophages was set at 1.00. These assays revealed no differences in relative migration rates across all conditions, with the relative migration rate of infected macrophages being 1.01, 1.04, and 1.10 for *L. infantum*, *L. major*, and *L. donovani*, respectively (**Figure 11A**).

Regarding infection rates, the naïve macrophages presented an infection rate of 2.56% which is indicative of false positive values (**Figure 11B**). For infected macrophages, the infection rates were 29.5%, 65.2%, and 37.6% for *L. infantum*, *L. major*, and *L. donovani*, respectively (**Figure 11B**).

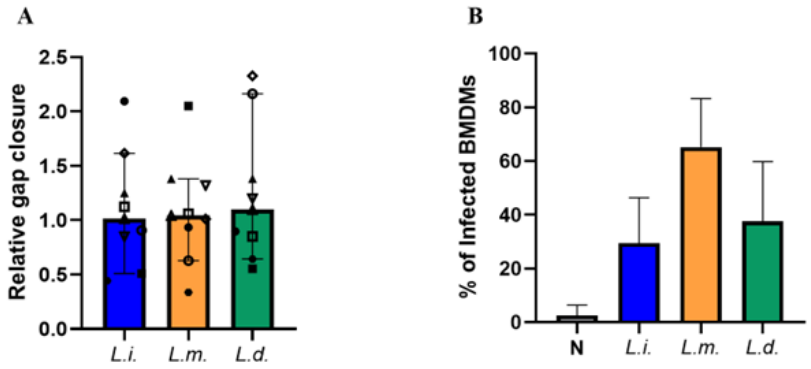

Figure 11. Wound healing migration assays revealed no differences in relative migration rates across all conditions. BMDM were kept naïve (N) or incubated with *L. major* (*L.m.*), *L. infantum* (*L.i.*) or *L. donovani* (*L.d.*) promastigotes for 3 h. Infections were interrupted by washing away non-phagocytosed parasites. **A)** Collective macrophage migration was assessed for 5 h, resorting to gap closure assays. For each independent experiment, the velocities of infected BMDM were normalized to the gap closure rate of naïve macrophages. Each symbol represents individual experiments. Values represent the means and standard deviations of nine individual experiments performed in triplicate. **B)** Eighteen hours p.i., cells were fixed for the estimation of infection rates through DAPI detection. Values represent the means and standard deviations of nine individual experiments performed in triplicate.

3.1.1. Testing Dasatinib effect on BMDMs migration

The addition of Dasatinib upon the BMDMs failed to significantly impair their migration, independently of infection status. Although no statistical significance was found, infected cells tended to migrate faster than the naïves, with a mean of 2.8 times faster for *L. infantum* infections, followed by 2.0 for *L. major* and 1.7 for *L. donovani* (**Figure 12A**). It was also observed that infected BMDMs treated with 100nM Dasatinib appeared to experience reduced gap closure rates, although not statistically significant. Remarkably, naïve macrophages appeared unaffected by the compound and displayed even faster migration rates at 1.3 (**Figure 12A**).

The infection rates of the infected macrophages without the inhibitor were 18.3%, 59.1%, and 27.3% for *L. infantum*, *L. major*, and *L. donovani*, respectively (**Figure 12B**). With the inhibitor, these rates were higher, although very similar, at 19.9%, 63.0%, and 32.7% for *L. infantum*, *L. major*, and *L. donovani*, respectively (**Figure 12B**). The false positive infection rate was determined to be 1.45% and 0.95%, for BMDMs with and without Dasatinib, respectively (**Figure 12B**).

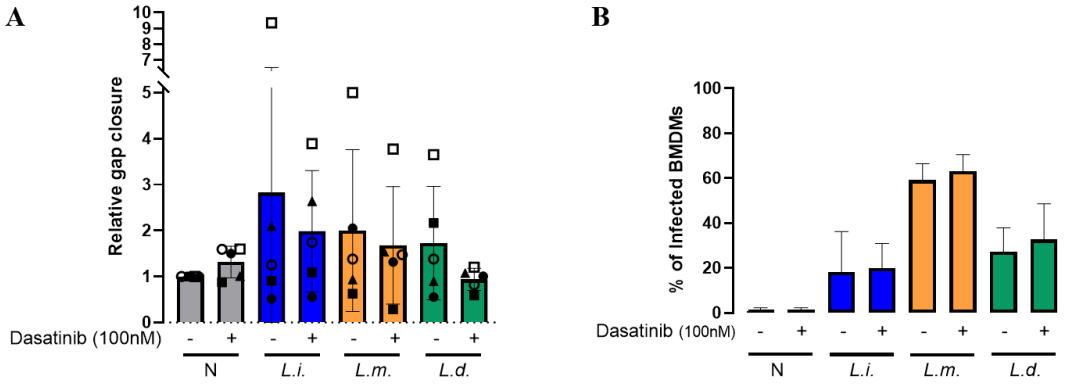

Figure 12. Dasatinib did not significantly impair macrophage migration or infection rates, independently of *Leishmania* species. BMDM were kept naïve (N) or incubated with *L. major* (*L.m.*), *L. infantum* (*L.i.*) or *L. donovani* (*L.d.*) promastigotes for 3 h. Infections were interrupted by washing away non-phagocytosed parasites and 100 nM Dasatinib or cDMEM was added to all conditions. **A)** Collective macrophage migration was assessed for 5 h, resorting to gap closure assays. For each independent experiment, the velocities of infected BMDM were normalized to the gap closure rate of naïve macrophages; Each symbol represents individual experiments. **B)** Eighteen hours p.i., cells were fixed for the estimation of infection rates through DAPI detection. Values represent the means and standard deviations of five individual experiments performed in triplicate.

3.1.2. Testing Wortmannin effect on BMDMs migration

Incubation of the macrophages with 200 nM Wortmannin also failed to impair wound closure. While no statistical significance was found, it was observed that exposure to this compound lead to a slight decrease in migration rates of *L. major*–infected BMDMs, decreasing from 0.88 to 0.65 (**Figure 13A**). In contrast, the BMDMs infected with *L. infantum* and *L. donovani* maintained their migration rates when in contact with the inhibitor, remaining at 1.0 and 1.1, respectively (**Figure 13A**).

As for the infection rates observed in the Wortmannin assays, the BMDMs that did not come into contact with the drug exhibited the following infection rates: *L. infantum* (44.5%), *L. major* (78.3%) and *L. donovani* (49.1%) (**Figure 13B**). Similarly, the macrophages in contact with Wortmannin had the following infection rates: *L. infantum* (44.8%), *L. major* (80.2%) and *L. donovani* (48.0%) (**Figure 13B**). The false positive infection rates ranged between 0.84% and 0.99%.

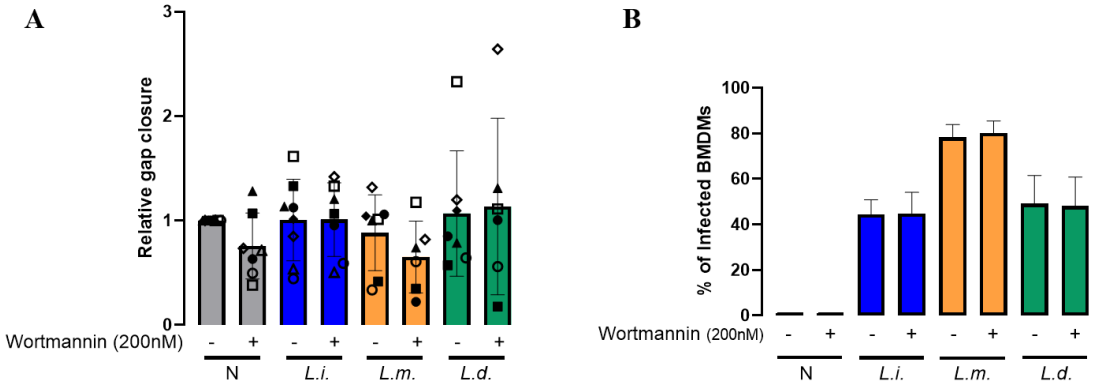

Figure 13. Wortmannin did not significantly impair macrophage migration or infection rates, independently of *Leishmania* species. BMDM were kept naïve (N) or incubated with *L. major* (*L.m.*), *L. infantum* (*L.i.*) or *L. donovani* (*L.d.*) promastigotes for 3 h. Infections were interrupted by washing away non-phagocytosed parasites and 200 nM Wortmannin or cDMEM was added to all conditions. **A)** Collective macrophage migration was assessed for 5 h, resorting to gap closure assays. For each independent experiment, the velocities of infected BMDM were normalized to the gap closure rate of naïve macrophages. Each symbol represents an individual experiment. **B)** Eighteen hours p.i., cells were fixed for the estimation of infection rates through DAPI detection. Values represent the means and standard deviations of six individual experiments performed in triplicate.

3.2. Random single cell migration assays

The inherent migration of the BMDMs upon infection by different species of *Leishmania* was assessed though live-cell microscopy by tracking individual cells in the absence of any physical or chemical stimuli. Images were analysed to retrieve three parameters: i) speed, as expression of macrophage velocity from one frame to the next – the track's speed was calculated as the average of all the instant speeds observed throughout the entire assay; ii) accumulated distance, the sum of the total distance travelled by each cell throughout the entire assay and iii) displacement, the distance between the cell's initial and final position. Macrophage's migration dynamics were followed for the entire duration of the assays, and speed of the cells was compared at different time points. We observed that, in the conditions of these assays, individual macrophage's speed remained constant independently of the duration of the analysis (**Figure 14**). Therefore, and to reduce the amount of raw data to manipulate, only the first 5 hours (100 time points) were used for subsequent analysis.

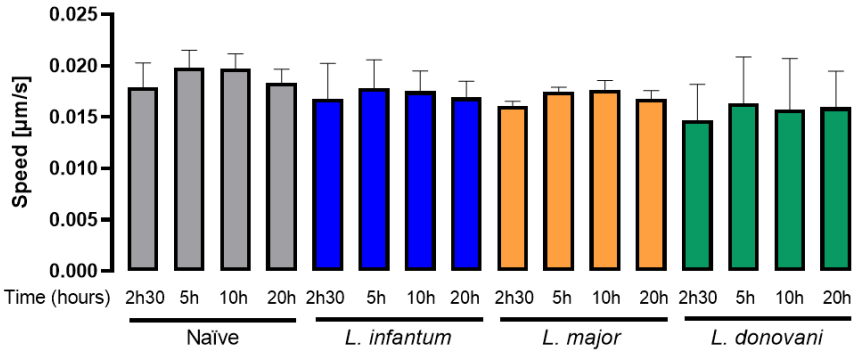

Figure 14. The speed of the individual macrophage remained constant independently of the duration of the analysis. Individual BMDM random migration was automatically assessed for 20 h, resorting to the Harmony software. The mean BMDMs velocities from all conditions were analysed during different time points, specifically 2 hours and 30 minutes, 5 hours, 10 hours, and 20 hours. Values represent means and standard deviations of one experiment performed in triplicate.

3.2.1. Automatic tracking using the Harmony software

Establishment of an analysis sequence in the Harmony software allowed for automatic single-cell tracking. For each condition, between 6000 – 21 000 tracks per condition were evaluated for their accumulated distance, displacement, and speed. However, since many of these tracks only covered short durations due to detection errors, it was established that only tracks traced for 100 time points would be included in the analysis to ensure a fair comparison. This resulted in only a portion of the tracks being analysed, ranging between 240 – 1110 tracks per condition. While the accumulated distance was similar between naïve (278 µm), *L. infantum* (268 µm) and *L. major*-infected macrophages (266 µm), the *L. donovani*-infected macrophages migrated slightly less (222 µm) (**Figure 15A**). The displacement of uninfected cells (22µm) was higher when compared to BMDMs infected with *L. infantum* (20 µm), *L. major* (19 µm), and *L. donovani* (17 µm), the latter reaching statistical significance (**Figure 15B**). Regarding speed, all macrophages displayed similar values, with average migration rates only differing in up to 0.0005 µm/s (0.0156 µm/s for naïve, 0.0154 µm/s for *L. infantum*, 0.0156 µm/s for *L. major,* and 0.0151 µm/s for *L. donovani*-infeceted macrophages) (**Figure 15C**). Finally, we analysed migration patterns by retrieving the x and y coordinates for individual cells throughout the assay. Evaluation of 10 randomly chosen cells of each condition (naive and infected with the different species) showed no visible and consistent patterns of macrophage migration (**Figure 15E,F**).

Infections rates were measured taking advantage of the CFSE dye used to stain the parasites, enabling us to subsequently differentiate between infected and bystander macrophages. These infection rates were notably higher when compared to the values obtained in the WH assays which relied on DAPI detection. The infection rates were as follows: *L. infantum* (50.0%), *L. major* (84.2%) and *L. donovani* (71.4%) (**Figure 15 D**). The false positive infection rate was determined to be 2.67%.

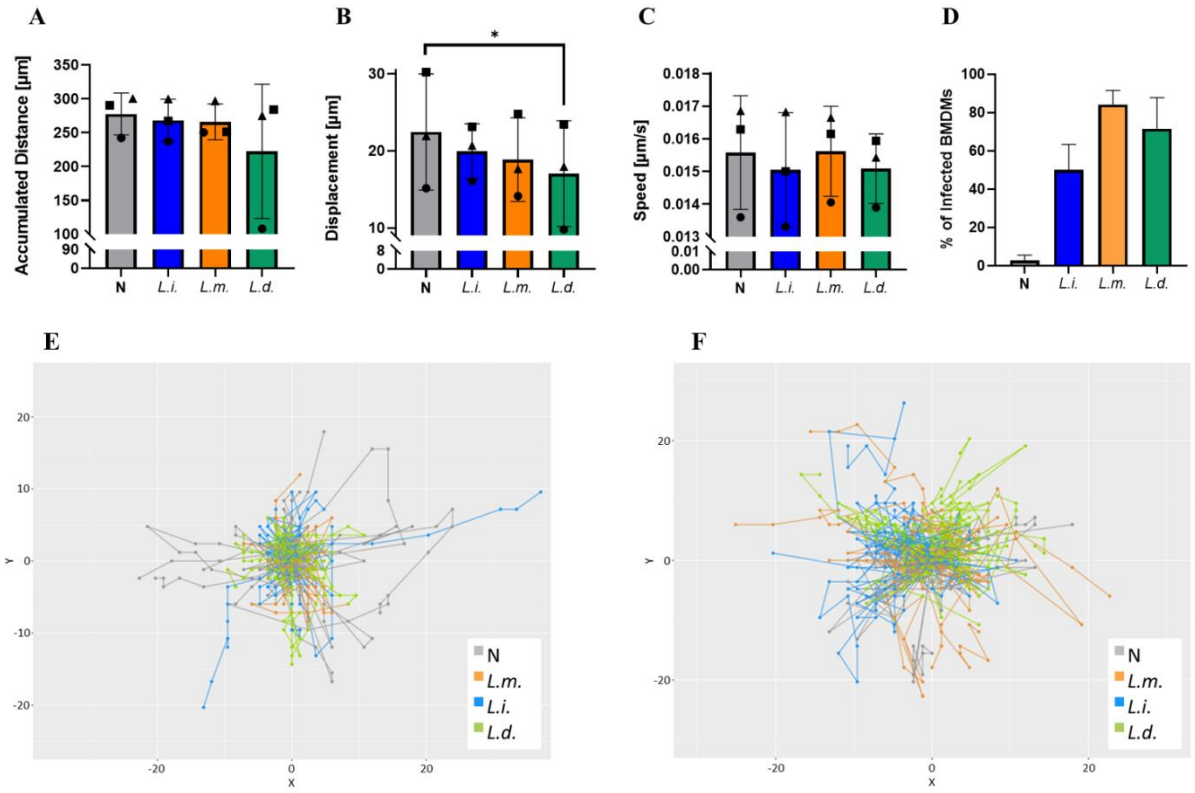

Figure 15. Automatic tracking of individual cell's random migration revealed naïve macrophages migrate slightly more than *Leishmania*-infected macrophages. BMDM were kept naïve (N) or incubated with *L. major* (*L.m.*), *L. infantum* (*L.i.*) or *L. donovani* (*L.d.*) promastigotes for 3 h. Infections were interrupted by washing away non-phagocytosed parasites. Individual cell migration was automatically assessed for 5 h, resorting to the Harmony software for the automatic tracking. The data from each track was analysed in order to obtain **A)** Accumulated distance, **B)** Displacement, and **C)** Speed. Each symbol represents an individual experiment. Bars represent the mean and standard deviation of eight independent experiments, each performed in triplicate. One-way ANOVA (Turkey) revealed statistically significant differences between data sets (*$p < 0.1$). **D)** Eighteen hours p.i., cells were fixed for the estimation of infection rates through CFSE detection. Values represent the means and standard deviations of three individual experiments performed in triplicate**. E, F)** Example of representative rose plot from two independent experiments displaying the random migration patterns N BMDMs in grey, *L.m.* in orange, *L.i.* in blue and *L.d* in green. Ten BMDMs per condition tracked automatically with the Harmony software.

3.2.2. MTrackJ manual tracking

The Harmony software does not allow for differentiation between infected cells and bystander cells that, while in contact with promastigotes, failed to internalize them. To take this information into consideration, and to confirm the accuracy of the automatic tracking, manual tracking was performed in the same assays with the help of the MTrackJ plugin. As previously established, tracks of at least 10 cells were measured for 5 hours (100 time points).

Overall, MTrackJ analysis resulted in higher values for accumulated distance (373-525 μm vs 222-278 μm, respectively) and speed (0.019-0.026 μm/s vs. 0.015-0.016 μm/s) in all instances when compared with Harmony data, while displacement stayed within the same range. No statistically significant differences (or even a visual trend) were found between infected and bystander macrophages in any of the parameters analysed.

L. infantum bystanders had similar accumulated distances as their infected counterparts (385 vs 373 μm, respectively), while *L. major* bystanders travelled longer distances than infected cells (525 vs 461 μm) (**Figure 16A**). Conversely, *L. donovani* bystanders showed smaller accumulated distance (386 vs 461 μm) (**Figure 16A**). In what regards to cell displacement, we found this parameter to be unresponsive to parasite infection, as the effect on bystander cells was varied. The bystanders of *L. infantum* (23 μm) and *L. donovani* (18 μm) displayed smaller distances than their infected counterparts (27 μm and 24 μm, respectively), while the opposite was observed in *L. major*-infected macrophages (26 μm for the infected and 33 μm for the bystanders) (**Figure 16B**). Finally, only the *L. donovani*-infected macrophages (0.023 μm/s) exhibited higher migration speeds relatively to the non-infected macrophages (0.020 μm/s). Indeed, both *L. infantum* and *L. major* bystanders (0.021 μm/s and 0.026 μm/s, respectively) migrated faster than the respective infected macrophages (0.019 μm/s and 0.024 μm/s) (**Figure 16C**).

Migration patterns were also analysed by retrieving the x and y coordinates for the individual cells for each of the time points. The migration of BMDMs bot not considering infection status and differentiating infected from bystanders showed no visible and consistent pattern of macrophage migration dependent on the condition (**Figure 16D, E**).

As the experiments analysed were the same as those previously subjected to automatic analysis, the infection rates are represented on **Figure 15D**.

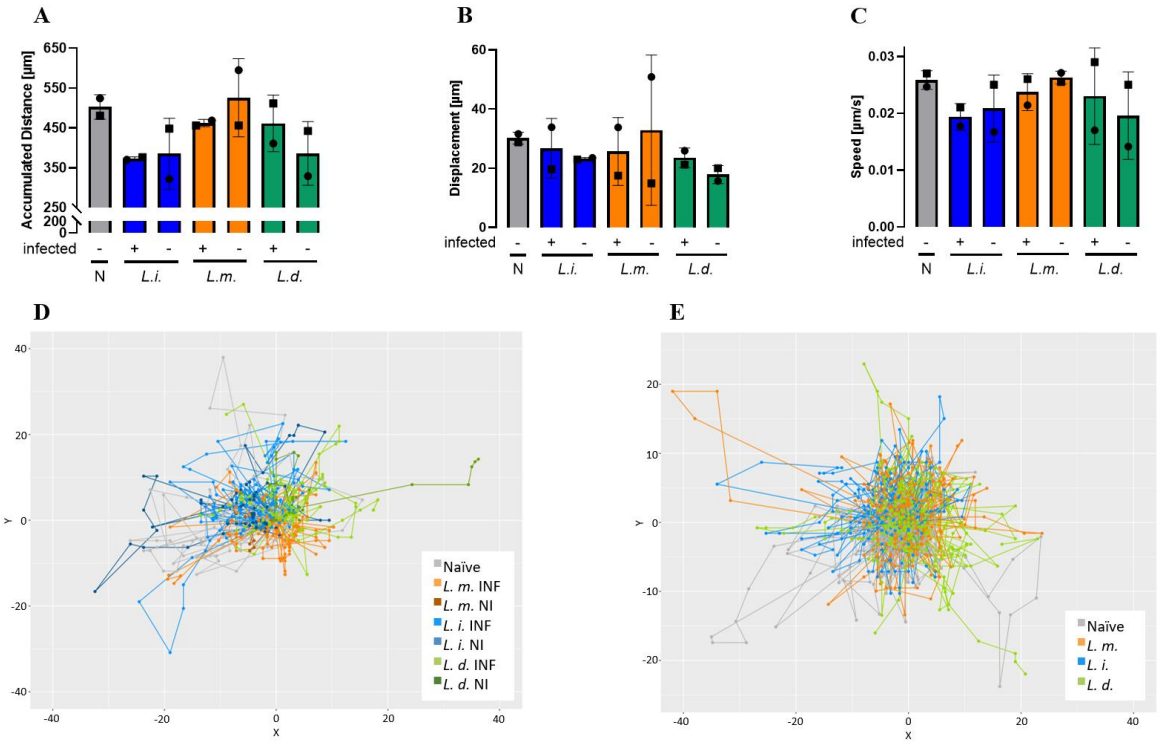

Figure 16. Manual tracking of individual cell's random migration revealed no consistent pattern of macrophages migration. BMDM were kept naïve (N) or incubated with *L. infantum* (*L.i.*), *L. major* (*L.m*) *L. donovani* promastigotes for 3 h. Infections were interrupted by washing away non-phagocytosed parasites. Individual cell migration was assessed for 18 h, resorting to the MTrackJ plugin from ImageJ for the manual tracking. The data from each track was analysed in order to obtain **A)** Accumulated distance, **B)** Displacement, and **C)** Speed. Bars represent means and standard deviations of eight independent experiments, each performed in triplicate. To track the migration patterns of BMDMs under different conditions, rose plots were developed with the aid of RStudio. **D)** Example of one representative rose plot displaying the random migration patterns of naïve N BMDMs, infected BMDMs with *L.m* (*L.m*. INF), *L. i.* (*L.i*. INF) or *L. d.* (*L.d.* INF), or non-infected bystander BMDMs in contact with *L. m.* (*L.m.* NI), *L. i.* (*L.i.* NI) or *L. d.* (*L.d*. NI); 10 tracks per condition. **E)** Example of one representative rose plot displaying the random migration patterns of N BMDMs or infected BMDMs with *L.m, L.i*., or *L.d.,* without distinction between the infected macrophages and the bystanders. Ten BMDMs per condition tracked manually with the aid of the MTrackJ plugin from ImageJ.

3.2.3. Chemical inhibitor assays

The impact of the two inhibitors, Dasatinib (200nM) and Wortmannin (400nM), was also tested in this assays to assess their impact on random migration. In this assays, the concentrations used were twice as high as the previous concentrations, as no noticeable effects were observed in the WH assays with the lower concentrations.

Automatic analysis with Harmony revealed that these drugs had no inhibitory effect on the macrophages' migration. If anything, *L. infantum*-infected macrophages treated with Wortmannin had a tendency to travel greater distances with higher speeds than controls (**Figure 18A-C**).

Manual analysis with MTrackJ confirmed that Wortmannin did not affect the accumulated distance, displacement, and speed of the macrophages, either infected with *Leishmania* or bystanders (**Figure 18D-F**). On the other hand, Dasatinib appeared to negatively impact both the accumulated distances and speeds of naïve and *Leishmania*-infected macrophages while it showed no effect in terms of displacement. Notably, Dasatinib-exposed naïve BMDMs migrated significantly less cumulative distances and at slower speeds than the drug free naïve BMDMs (**Figure 18D, F**). No migration trend was observed for the bystander macrophages regardless of the parasites they contacted.

In the migration experiments described above, infection rates for *Leishmania*-infected macrophages that did not come into contact with any drug were as follows: *L. infantum* (73.03%), *L. major* (94.98%), and *L. donovani* (88.77%). For those exposed to 200nM Dasatinib, the infection rates were: *L. infantum* (78.52%), *L. major* (95.59%), and *L. donovani* (89.81%). Finally, the macrophages that were exposed to 400nM Wortmannin had the following infection rates: *L. infantum* (93.79%), *L. major* (75.37%), and *L. donovani* (85.74%) (**Figure 17**). The false positive infection rates ranged from 0.28% to 1.09%.

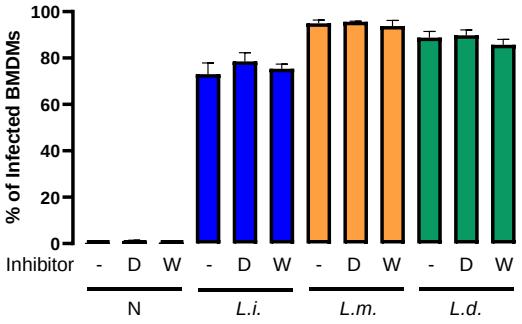

Figure 17. Dasatinib and Wortmannin did not impact BMDM infection rates in the manual RSC migration assays, independently of *Leishmania* species. BMDMs were kept naïve (N) or incubated with *L. major* (*L.m.*), *L. infantum* (*L.i.*) or *L. donovani* (*L.d.*) promastigotes for 3 h. Infections were interrupted by washing away non-phagocytosed parasites and 200 nM Dasatinib, 400 nM Wortmannin or cDMEM was added to all conditions. Eighteen hours p.i., cells were fixed for the estimation of infection rates through CFSE detection. Values represent the means and standard deviations of two individual experiments performed in triplicate.

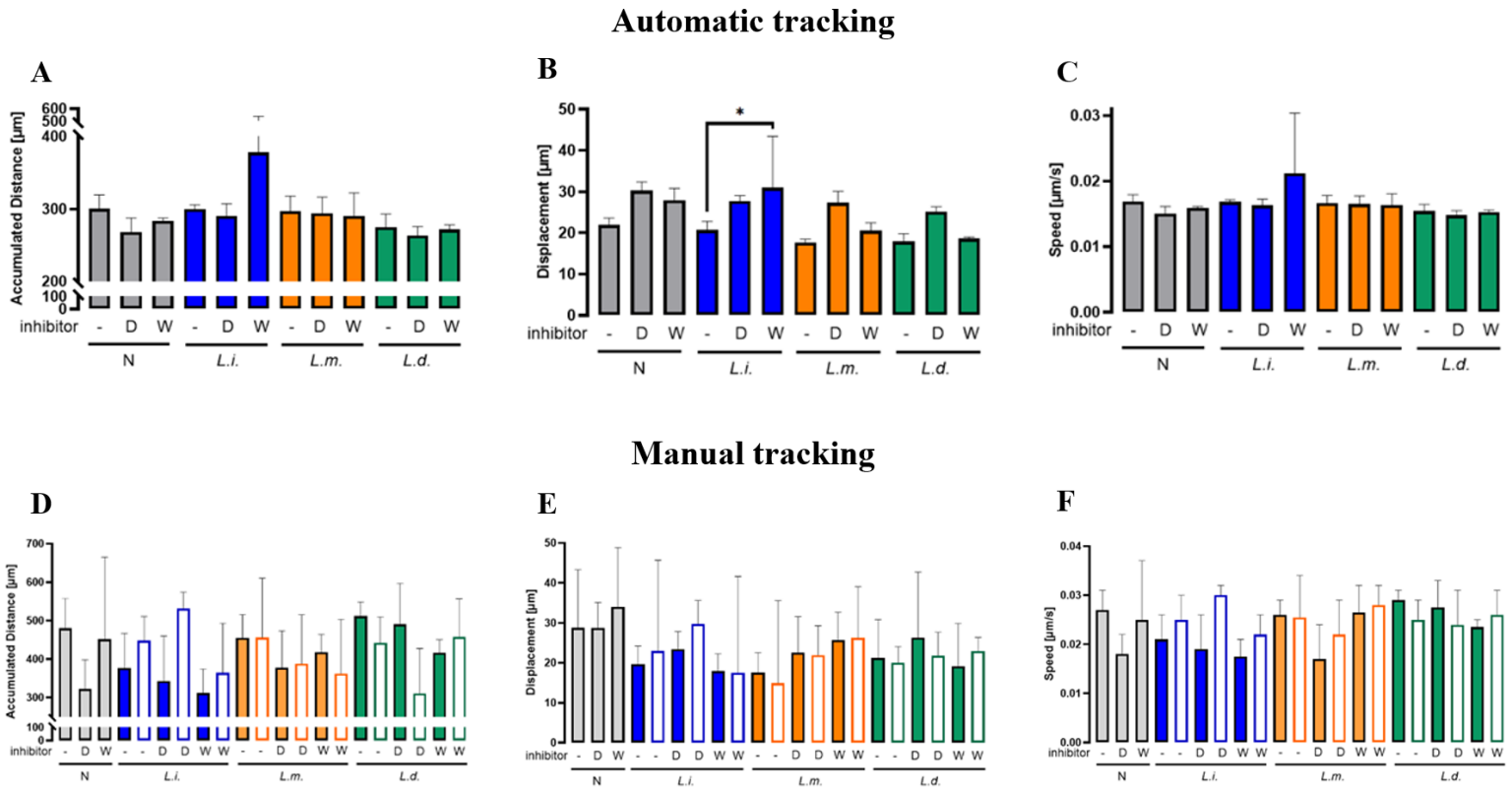

Figure 18. Automatic and manual tracking of individual cell's random migration showed no consistent impact of the drugs on the macrophage's migration. BMDM were kept naïve (N) or incubated with *L. major* (*L.m.*), *L. infantum* (*L.i*) or *L. donovani* (*L.d.*) promastigotes for 3 h. Infections were interrupted by washing away non-phagocytosed parasites and 200 nM Dasatinib (D), 400 nM Wortmannin (W) or cDMEM (-) was added to all conditions. Individual cell migration was automatically assessed for 5 h, resorting to the Harmony software. The data from each track was analysed to obtain **A)** Accumulated distance, **B)** Displacement, and **C)** Speed. Values represent the means and standard deviations of one experiment performed in triplicate. Alternatively, individual cell migration was assessed for 18 h, resorting to the MTrackJ plugin from ImageJ for the manual tracking. The data from each track was once again analysed to obtain **D)** Accumulated distance, **E)** Displacement, and **F)** Speed. represent means and standard deviations of one experiment performed in triplicate. The solid colour bars represent the infected macrophages while the bars with the fill pattern represent the bystander macrophages.

3.3. Macrophage morphology and migration

In the course of the RSC migration assays, it became evident that a subset of BMDMs exhibited limited movement throughout the entire assay duration. These macrophages displayed a distinctive round morphology devoid of extensions. Therefore, to investigate the potential impact of cell morphology on macrophage migration, we assessed cell roundness using Harmony software. (**Supplementary Figure 3**).

It was determined that these cells consistently exhibited a roundness value exceeding 0.92, and they remained almost stationary, barely moving from their initial position within the frame (**Supplementary Figure 3**). This criterium was used to categorize the macrophages into round/immobile and not-round/mobile cells to be analysed separately. These round macrophages comprised approximately 20-27% of all cells in the assays (**Figure 19**).

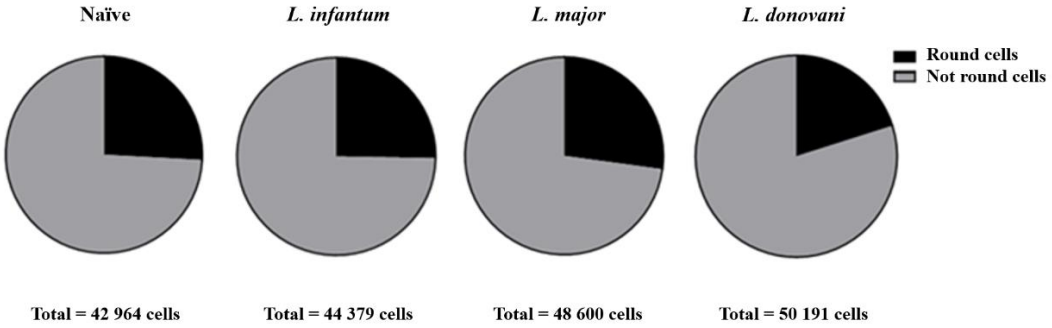

Figure 19. Around one quarter of all detected BMDMs displayed a rounder shape and lack of extensions, associated with less motility. The morphology of naïve and *L. infantum*, *L. major* and *L. donovani* infected-BMDMs from previous assays was analysed. Round cells were defined as cells with roundness > 0.92.

After this analysis, it was determined that the cells with roundness > 0.92 presented lower accumulated distances (13.2 for naïves, 14.4 for *L. infantum*, 15.0 for *L. major* and 13.3 for *L. donovani*) (**Figure 20A**), displacements (5.1 for naïve, 4.6 for *L. infantum*, 4.9 for *L. major* and 4.3 for *L. donovani*) (**Figure 20B**) and speed (0.014 for naïve and *L. major* and 0.013 for *L. infantum* and *L. donovani*) (**Figure 20C**) than those obtained when no morphology selection is applied.

Considering only the non-round/mobile cells tracked by the Harmony software, it became evident that naïve macrophages displayed greater accumulated distance, displacement, and speed than infected BMDMs (**Figure 20D-F**). For both accumulated distance and speed, the difference between the naïve macrophages and the *L. infantum*-infected was significant. This pattern did not extend to displacement, as *L. infantum*-infected macrophages exhibited more extensive migration

compared to those infected by *L. major* and *L. donovani*, both of which showed significantly reduced migration when compared to the naïve macrophages.

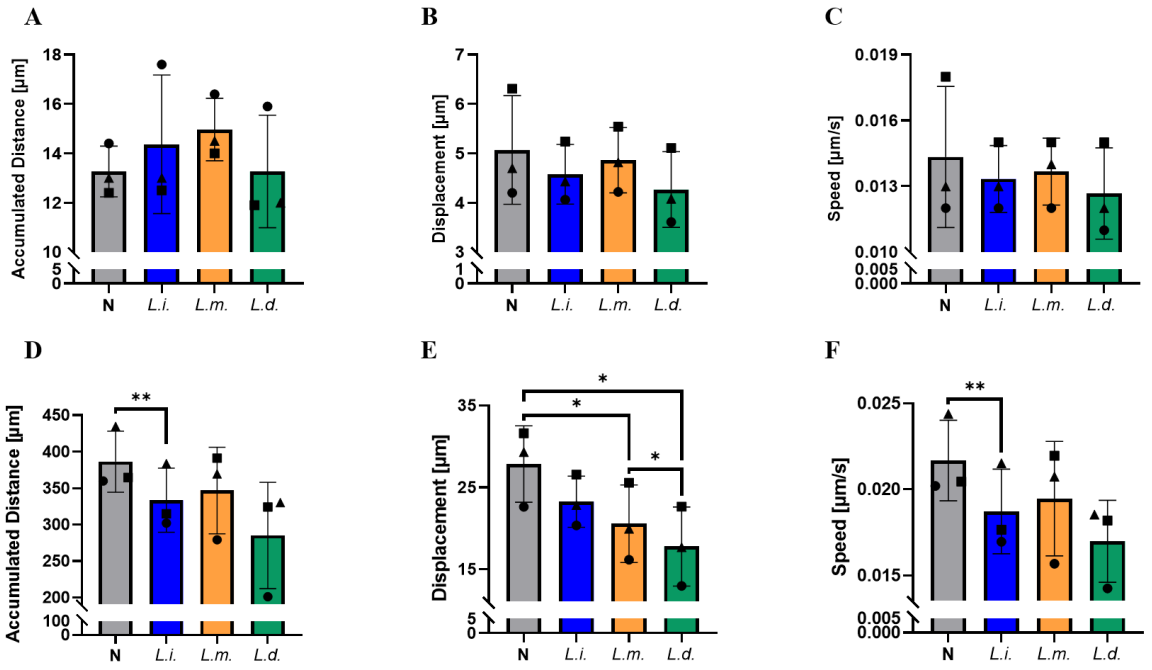

Figure 20. Round BMDMs exhibit diminished motility relative to non-round counterparts, with naïve (N) non-round cells showcasing faster and more extensive migration than *L. infantum* (L.i.), *L. major* (*L.m.*) and *L. donovani* (*L. d.*) infected-BMDMs. The morphology of all detected BMDMs from the previous RSC migration assays was analysed, including naïve (N) and *L. infantum*, *L. major* and *L. donovani* infected-BMDMs. Round BMDMs' (roundness > 0.92) tracks were analysed to obtain the **A)** Accumulated distance, **B)** Displacement, and **C)** Speed. Non-round BMDMs' (roundness ≤ 0.92) tracks were analysed to obtain the **D)** Accumulated distance, **E)** Displacement, and **F)** Speed. Each symbol represents an individual experiment. Values represent the means and standard deviations of three individual experiments performed in triplicate.

This analysis enabled the determination of the mean values for speed, accumulated distance and displacement associated with round/immobile and not-round/mobile phenotype cells (**Table 5**). These values were used as criteria to exclude round/not-moving cells from the tracks obtained from MJTrack analysis.

Following the exclusion of data associated with round BMDMs from the MTrackJ results, the data was shown not to be consistent with the findings obtained from the Harmony software. No statistically significant differences were observed among the non-round BMDMs (**Figures 21A-C**). All infected cells and their corresponding bystanders travelled similar cumulative and displacement distances, the only exception being *L. donovani* bystanders which exhibited superior displacement, and *L. major* bystanders which had greater cumulative migration (**Figure 21A,B**). In terms of speed,

all bystander cells were slightly faster than their infected counterparts, except for *L. donovani* (**Figure 21C**).

Table 5. Mean values of accumulated distance, displacement, and speed of the round BMDMs retrieved after Harmony analysis.

	Accumulated Distance (µm)				Displacement (µm)				Speed (µm/s)			
Date	N	*L.i.*	*L.m.*	*L.d.*	N	*L.i.*	*L.m.*	*L.d.*	N	*L.i.*	*L.m.*	*L.d.*
EXP01	14.4	17.6	16.4	15.9	4.20	4.06	4.22	3.71	0.012	0.012	0.012	0.011
EXP02	12.4	12.5	14.0	11.9	6.31	5.24	5.54	5.11	0.018	0.015	0.015	0.015
EXP03	13.0	13.0	14.5	12.0	4.70	4.43	4.82	3.91	0.013	0.013	0.014	0.012
Mean	13.3	14.4	15.0	13.3	5.07	4.58	4.86	4.24	0.014	0.013	0.014	0.013

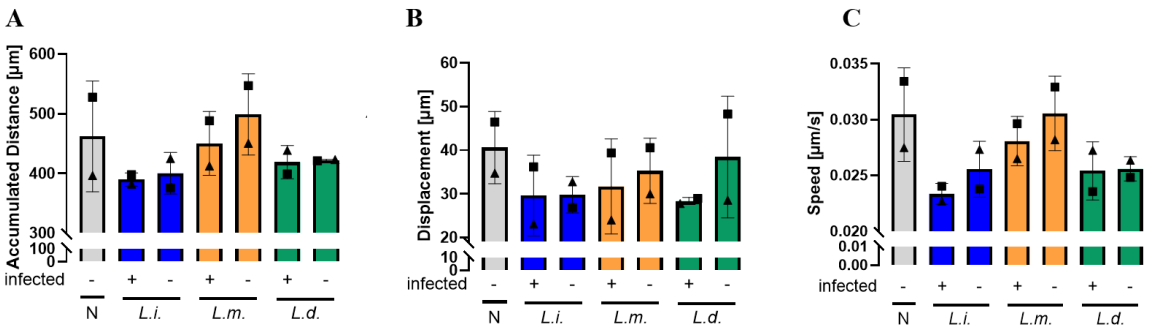

Figure 21. The exclusion of data associated with round BMDMs from the MTrackJ results revealed no consistent pattern of macrophages migration. The morphology of all detected BMDMs from the previous RSC migration assays was analysed, including naïve (N) or incubated with *L. major* (*L.m.*), *L. infantum* (*L.i.*) or *L. donovani* (*L.d.*) infected-BMDMs. Values associated with round BMDMs were excluded from the MTrackJ analysis and the assays reanalysed to obtain the non-round BMDMs' **A)** Accumulated distance, **B)** Displacement, and **C)** Speed. Each symbol represents an individual experiment. Values represent the means and standard deviations of three individual experiments performed in triplicate.

When the inhibitors data was re-analysed using Harmony, Dasatinib appeared to only have effect on the accumulated distance and speed, particularly evident in the case of naïve macrophages (**Figure 22A-C**). Wortmannin appeared not to have a consistent effect on any BMDMs, regardless of infection status (**Figure 22A-C**).

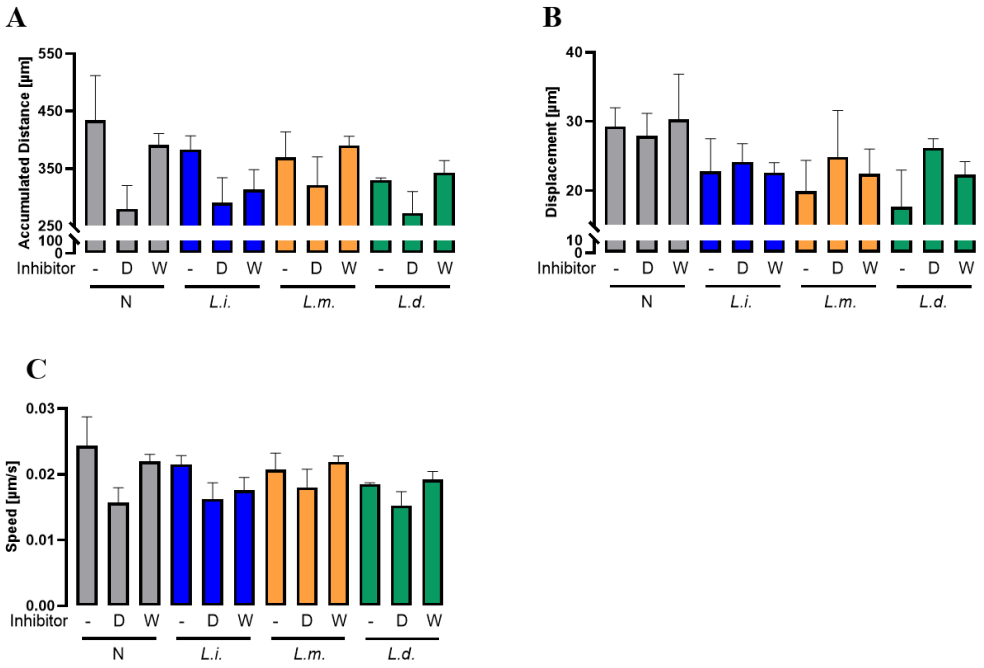

Figure 22. The exclusion of data associated with round BMDMs from the Harmony results revealed that Dasatinib only had a slight effect on the accumulated distance and speed of all BMDMs regardless of infection status, while Wortmannin showed no effect. The chemical inhibitor assay performed with the aid of the Harmony software was reanalysed excluding values associated with round BMDMs in order to obtain the non-round BMDMs' **A)** Accumulated distance, **B)** Displacement, and **C)** Speed. Values represent the means and standard deviations of one experiment performed in triplicate.

The removal of the round cell-associated values from the MtrackJ analysis did not yield in different results from those accounting for all cell morphologies, as no significant inhibitory effect was observed from either Dasatinib or Wortmannin (**Figure 23A-C**). However, it was observed that *L. infantum* bystander BMDMs tended to migrate more and faster than their infected counterparts (**Figure 23A-C**).

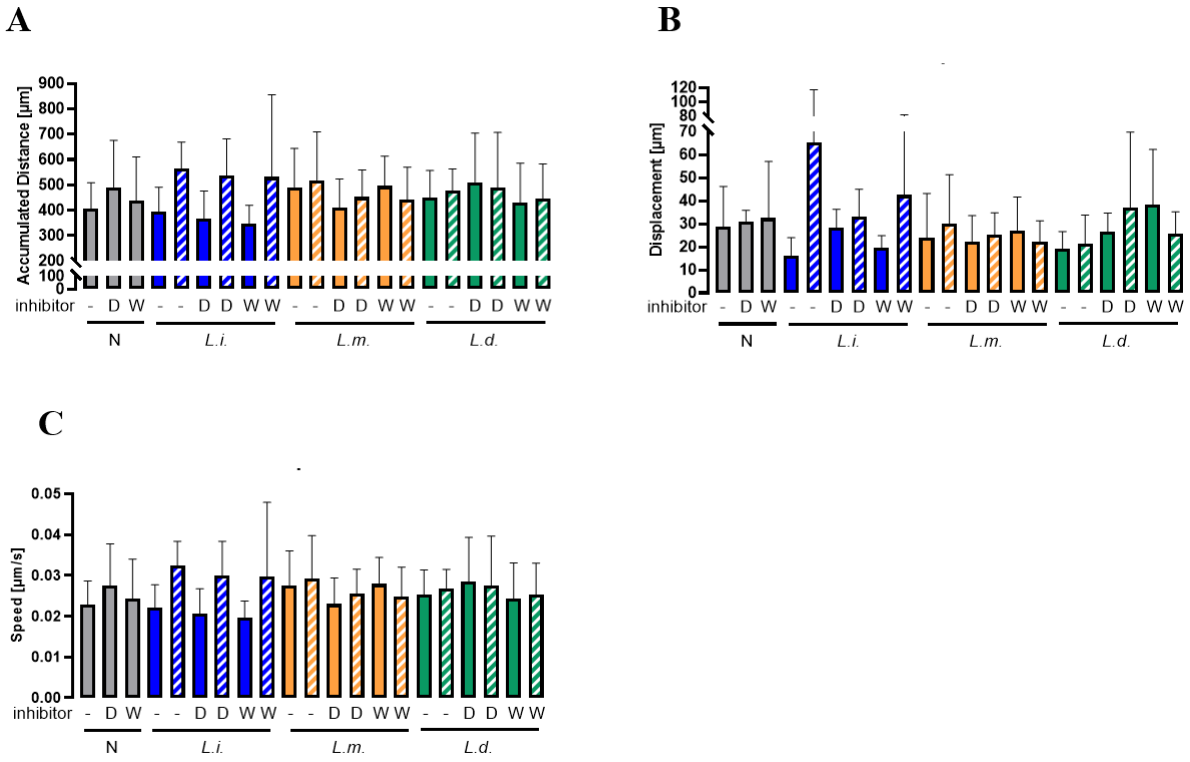

Figure 23. The exclusion of data associated with round BMDMs from the MTrackJ Dasatinib and Wortmannin had no consistent effect migration regardless of infection status. The chemical inhibitor assay performed with the aid of the MtrackJ software was reanalysed excluding values associated with round BMDMs in order to obtain the non-round BMDMs' **A)** Accumulated distance, **B)** Displacement, and **C)** Speed. Values represent the means and standard deviations of one experiment performed in triplicate. The solid colour bars represent the infected macrophages while the bars with the fill pattern represent the bystander macrophages.

Discussion

Millions of people worldwide suffer from leishmaniasis manifesting in either cutaneous or life-threatening visceral forms, with specific *Leishmania* species associated with distinct clinical presentations. The mechanism behind why some parasite species like *L. major* tend to remain on the skin, while *L. infantum* and *L. donovani* disseminate to internal organs is still unknown. In this thesis we consider the hypothesis that macrophages play a crucial role in the dissemination process. The first part of the thesis aimed at setting up the methodologies required to examine this assumption and their underlying mechanisms. The developed protocols were subsequently used to compare the migration of macrophages infected by cutaneous and visceral species with that of non-infected cells.

1. Metacyclic selection and detection of infection

The study of the impact of intracellular parasites on their host cells relies on high rates of infection. These may be achieved through optimization of the infection protocols, i.e selection of infective parasite forms, but also by enhancing our ability to detect said infections with accuracy.

To ensure systematic high infections, two methods for isolation of metacyclic promastigotes were explored. Both the PNA and the Ficoll metacyclic isolation methods have been established for various *Leishmania* species [89, 91-93, 96, 103-105, 107, 108]. However, we found that none of these methods delivered meaningful enrichment of parasites with morphologies associated with metacyclic forms in the infective inoculum. Accordingly, the selected parasites also failed to increase infection rates in BMDMs when compared to the unselected cultures.

A more precise alternative, that also relies on the morphological characteristics of metacyclic promastigotes, involves their identification through the analysis of forward scatter (FSC) versus side scatter (SSC) intensity using flow cytometry[105]. However, it is important to mention that parasite sorting through cytometry is not ideal due to possible cross contamination between equipment usage. This analysis enables the differentiation of two distinct subpopulations displaying clearly different FSC intensities, which correspond to different cell sizes. Metacyclic promastigotes, recognized by their short body and long flagellum, exhibit FSC^{low}, while the remaining promastigotes are identified as FSC^{high} [105]. Additionally, as an alternative to PNA, monoclonal antibodies (mAb)s have been developed to selectively bind to lectins associated with the metacyclic form, providing a more reliable option for detection [139].

It is important to acknowledge that relying solely on morphology and lectin detection may not be sufficient for identifying metacyclogenesis in parasites. Metacyclogenesis is associated with alterations in parasite morphology, but it is also accompanied by changes in parasite gene expression

[105]. Through gene expression analysis, specific up-regulated genes in metacyclic forms have been identified, including the hydrophilic acylated surface protein (HASP), which is present on the plasma membrane of infective parasite stages exclusively [140]. Antibodies targeting this protein have been demonstrated to selectively bind to metacyclic promastigotes [141]. Furthermore, mAbs have been developed to bind to procyclic-LPG fragments, enabling the negative selection of metacyclic promastigotes [98, 142, 143]

Other factors such as the number of days in culture and the number of passages *in vitro* appear to have a greater influence on parasite infectivity [95, 96, 141]. In this regard, we also observed that longer culture times (9-12 days) correlated with higher proportion of metacyclic promastigotes for *L. infantum* and *L. major*. Taking these findings into account, as well as previous observations from our research team (unpublished data), we opted to infect BMDMs with unselected stationary cultures that had been cultured for 12 days in the case of *L. major* and 9 days for *L. infantum* and *L. donovani*.

Accurate detection of infected cells is crucial to distinguish phenotypes of cells with internalized parasites from those of bystanders, or even to identify subtle effects occurring only in parasitized cell populations. Also, it is important to outline that the overall result of a migration experiment may be overlooked if the altered behaviour is specific to infected cells and these are in low number, as occurs in underachieving infections.

Routine protocol for determination of *in vitro* parasite burden in the host lab resorted to DAPI labelling for parasite identification [144]. This approach, while relatively inexpensive, fast, and simple for a high throughput assessment, presented some limitations, which resulted in under representation of infection rates. Specifically, we found that the nuclei of macrophages, which are several times bigger than the those of parasites, prevented accurate detection of parasites co-localizing or standing in close proximity. Furthermore, strong accumulation of DAPI signal in macrophage's nuclei could often lead to low background/signal ratios in areas with high cell confluency, resulting in difficulties to accurately detecting parasites. In the case of *L. major* infections, these problems were less impactful since, on average, this species resulted in a larger number of parasites per macrophage (1.5-2 times more parasites per macrophage). Therefore, despite the detection challenges, the increased parasite load within each macrophage raised the probability of parasite detection. These problems were successful surpassed by pre-staining the promastigotes with CFSE.

CFSE is an intra-cytoplasmic fluorochrome that allows for the analysis of large populations while not decreasing *Leishmania* infectivity [145]. This method is not only used to detect cells by flow cytometry but also regular fluorescent microscopy [138]. CFSE also enables the assessment of

cell divisions within each population, as fluorescence is halved with each cell division. This feature allows for the monitoring of cell proliferation without adversely affecting cellular function [146]. Through the use of CFSE to label parasites, we achieved a more precise determination of infection rates, resulting in an observed increase of these when compared to the previous protocol. This is evident when comparing the infection rates in **Figure 11B, Figure 12B** and **Figure 13B**, which relied on DAPI detection, with those in **Figure 15D** and **Figure 17**, where CFSE-stained parasites were employed.

2. Inhibitors' cytotoxicity assessment

One of the main objectives of this project was to determine the impact of the chemical inhibitors Dasatinib and Wortmannin in the migration of naïve and *Leishmania*-infected macrophages.

Wortmannin, a pan-inhibitor of PI3K, was shown by different authors to impede migration of primary cells , including neutrophils isolated from human blood in CXCL8-dependent migration, human Tenon's fibroblasts, HUVEC cells, MSC isolated from BALB/c mice, and epidermal keratinocytes from Sprague Dawley rats [147-152]. This drug has also exhibited migratory inhibition in various cell lines, such as MC3T3, CD133-over expressing GBC-SD, 5637 and T-24 [153-155]. These effects were observed in both 2D and 3D migration assays, with inhibitor concentrations ranging from 50nM to 10μM [30-37].

Dasatinib is a Src inhibitor known to suppress Src phosphorylation and, subsequently, inhibit Src-associated cell migration and angiogenesis [156]. In transwell assays, concentrations of 0.2 to 10μM of Dasatinib were shown to inhibit sorafenib-induced cell migration in cell lines like Chang liver, PLC/PRF/5, and HepG2 [156]. Additionally, it suppressed the EFhd2-mediated migration of RAW264.7 macrophages[157]. Conversely, at concentration of 10 or 50 nM, this inhibitor has been reported to enhance the migration of monocyte-derived dendritic cells toward a CCL19 gradient without altering the expression of its receptor, CCR7 [158].

In order to correctly interpret any effect of the inhibitors on migration of *Leishmania*-infected macrophages, we had to first establish that these inhibitors had no cytotoxicity for these cells. Our investigation revealed a 50% survival rate of BMDM at 1500 nM Desatinib, and no impact of Wortmannin at any of the concentrations tested. Both drugs were diluted in DMSO, which only seem to affect macrophages at concentrations above 3.52×10^8 nM. Consequently, we concluded that, at the concentrations used in the migration experiments, the inhibitors were not cytotoxic to BMDMs. On other words, they could safely be used to understand *Leishmania*-triggered migration of host cells.

3. Migration assays

WH assays were performed to study the impact of *Leishmania* on migration of their host cells, and of Dasatinib and Wortmannin on that process. We have found a high variability in the assays, that persisted even upon intra-assay normalization to naïve untreated controls. As such, no consistent pattern was observed in non-treated cells regardless of infection, with infected cells either migrating more or less than non-infected macrophages from assay to assay. Furthermore, no tendency could be detected between macrophages in contact with the inhibitor and those without. These experiences presented different infection rates, which could justify the variances. However, since infections were performed with the same *Leishmania* strains under the same conditions, we suspect that the different infection rates were due to errors in the parasite detection method employed, which relied on DAPI, rather than variations in the infections themselves.

The results obtained during this work are not in accordance with our group previous findings, where it was found that *L. infantum*, but not *L. major*, persistently enhanced macrophage migration, and the drugs had inhibitory effects on migration rates – while 200 nM Wortmannin impacted migration of all macrophages, 100 nM Dasatinib inhibited migration of naïve and *L. major*-infected cells, but not of *L. infantum* parasitized ones. However, in the current study, introduction of inhibitors had no statistically significant effect in any case.

The variations found between present and past results cannot be attributed to a single factor but, rather, highlight the potential limitations of the WH assay model for our research. Several studies outlined the many sources of variability that can influence the outcome of WH experiments. Firstly, manual creation of wounds with a pipette tip results in variations in wound size and shape between wells, even if using the same type of tip [109]. Additionally, determining the appropriate time interval to calculate relative gap closure is challenging, as cell behaviour can change along the assays, particularly as the wound approaches closure, where cells tend to slow down their migration. This makes it difficult to establish a common interval where macrophage migration is solely dependent on the experimental condition, without being influenced by wound morphology. We tried to overcome, or at least diminish, this by only taking into account a portion of the assay, where the wounds were far from resolved, to calculate the relative migration. However, the intra-assay variability remained high.

Furthermore, the mechanical process of scratching can cause damage to the cells and underlying extracellular matrix [110, 159]. As the extent of this damage is difficult to assess, its contribution to migratory behaviour of the cells remains largely unknown. The additional washing step designed to remove detached cells from the well can stress BMDMs within the monolayer [160]. An alternative approach that could overcome these limitations involves using a physical barrier to

create cell-free areas when plating macrophages. Once the monolayer is established, the physical barrier can be removed without the need for manual scratching. This method has been reported to introduce less variability compared to manual wounding with a pipette tip [161]. However, in our hands, this procedure resulted in the detachment of a significant portion of the cells and disruption of the monolayer.

Overall, the WH method did not yield consistent results in our study. One possibility is that the limitations and drawbacks of the method mentioned above are responsible for this.

Migration dynamics were further analysed resorting to RSC, which allowed for the tracking of individual cells without addition of any stimuli, such as the cell-free area in the WH assay. Depending on the software used for image processing, this method may even enable differentiation between infected and bystander macrophages. We observed that, in these assays individual macrophage speed remained constant regardless of the time point used for analysis. Therefore, we restricted RSC experiments to the first 5 hours, in order to reduce the amount to data to process. When analysing individual tracks, we observed a clear back and forward migration pattern of macrophages (**Figure 15E,F and Figure 16D,E**). Thus, even though they usually migrated for thousands of micrometres during the period of the assay, their displacement stayed within a range of less than a hundred micrometres. This type of movement has been described in studies where non-stimulated macrophages displayed rose plots similar to the ones we obtained [162, 163]. We noted that the speed achieved by BMDMs in our assays was around 0.014-0.020 μm/s, which is similar to what has been reported by other authors [164, 165].

The automatic tracking using the Harmony software allows for a fast and systematic detection of macrophages but does not differentiate on the infection status of the cell. This method significantly increases the number of macrophages that can be analysed within a much shorter timeframe, compared to manual tracking. Additionally, automatic tracking offers a level of precision that is often challenging to achieve through manual tracking, where selecting a consistent reference point (e.g., cell nucleus or cell centre) over time can be challenging. Furthermore, it helps to eliminate potential inconsistencies that might arise between different operators. Successful automatic tracking relied on digital phase-contrast images, since cell segmentation in brightfield images tend to be error-prone [166]. Fluorescence microscopy was only employed at the beginning and at the end of each assay to access the infection rates, given the risk that phototoxicity, would impair or kill the cells [167]. Further optimization of the acquisition settings could surpass this issue, however in the present conditions, this analysis is not able to discern between infected and bystander cells. This approach has other limitations, such as the difficulty in the segmentation of closely adjacent cells and the potential detection of cell morphology changes as movement, leading to exaggerated speed values.

Moreover, cell movements and alterations in morphology could often lead to objects getting out of focus, resulting in only a portion of the tracks completing the entire 5 hours.

To address the concerns outlined in the previous paragraph, a manual tracking approach with brightfield images was also employed to validate the accuracy of the automatic method. Manual tracking offers the advantage of distinguishing between infected and bystander cells while also eliminating problems associated with slight changes in focus. On the downside, manual tracking is laborious, time intensive and operator dependent which hard limits the number of cells that can be analysed.

In the RSC migration assays analysed automatically, naïve BMDMs displayed higher accumulated distance and displacement than the *Leishmania*-infected macrophages, although this was only statistically significant for displacement. Conversely, no trend was observed in the manual tracking of the same RSCM assays. The only consistent observation in this analysis was that *L. major* bystanders exhibited higher migration values, while *L. donovani* bystanders displayed lower migration values. It is important to notice that values of accumulated distance were higher in the manual tracking analysis since they account for the back and forward motion of the cells, while speed values were not affected by this since they reflect the mean of all the frame-to-frame velocities for each cell. Overall, the parameters in study showed great variability within the experimental groups.

In migration assays performed with no introduction of a chemical stimulus, it is expected that the BMDMs movements were primarily regulated by the presence of M-CSF, which was added as a supplement to the cell culture medium. While the detailed signalling cascade activated by M-CSF is not yet fully understood, PI3K and SFKs have been described to play a role in regulating macrophage migration [168-170]. Dasatinib and Wortmannin should disturb these signalling pathways and halt macrophage migration, however once more, no statistical differences were found between cells treated and not treated with these inhibitors, both by automatic and manual analysis. To our knowledge, no other article has been published on the effect of these drugs on BMDM migration, besides the one from our group [61].

No single reason can explain why these inhibitors, despite their well-documented inhibitory properties in other cell types, they presented no effect in our assays. One point that is worth noting is that the majority of the studies resorted to directional migration assays, relying on chemokines to stimulate cell migration. In those assays, drugs were shown to impair the chemokine-dependent migration. In fact, the use of PI3K and Src inhibitors has provided evidence that the activation of these kinases plays a central role in chemokine receptor-stimulated chemotaxis as well as polarization [169, 171]. Thus, as the RSC migration assay relies on the unstimulated migration of macrophages without any specific cues, this assay may not be ideal for testing the effects of these drugs on BMDM migration.

4. Effect of morphology on BMDM migration

Analysis of the acquired images revealed that approximately one quarter of the cells displayed a distinct round morphology that was associated with decreased motility, relatively to the remaining cells. This observation was consistent for all experimental groups, independently of infection or treatment. When these cells were excluded from the data set, automatic tracking analysis showed that naïve macrophages migrated more and faster than *Leishmania*-infected macrophages. However, manual tracking results did not show a similar trend and no statistical differences were observed. All infected cells and corresponding bystanders run similar cumulative and displacement distances, with the possible exception of *L. donovani*. Interstingly, bystander BMDMs were slightly faster than their infected counterparts, but without statistical significance.

When the chemical inhibitor assays were reanalysed excluding the round cell-associated values, it was seen that while Dasatinib appeared to have a visual effect on the accumulated distance and speed, Wortmannin appeared not to affect the any BMDMs regardless of the infection status.

Studies on BMDMs have shown that depending on the macrophage polarization, these can have very different morphologies – while M1 macrophages are associated with a flat and round morphology, the M2 macrophages tend to have an elongated morphology [172, 173]. Furthermore, the organization of the cytoskeleton is also reported to vary depending on the polarization of the macrophage, with M1 macrophages displaying actin clusters around the nucleus and M2 macrophages having more actin at the cell periphery [173]. These cytoskeletal differences align with the observation that M2 macrophages tend to be more elongated and motile, allowing for faster migration, while M1 macrophages exhibit stronger adhesion properties and reduced motility, resulting in limited migration [173, 174]. However, as both naïve and *Leishmania*-infected macrophages had similar proportions of round and non-round cells, this polarization does not seem to be triggered by the infection.

Conclusion

This MSc thesis delved into various aspects of *Leishmania* infection and its impact on macrophage migration. Here, we explored two methods, PNA negative selection and Ficoll gradient, for enrichment of metacyclic parasites with the goal of reaching consistent higher infection rates in *in vitro* BMDMs. We concluded that, in our experimental conditions, neither of these methodologies led to significant improvements in the infection rates. However, several other alternatives for metacyclic selection could also be tested, such as HASP mAbs. On the other hand, pre-labelling of promastigotes with CFSE proved to be an accurate and reliable approach for the identification of infected macrophages and for quantification of infections.

Regarding macrophage migration, the WH assays failed to yield consistent results. One possible motive for this relies on the various limitations and sources of variability, which could hinder the interpretation of the data and therefore our capacity to retrieve conclusions about the biological phenomena. However, these differences could be also due to biological variability. The RSC migration assays provided a more in-depth and precise analysis of individual macrophage migration patterns. In the assay conditions, macrophage migration seemed to be mostly unaffected by *Leishmania* infection, regardless of species. Despite the well-documented inhibitory properties of Dasatinib and Wortmannin in other cell types, these inhibitors did not have a significant effect on macrophage migration in the context of this study. These inconsistencies may be explained by not only the difference in cell type but also by the type of migration assay in use, we plan to test these inhibitors in chemotaxis assays, where the cells migrate towards a stimulus.

Analysis of cell morphology and migration revealed that macrophage polarization may play a role in migration patterns, but further investigations are needed to elucidate the specific mechanisms involved and the role of parasite infection in this phenomenon.

In conclusion, this thesis has shed light on the intricate interplay between *Leishmania* parasites and macrophages, emphasizing the importance of infection detection methods and the complexity of studying macrophage migration in response to infection. The findings suggest that traditional WH and RSC migration assays may have some limitations in yielding consistent results that reflect the macrophage behaviour, and thus other migration assays should be tested, including microfluidic devices and transwell 3D assays. The results regarding the impact of Dasatinib and Wortmannin on macrophage migration emphasize the necessity for further research to determine which migration assays should be employed and to elucidate the underlying mechanisms and their role in *Leishmania*-infected macrophages. Additionally, the observation of distinct macrophage morphologies and their potential association with different polarization states highlights the intricate nature of macrophage despite the common differentiation process. Overall, this research contributed

with valuable insights to the field of leishmaniasis and macrophage biology, however, further studies are necessary to understand of the complex host-parasite interactions in this context.

References

1. Knapp, A. P., & Alpern, J. D., *Cutaneous Leishmaniasis.* The New England journal of medicine, 2020. **382**(2): p. e2.
2. Ordaz-Farías, A., et al., *Case report: Transient success using prolonged treatment with miltefosine for a patient with diffuse cutaneous leishmaniasis infected with Leishmania mexicana mexicana.* The American journal of tropical medicine and hygiene, 2013. **88 1**: p. 153-6.
3. Calvopina, M., et al., *Leishmania isoenzyme polymorphisms in Ecuador: Relationships with geographic distribution and clinical presentation.* BMC Infectious Diseases, 2006. **6**(1): p. 139.
4. Joshi, S.D., Bajracharya, B.L., & Baral, M.R., *Kala-azar (visceral Leishmaniasis) from Khotang.* Kathmandu University medical journal, 2006. **4 2**: p. 232-4.
5. Baneth, G. & Solano-Gallego, L., *Leishmaniasis.* Veterinary Clinics of North America: Small Animal Practice, 2022. **52**(6): p. 1359-1375.
6. Burza, S., S.L. Croft, & Boelaert, M., *Leishmaniasis.* Lancet, 2018. **392**(10151): p. 951-970.
7. World Health Organization. *Leishmaniasis*. 2023 12 January 2023; Available from: https://www.who.int/news-room/fact-sheets/detail/leishmaniasis.
8. Maxfield, L., & Crane, J. S., *Leishmaniasis*. In StatPearls, 2023; Available from: https://www.ncbi.nlm.nih.gov/books/NBK531456/.
9. Torres-Guerrero, E., et al., *Leishmaniasis: a review.* F1000Res, 2017. **6**: p. 750.
10. World Health Organization, *Global Health Observatory data repository - Leishmaniasis*. 2023.
11. Tabbabi, A., *Review of Leishmaniasis in the Middle East and North Africa.* Afr Health Sci, 2019. **19**(1): p. 1329-1337.
12. Akhoundi, M., et al., *A Historical Overview of the Classification, Evolution, and Dispersion of Leishmania Parasites and Sandflies.* PLoS Negl Trop Dis, 2016. **10**(3): p. e0004349.
13. Bates, P.A., *Transmission of Leishmania metacyclic promastigotes by phlebotomine sand flies.* Int J Parasitol, 2007. **37**(10): p. 1097-106.
14. Espinosa, O.A., et al., *An appraisal of the taxonomy and nomenclature of trypanosomatids presently classified as Leishmania and Endotrypanum.* Parasitology, 2018. **145**(4): p. 430-442.
15. Kwakye-Nuako, G., et al., *Description, Biology, and Medical Significance of Leishmania (Mundinia) Chancei n. sp. (Kinetoplastea: Trypanosomatidae) from Ghana and Leishmania (Mundinia) Procaviensis n. sp. (Kinetoplastea: Trypanosomatidae) from Namibia.* Journal of Parasitology, 2023. **109**(1): p. 43-50, 8.
16. Kevric, I., M.A. Cappel, & Keeling, J.H., *New World and Old World Leishmania Infections: A Practical Review.* Dermatol Clin, 2015. **33**(3): p. 579-93.
17. Sereno, D., *Leishmania (Mundinia) spp.: from description to emergence as new human and animal Leishmania pathogens.* New Microbes New Infect, 2019. **30**: p. 100540.
18. Steverding, D., *The history of leishmaniasis.* Parasit Vectors, 2017. **10**(1): p. 82.
19. Sunter, J. & Gull, K., *Shape, form, function and Leishmania pathogenicity: from textbook descriptions to biological understanding.* Open Biol, 2017. **7**(9).
20. Thakur, S., J. Joshi, & Kaur, S., *Leishmaniasis diagnosis: an update on the use of parasitological, immunological and molecular methods.* J Parasit Dis, 2020. **44**(2): p. 253-272.
21. Serafim, T.D., et al., *Leishmaniasis: the act of transmission.* Trends in Parasitology, 2021. **37**(11): p. 976-987.
22. Landfear, S.M., *New Vistas in the Biology of the Flagellum-Leishmania Parasites.* Pathogens, 2022. **11**(4).
23. Serafim, T.D., et al., *Sequential blood meals promote Leishmania replication and reverse metacyclogenesis augmenting vector infectivity.* Nat Microbiol, 2018. **3**(5): p. 548-555.

24. Toepp, A.J. & Petersen, C.A., *The balancing act: Immunology of leishmaniosis.* Res Vet Sci, 2020. **130**: p. 19-25.
25. Young, J. & Kima, P.E., *The Leishmania Parasitophorous Vacuole Membrane at the Parasite-Host Interface.* Yale J Biol Med, 2019. **92**(3): p. 511-521.
26. Liévin-Le Moal, V. & Loiseau, P.M., *Leishmania hijacking of the macrophage intracellular compartments.* Febs j, 2016. **283**(4): p. 598-607.
27. Castro, R., et al., *The ultrastructure of the parasitophorous vacuole formed by Leishmania major.* J Parasitol, 2006. **92**(6): p. 1162-70.
28. Kaye, P. & Scott, P., *Leishmaniasis: complexity at the host–pathogen interface.* Nature Reviews Microbiology, 2011. **9**(8): p. 604-615.
29. Veras, P.S.T., et al., *Elucidating the role played by bone marrow in visceral leishmaniasis.* Frontiers in Cellular and Infection Microbiology, 2023. **13**.
30. de Vries, H.J.C. & Schallig, H.D., *Cutaneous Leishmaniasis: A 2022 Updated Narrative Review into Diagnosis and Management Developments.* Am J Clin Dermatol, 2022. **23**(6): p. 823-840.
31. Dinc, R., *Leishmania Vaccines: the Current Situation with Its Promising Aspect for the Future.* Korean J Parasitol, 2022. **60**(6): p. 379-391.
32. Pacheco-Fernandez, T., et al., *Field-Deployable Treatments For Leishmaniasis: Intrinsic Challenges, Recent Developments and Next Steps.* Res Rep Trop Med, 2023. **14**: p. 61-85.
33. Kumari, S., et al., *Amphotericin B: A drug of choice for Visceral Leishmaniasis.* Acta Tropica, 2022. **235**: p. 106661.
34. Lamotte, S., et al., *The enemy within: Targeting host–parasite interaction for antileishmanial drug discovery.* PLOS Neglected Tropical Diseases, 2017. **11**(6): p. e0005480.
35. van Griensven, J., et al., *The status of combination therapy for visceral leishmaniasis: an updated review.* Lancet Infect Dis, 2023.
36. Kapil, S., P.K. Singh, & Silakari, O., *An update on small molecule strategies targeting leishmaniasis.* European Journal of Medicinal Chemistry, 2018. **157**: p. 339-367.
37. Gupta, G., S. Oghumu, & Satoskar, A.R., *Mechanisms of immune evasion in leishmaniasis.* Adv Appl Microbiol, 2013. **82**: p. 155-84.
38. Ashburn, T.T. & Thor, K.B., *Drug repositioning: identifying and developing new uses for existing drugs.* Nat Rev Drug Discov, 2004. **3**(8): p. 673-83.
39. Pushpakom, S., et al., *Drug repurposing: progress, challenges and recommendations.* Nat Rev Drug Discov, 2019. **18**(1): p. 41-58.
40. Abbas, A.K., A.H. Lichtman, & Pillai, S., *Cells and Tissues of the Immune System*, in *Cellular and Molecular Immunology*, E.H. Sciences, Editor. 2017. p. 13-36.
41. National Institute of Allergy and Infectious Diseases. *Immune Cells*. 2014; Available from: https://www.niaid.nih.gov/research/immune-cells.
42. Wynn, T.A., A. Chawla, & Pollard, J.W., *Macrophage biology in development, homeostasis and disease.* Nature, 2013. **496**(7446): p. 445-55.
43. Almeida, F.S., et al., *Leishmaniasis: Immune Cells Crosstalk in Macrophage Polarization.* Tropical Medicine and Infectious Disease, 2023. **8**(5): p. 276.
44. Goto, Y. & Mizobuchi, H., *Pathological roles of macrophages in Leishmania infections.* Parasitology International, 2023. **94**: p. 102738.
45. Talkenberger, K., et al., *Amoeboid-mesenchymal migration plasticity promotes invasion only in complex heterogeneous microenvironments.* Sci Rep, 2017. **7**(1): p. 9237.
46. Maridonneau-Parini, I., *Control of macrophage 3D migration: a therapeutic challenge to limit tissue infiltration.* Immunol Rev, 2014. **262**(1): p. 216-31.
47. Dey, R., et al., *Gut Microbes Egested during Bites of Infected Sand Flies Augment Severity of Leishmaniasis via Inflammasome-Derived IL-1β.* Cell Host and Microbe, 2018. **23**(1): p. 134-143.e6.
48. Guimaraes-Costa, A.B., et al., *A sand fly salivary protein acts as a neutrophil chemoattractant.* Nature Communications, 2021. **12**(1).

49. Liu, D., & Uzonna, J.E., *The early interaction of Leishmania with macrophages and dendritic cells and its influence on the host immune response.* Frontiers in Cellular and Infection Microbiology, 2012. **2**.
50. Linehan, S.A., Martinez-Pomares, L., & Gordon, S., *Mannose receptor and scavenger receptor: two macrophage pattern recognition receptors with diverse functions in tissue homeostasis and host defense.* Adv Exp Med Biol, 2000. **479**: p. 1-14.
51. van Zandbergen, G., et al., *Cutting edge: neutrophil granulocyte serves as a vector for Leishmania entry into macrophages.* J Immunol, 2004. **173**(11): p. 6521-5.
52. Puentes, S.M., et al., *Serum resistance of metacyclic stage Leishmania major promastigotes is due to release of C5b-9.* J Immunol, 1990. **145**(12): p. 4311-6.
53. Faria, M.S., et al., *Leishmania inhibitor of serine peptidase 2 prevents TLR4 activation by neutrophil elastase promoting parasite survival in murine macrophages.* J Immunol, 2011. **186**(1): p. 411-22.
54. Ribeiro-Gomes, F.L., et al., *Neutrophils activate macrophages for intracellular killing of Leishmania major through recruitment of TLR4 by neutrophil elastase.* J Immunol, 2007. **179**(6): p. 3988-94.
55. Tabatabaee, P. A., et al., *Leishmania major: Secreted antigens of Leishmania major promastigotes shift the immune response of the C57BL/6 mice toward Th2 in vitro.* Experimental Parasitology, 2011. **127**(1): p. 46-51.
56. Olivier, M., Gregory, D. J., & Forget, G., *Subversion mechanisms by which Leishmania parasites can escape the host immune response: a signaling point of view.* Clin Microbiol Rev, 2005. **18**(2): p. 293-305.
57. Scianimanico, S., et al., *Impaired recruitment of the small GTPase rab7 correlates with the inhibition of phagosome maturation by Leishmania donovani promastigotes.* Cellular Microbiology, 1999. **1**(1): p. 19-32.
58. Prina, E., et al., *Presentation of the protective parasite antigen LACK by Leishmania-infected macrophages.* J Immunol, 1996. **156**(11): p. 4318-27.
59. Chandra, D., & Naik, S., *Leishmania donovani infection down-regulates TLR2-stimulated IL-12p40 and activates IL-10 in cells of macrophage/monocytic lineage by modulating MAPK pathways through a contact-dependent mechanism.* Clin Exp Immunol, 2008. **154**(2): p. 224-34.
60. Meddeb-Garnaoui, A., Zrelli, H., & Dellagi, K., *Effects of tropism and virulence of Leishmania parasites on cytokine production by infected human monocytes.* Clin Exp Immunol, 2009. **155**(2): p. 199-206.
61. Rocha, M.I., et al., *Leishmania infantum Enhances Migration of Macrophages via a Phosphoinositide 3-Kinase γ-Dependent Pathway.* ACS Infect Dis, 2020. **6**(7): p. 1643-1649.
62. Figueira, C.P., et al., *Leishmania infection modulates beta-1 integrin activation and alters the kinetics of monocyte spreading over fibronectin.* Scientific Reports, 2015. **5**(1): p. 12862.
63. Pinheiro, N.F., Jr., et al., *Leishmania infection impairs beta 1-integrin function and chemokine receptor expression in mononuclear phagocytes.* Infect Immun, 2006. **74**(7): p. 3912-21.
64. Maretti-Mira, A.C., et al., *MMP-9 activity is induced by Leishmania braziliensis infection and correlates with mucosal leishmaniasis.* Acta Trop, 2011. **119**(2-3): p. 160-4.
65. de Menezes, J.P., et al., *Leishmania infection inhibits macrophage motility by altering F-actin dynamics and the expression of adhesion complex proteins.* Cell Microbiol, 2017. **19**(3).
66. Luz, Y., et al., *Leishmania infection alters macrophage and dendritic cell migration in a three-dimensional environment.* Frontiers in Cell and Developmental Biology, 2023. **11**.
67. Mazumder, S., et al., *Leishmania LPG interacts with LRR5/LRR6 of macrophage TLR4 for parasite invasion and impairs the macrophage functions.* Pathog Dis, 2023. **81**.
68. Kima, P. E., *PI3K signaling in Leishmania infections.* Cell Immunol, 2016. **309**: p. 19-22.

69. Vanhaesebroeck, B., et al., *The emerging mechanisms of isoform-specific PI3K signalling.* Nature Reviews Molecular Cell Biology, 2010. **11**(5): p. 329-341.
70. Leevers, S. J., Vanhaesebroeck, B., & Waterfield, M. D., *Signalling through phosphoinositide 3-kinases: the lipids take centre stage.* Curr Opin Cell Biol, 1999. **11**(2): p. 219-25.
71. Gross, C., & Bassell, G. J., *Neuron-specific regulation of class I PI3K catalytic subunits and their dysfunction in brain disorders.* Frontiers in Molecular Neuroscience, 2014. **7**.
72. Khadem, F., et al., *Deficiency of p110δ isoform of the phosphoinositide 3 kinase leads to enhanced resistance to Leishmania donovani.* PLoS Negl Trop Dis, 2014. **8**(6): p. e2951.
73. Cummings, H.E., et al., *Critical role for phosphoinositide 3-kinase gamma in parasite invasion and disease progression of cutaneous leishmaniasis.* Proceedings of the National Academy of Sciences of the United States of America, 2012. **109**(4): p. 1251-1256.
74. Shi, X., et al., *Research progress on the PI3K/AKT signaling pathway in gynecological cancer (Review).* Mol Med Rep, 2019. **19**(6): p. 4529-4535.
75. Tariq, K., & Luikart, B. W., *Striking a balance: PIP2 and PIP3 signaling in neuronal health and disease.* Exploration of Neuroprotective Therapy, 2021. **1**(2): p. 86-110.
76. Yu, M., et al., *Development and safety of PI3K inhibitors in cancer.* Arch Toxicol, 2023. **97**(3): p. 635-650.
77. Sheridan, C., & Downward, J., *Inhibiting the RAS–PI3K Pathway in Cancer Therapy*, in *The Enzymes*, F. Tamanoi and C.J. Der, Editors. 2013, Academic Press. p. 107-136.
78. Camps, M., et al., *Blockade of PI3Kgamma suppresses joint inflammation and damage in mouse models of rheumatoid arthritis.* Nat Med, 2005. **11**(9): p. 936-43.
79. Pottier, C., et al., *Tyrosine Kinase Inhibitors in Cancer: Breakthrough and Challenges of Targeted Therapy.* Cancers (Basel), 2020. **12**(3).
80. Sun, P., & Meng, L. H., *Emerging roles of class I PI3K inhibitors in modulating tumor microenvironment and immunity.* Acta Pharmacologica Sinica, 2020. **41**(11): p. 1395-1402.
81. Marim, F.M., et al., *A method for generation of bone marrow-derived macrophages from cryopreserved mouse bone marrow cells.* PLoS One, 2010. **5**(12): p. e15263.
82. Mendoza, R., et al., *Mouse Bone Marrow Cell Isolation and Macrophage Differentiation.* Methods Mol Biol, 2022. **2455**: p. 85-91.
83. Ying, W., et al., *Investigation of macrophage polarization using bone marrow derived macrophages.* J Vis Exp, 2013(76).
84. Trouplin, V., et al., *Bone marrow-derived macrophage production.* J Vis Exp, 2013(81): p. e50966.
85. Goodrum, K. J., *Complement Component C3 Secretion by Mouse Macrophage-Like Cell Lines.* Journal of Leukocyte Biology, 1987. **41**(4): p. 295-301.
86. Wang, C., et al., *Characterization of murine macrophages from bone marrow, spleen and peritoneum.* BMC Immunology, 2013. **14**(1): p. 6.
87. da Silva, R.L., et al., *Leishmania donovani infection suppresses Allograft Inflammatory Factor-1 in monocytes and macrophages to inhibit inflammatory responses.* Scientific Reports, 2021. **11**(1): p. 946.
88. Palacios, G., et al., *Gene Expression Profiling of Classically Activated Macrophages in Leishmania infantum Infection: Response to Metabolic Pre-Stimulus with Itaconic Acid.* Tropical Medicine and Infectious Disease, 2023. **8**(5): p. 264.
89. Al-Bayati, N. & Saleem, N., *Purification of Metacyclic Leishmanial Promastigotes by Using Peanut Lectin Agglutinin Test.* 2017.
90. Yao, C., et al., *Leishmania chagasi: homogenous metacyclic promastigotes isolated by buoyant density are highly virulent in a mouse model.* Exp Parasitol, 2008. **118**(1): p. 129-33.
91. Alcolea, P.J., et al., *In vitro infectivity and differential gene expression of Leishmania infantum metacyclic promastigotes: negative selection with peanut agglutinin in culture versus isolation from the stomodeal valve of Phlebotomus perniciosus.* BMC Genomics, 2016. **17**(1): p. 375.

92. Chanmol, W., et al., *Stimulation of metacyclogenesis in Leishmania (Mundinia) orientalis for mass production of metacyclic promastigotes.* Frontiers in Cellular and Infection Microbiology, 2022. **12**.
93. Alcolea, P.J., et al., *Genome-wide analysis reveals increased levels of transcripts related with infectivity in peanut lectin non-agglutinated promastigotes of Leishmania infantum.* Genomics, 2009. **93**(6): p. 551-64.
94. Sacks, D.L., S. Hieny, & Sher, A., *Identification of cell surface carbohydrate and antigenic changes between noninfective and infective developmental stages of Leishmania major promastigotes.* J Immunol, 1985. **135**(1): p. 564-9.
95. Bhaumik, S.K., et al., *Virulence attenuation of a UDP-galactose/N-acetylglucosamine β1,4 galactosyltransferase expressing Leishmania donovani promastigote.* Glycoconjugate Journal, 2008. **25**(5): p. 459-472.
96. Sacks, D.L., et al., *Stage-specific binding of Leishmania donovani to the sand fly vector midgut is regulated by conformational changes in the abundant surface lipophosphoglycan.* J Exp Med, 1995. **181**(2): p. 685-97.
97. Sacks, D.L. & da Silva, R.P, *The generation of infective stage Leishmania major promastigotes is associated with the cell-surface expression and release of a developmentally regulated glycolipid.* J Immunol, 1987. **139**(9): p. 3099-106.
98. Pinto-da-Silva, L.H., et al., *Leishmania (Viannia) braziliensis metacyclic promastigotes purified using Bauhinia purpurea lectin are complement resistant and highly infective for macrophages in vitro and hamsters in vivo.* Int J Parasitol, 2002. **32**(11): p. 1371-7.
99. Almeida, M.C., et al., *Metacyclogenesis of Leishmania (Viannia) braziliensis in vitro: evidence that lentil lectin is a marker of complement resistance and enhanced infectivity.* Trans R Soc Trop Med Hyg, 1993. **87**(3): p. 325-9.
100. Späth, G.F. & Beverley, S.M., *A Lipophosphoglycan-Independent Method for Isolation of Infective Leishmania Metacyclic Promastigotes by Density Gradient Centrifugation.* Experimental Parasitology, 2001. **99**(2): p. 97-103.
101. Rosado, M., et al., *Advances in biomarker detection: Alternative approaches for blood-based biomarker detection*, in *Advances in Clinical Chemistry*, G.S. Makowski, Editor. 2019, Elsevier. p. 141-199.
102. Moreira, D., et al., *Impact of Continuous Axenic Cultivation in Leishmania infantum Virulence.* PLOS Neglected Tropical Diseases, 2012. **6**(1): p. e1469.
103. Giraud, E., et al., *Quantifying Leishmania Metacyclic Promastigotes from Individual Sandfly Bites Reveals the Efficiency of Vector Transmission.* Communications Biology, 2019. **2**(1): p. 84.
104. Findlay, R.C., et al., *High-speed, three-dimensional imaging reveals chemotactic behaviour specific to human-infective Leishmania parasites.* eLife, 2021. **10**: p. e65051.
105. Saraiva, E.M., et al., *Flow cytometric assessment of Leishmania spp metacyclic differentiation: Validation by morphological features and specific markers.* Experimental Parasitology, 2005. **110**(1): p. 39-47.
106. Matte, C., Arango Duque, G. & Descoteaux, A., *Leishmania donovani Metacyclic Promastigotes Impair Phagosome Properties in Inflammatory Monocytes.* Infect Immun, 2021. **89**(7): p. e0000921.
107. Dias, B.R.S., et al., *Autophagic Induction Greatly Enhances Leishmania major Intracellular Survival Compared to Leishmania amazonensis in CBA/j-Infected Macrophages.* Frontiers in Microbiology, 2018. **9**.
108. Jara, M., et al., *Transcriptional Shift and Metabolic Adaptations during Leishmania Quiescence Using Stationary Phase and Drug Pressure as Models.* Microorganisms, 2022. **10**(1): p. 97.
109. Vang Mouritzen, M. & Jenssen, H., *Optimized Scratch Assay for In Vitro Testing of Cell Migration with an Automated Optical Camera.* J Vis Exp, 2018(138).
110. Ashby, W.J. & Zijlstra, A., *Established and novel methods of interrogating two-dimensional cell migration.* Integr Biol (Camb), 2012. **4**(11): p. 1338-50.

111. Jonkman, J.E., et al., *An introduction to the wound healing assay using live-cell microscopy.* Cell Adh Migr, 2014. **8**(5): p. 440-51.
112. van Horssen, R. & ten Hagen, T.L.M., *Crossing barriers: The new dimension of 2D cell migration assays.* Journal of Cellular Physiology, 2011. **226**(1): p. 288-290.
113. Hong, J., et al., *Electrical cell-substrate impedance sensing as a non-invasive tool for cancer cell study.* Analyst, 2011. **136**(2): p. 237-45.
114. Nie, F.Q., et al., *On-chip cell migration assay using microfluidic channels.* Biomaterials, 2007. **28**(27): p. 4017-22.
115. Kroening, S. & Goppelt-Struebe, M. , *Analysis of matrix-dependent cell migration with a barrier migration assay.* Sci Signal, 2010. **3**(126): p. pl1.
116. Georgescu, W., et al., *Model-controlled hydrodynamic focusing to generate multiple overlapping gradients of surface-immobilized proteins in microfluidic devices.* Lab Chip, 2008. **8**(2): p. 238-44.
117. Takayama, S., et al., *Patterning cells and their environments using multiple laminar fluid flows in capillary networks.* Proc Natl Acad Sci U S A, 1999. **96**(10): p. 5545-8.
118. Cory, G., *Scratch-Wound Assay*, in *Cell Migration: Developmental Methods and Protocols*, C.M. Wells and M. Parsons, Editors. 2011, Humana Press: Totowa, NJ. p. 25-30.
119. Dang, I. & Gautreau, A,, *Random Migration Assays of Mammalian Cells and Quantitative Analyses of Single Cell Trajectories.* Methods Mol Biol, 2018. **1749**: p. 1-9.
120. Thüroff, F., et al., *Bridging the gap between single-cell migration and collective dynamics.* Elife, 2019. **8**.
121. Phase Focus Limited, *Automated Random Cell Migration Assay*. 2019.
122. Axion Bio Systems. *Wound healing assays: single-cell migration assays*. 2023; Available from: https://cytosmart.com/resources/resources/wound-healing-assays-single-cell-migration-assays.
123. Justus, C.R., et al., *In vitro cell migration and invasion assays.* J Vis Exp, 2014(88).
124. Justus, C.R., et al., *Transwell In Vitro Cell Migration and Invasion Assays.* Methods Mol Biol, 2023. **2644**: p. 349-359.
125. Kramer, N., et al., *In vitro cell migration and invasion assays.* Mutation Research/Reviews in Mutation Research, 2013. **752**(1): p. 10-24.
126. Kashem, M.A., et al., *TILRR Promotes Migration of Immune Cells Through Induction of Soluble Inflammatory Mediators.* Frontiers in Cell and Developmental Biology, 2020. **8**.
127. Zengel, P., et al., *μ-Slide Chemotaxis: A new chamber for long-term chemotaxis studies.* BMC Cell Biology, 2011. **12**(1): p. 21.
128. Zigmond, S.H., *Ability of polymorphonuclear leukocytes to orient in gradients of chemotactic factors.* J Cell Biol, 1977. **75**(2 Pt 1): p. 606-16.
129. Ibidi GMBH. *Chemotaxis Assays*. 2023; Available from: https://ibidi.com/content/310-chemotaxis-assays.
130. Zicha, D., G.A. Dunn, and A.F. Brown, *A new direct-viewing chemotaxis chamber.* Journal of Cell Science, 1991. **99**(4): p. 769-775.
131. Howard, M.K., G. Sayers, & Miles, M.A., *Leishmania donovani metacyclic promastigotes: transformation in vitro, lectin agglutination, complement resistance, and infectivity.* Exp Parasitol, 1987. **64**(2): p. 147-56.
132. Meijering, E., O. Dzyubachyk, & Smal, I., *Methods for Cell and Particle Tracking*, in *Methods in Enzymology*, P.M. conn, Editor. 2012, Academic Press. p. 183-200.
133. Wickham, H., *ggplot2: Elegant Graphics for Data Analysis*. 2016, Springer-Verlag New York.
134. Merck KGaA, *Ficoll® 400 for Gradient Centrifugation*. 20/09/2023]; Available from: https://www.sigmaaldrich.com/PT/en/technical-documents/protocol/cell-culture-and-cell-culture-analysis/primary-cell-culture/ficoll-400.
135. Serafim, T.D., et al., *Leishmania metacyclogenesis is promoted in the absence of purines.* PLoS Negl Trop Dis, 2012. **6**(9): p. e1833.
136. Thermo Fisher Scientific Inc., *CellTrace™ Cell Proliferation Kits User Guide*. 2017.

137. Pereira, T.F., et al., *Fluorescence-based method is more accurate than counting-based methods for plotting growth curves of adherent cells.* BMC Research Notes, 2020. **13**(1): p. 57.
138. Viana, A.G., et al., *Infection of Human Monocytes with Leishmania infantum Strains Induces a Downmodulated Response when Compared with Infection with Leishmania braziliensis.* Front Immunol, 2017. **8**: p. 1896.
139. Soares, R.P.P., et al., *Leishmania chagasi: lipophosphoglycan characterization and binding to the midgut of the sand fly vector Lutzomyia longipalpis.* Molecular and Biochemical Parasitology, 2002. **121**(2): p. 213-224.
140. Coutinho-Abreu, I.V., et al., *Distinct gene expression patterns in vector-residing Leishmania infantum identify parasite stage-enriched markers.* PLoS Negl Trop Dis, 2020. **14**(3): p. e0008014.
141. Sádlová, J., et al., *The stage-regulated HASPB and SHERP proteins are essential for differentiation of the protozoan parasite Leishmania major in its sand fly vector, Phlebotomus papatasi.* Cell Microbiol, 2010. **12**(12): p. 1765-79.
142. Mahoney, A.B., et al., *Intra-species and stage-specific polymorphisms in lipophosphoglycan structure control Leishmania donovani-sand fly interactions.* Biochemistry, 1999. **38**(31): p. 9813-23.
143. Courret, N., et al., *Presentation of the Leishmania antigen LACK by infected macrophages is dependent upon the virulence of the phagocytosed parasites.* Eur J Immunol, 1999. **29**(3): p. 762-73.
144. Gomes-Alves, A.G., et al., *Development of an automated image analysis protocol for quantification of intracellular forms of Leishmania spp.* PLoS One, 2018. **13**(8): p. e0201747.
145. Gonçalves, R., et al., *A sensitive flow cytometric methodology for studying the binding of L. chagasito canine peritoneal macrophages.* BMC Infectious Diseases, 2005. **5**(1): p. 39.
146. Messaritakis, I., et al., *Leishmania donovani s.l.: Evaluation of the proliferation potential of promastigotes using CFSE staining and flow cytometry.* Experimental Parasitology, 2010. **125**(4): p. 384-388.
147. Martin, K.J., et al., *The role of phosphoinositide 3-kinases in neutrophil migration in 3D collagen gels.* PLoS One, 2015. **10**(2): p. e0116250.
148. Gao, Z., et al., *SIRT1 mediates Sphk1/S1P-induced proliferation and migration of endothelial cells.* Int J Biochem Cell Biol, 2016. **74**: p. 152-60.
149. Aquino-Martínez, R., A.P. Angelo, & Pujol, F.V., *Calcium-containing scaffolds induce bone regeneration by regulating mesenchymal stem cell differentiation and migration.* Stem Cell Research & Therapy, 2017. **8**(1): p. 265.
150. Pan, F., et al., *High glucose inhibits ClC-2 chloride channels and attenuates cell migration of rat keratinocytes.* Drug Des Devel Ther, 2015. **9**: p. 4779-91.
151. Carducci, A., et al., *GMP-grade platelet lysate enhances proliferation and migration of tenon fibroblasts.* FBE, 2016. **8**(1): p. 84-99.
152. Araki, N., M.T. Johnson, & Swanson, J.A., *A role for phosphoinositide 3-kinase in the completion of macropinocytosis and phagocytosis by macrophages.* J Cell Biol, 1996. **135**(5): p. 1249-60.
153. Su, P., et al., *MACF1 promotes osteoblastic cell migration by regulating MAP1B through the GSK3beta/TCF7 pathway.* Bone, 2022. **154**: p. 116238.
154. Li, C., et al., *CD133 promotes gallbladder carcinoma cell migration through activating Akt phosphorylation.* Oncotarget, 2016. **7**(14): p. 17751-9.
155. Cho, T.M., W.J. Kim, & Moon, S.K., *AKT signaling is involved in fucoidan-induced inhibition of growth and migration of human bladder cancer cells.* Food Chem Toxicol, 2014. **64**: p. 344-52.
156. Cheng, C.C., et al., *Sorafenib combined with dasatinib therapy inhibits cell viability, migration, and angiogenesis synergistically in hepatocellular carcinoma.* Cancer Chemotherapy and Pharmacology, 2021. **88**(1): p. 143-153.

157. Tu, Y., et al., *EFhd2/swiprosin-1 regulates LPS-induced macrophage recruitment via enhancing actin polymerization and cell migration.* Int Immunopharmacol, 2018. **55**: p. 263-271.
158. Nerreter, T., et al., *Dasatinib enhances migration of monocyte-derived dendritic cells by reducing phosphorylation of inhibitory immune receptors Siglec-9 and Siglec-3.* Exp Hematol, 2014. **42**(9): p. 773-82.e1-3.
159. Solbu, A.A., et al., *Assessing cell migration in hydrogels: An overview of relevant materials and methods.* Mater Today Bio, 2023. **18**: p. 100537.
160. Bouchalova, P. and P. Bouchal, *Current methods for studying metastatic potential of tumor cells.* Cancer Cell Int, 2022. **22**(1): p. 394.
161. Pijuan, J., et al., *In vitro Cell Migration, Invasion, and Adhesion Assays: From Cell Imaging to Data Analysis.* Frontiers in Cell and Developmental Biology, 2019. **7**.
162. Lewis, L., et al., *Stage Specific Assessment of Candida albicans Phagocytosis by Macrophages Identifies Cell Wall Composition and Morphogenesis as Key Determinants.* PLoS pathogens, 2012. **8**: p. e1002578.
163. García-Sánchez, M., et al., *Differential Responses of Bovine Monocyte-Derived Macrophages to Infection by Neospora caninum Isolates of High and Low Virulence.* Frontiers in Immunology, 2019. **10**.
164. Murray, M.Y., et al., *Macrophage migration and invasion is regulated by MMP10 expression.* PLoS One, 2013. **8**(5): p. e63555.
165. St-Pierre, J. & Ostergaard, H., *A Role for the Protein Tyrosine Phosphatase CD45 in Macrophage Adhesion through the Regulation of Paxillin Degradation.* PloS one, 2013. **8**: p. e71531.
166. Letzsch, S. & Böttcher, K., *Digital Phase Imaging: Cell Detection and Analysis without Fluorescent Staining using the Opera High Content Screening System*, I. PerkinElmer, Editor. 2011.
167. Cordelières, F.P., et al., *Automated cell tracking and analysis in phase-contrast videos (iTrack4U): development of Java software based on combined mean-shift processes.* PLoS One, 2013. **8**(11): p. e81266.
168. Dwyer, A.R., E.L. Greenland, & Pixley, F.J., *Promotion of Tumor Invasion by Tumor-Associated Macrophages: The Role of CSF-1-Activated Phosphatidylinositol 3 Kinase and Src Family Kinase Motility Signaling.* Cancers, 2017. **9**(6): p. 68.
169. Faccio, R., et al., *M-CSF Regulates the Cytoskeleton via Recruitment of a Multimeric Signaling Complex to c-Fms Tyr-559/697/721*.* Journal of Biological Chemistry, 2007. **282**(26): p. 18991-18999.
170. Mouchemore, K.A., et al., *Specific inhibition of PI3K p110δ inhibits CSF-1-induced macrophage spreading and invasive capacity.* Febs j, 2013. **280**(21): p. 5228-36.
171. Sotsios, Y. and S.G. Ward, *Phosphoinositide 3-kinase: a key biochemical signal for cell migration in response to chemokines.* Immunol Rev, 2000. **177**: p. 217-35.
172. McWhorter, F.Y., et al., *Modulation of macrophage phenotype by cell shape.* Proc Natl Acad Sci U S A, 2013. **110**(43): p. 17253-8.
173. Vereyken, E.J., et al., *Classically and alternatively activated bone marrow derived macrophages differ in cytoskeletal functions and migration towards specific CNS cell types.* J Neuroinflammation, 2011. **8**: p. 58.
174. Cui, K., et al., *Distinct Migratory Properties of M1, M2, and Resident Macrophages Are Regulated by αDβ2 and αMβ2 Integrin-Mediated Adhesion.* Frontiers in Immunology, 2018. **9**.

Supplementary Data

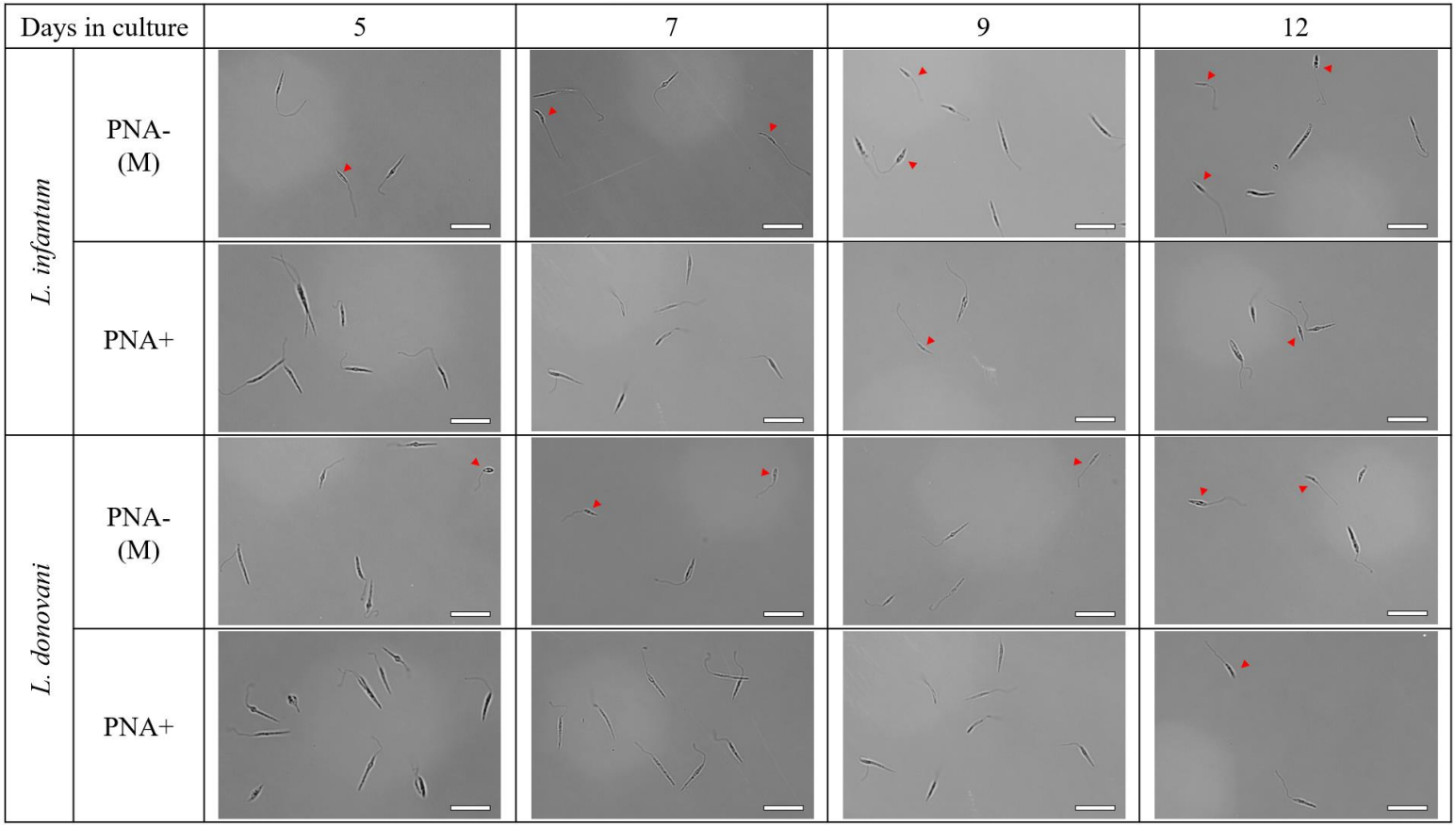

Supplementary Figure 1. Images acquired with an Olympus CX33 upright microscope with a 40x objective connected to a digital camera depicting *L. donovani* and *L. infantum* parasites after PNA selection. Metacyclic promastigotes are expected to remain in the PNA negative fraction [PNA- (M)], and not in the PNA positive fraction (PNA+). The red arrows are directed at parasites with metacyclic-associated morphology. Scale represents 10µm.

Days in culture	9	12
L. infantum	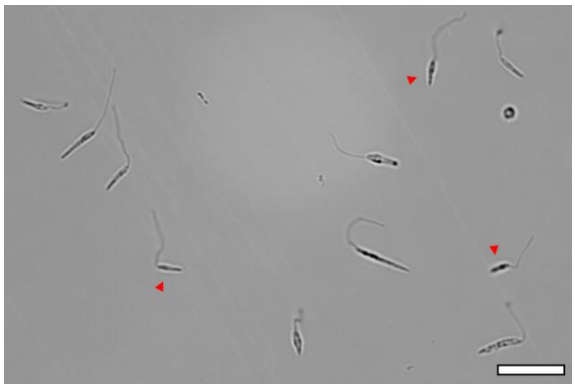	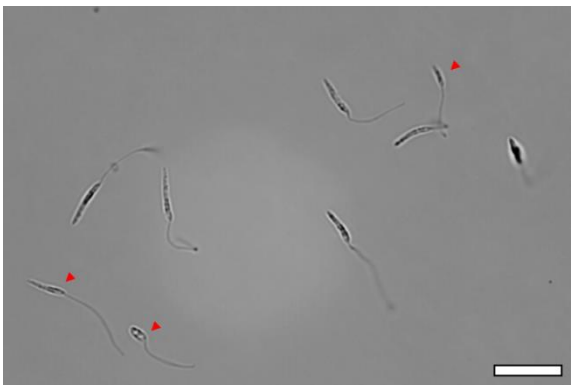
L. donovani	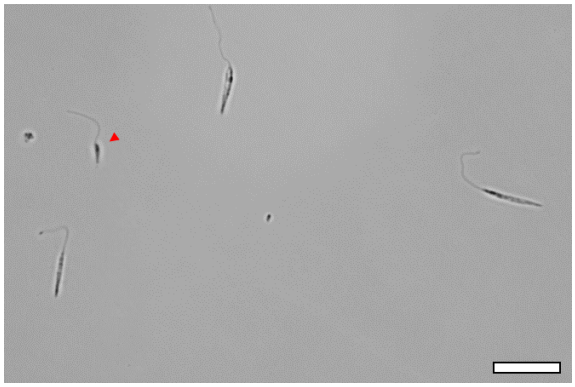	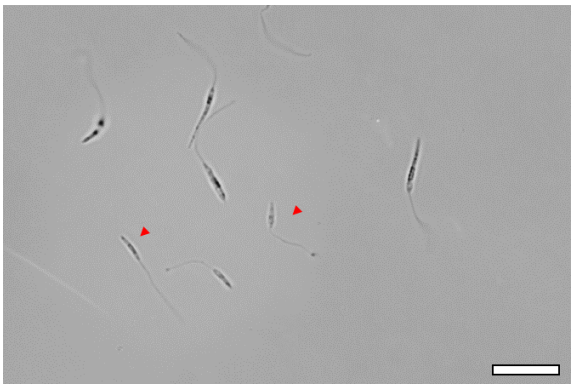

Supplementary Figure 2. Images acquired with an Olympus CX33 upright microscope with a 40x objective connected to a digital camera depicting *L. donovani* and *L. infantum* parasites after Ficoll selection. The photographed Ficoll phase was expected to select the metacyclic promastigotes. The red arrows are directed at parasites with metacyclic-associated morphology. Scale represents 10µm.

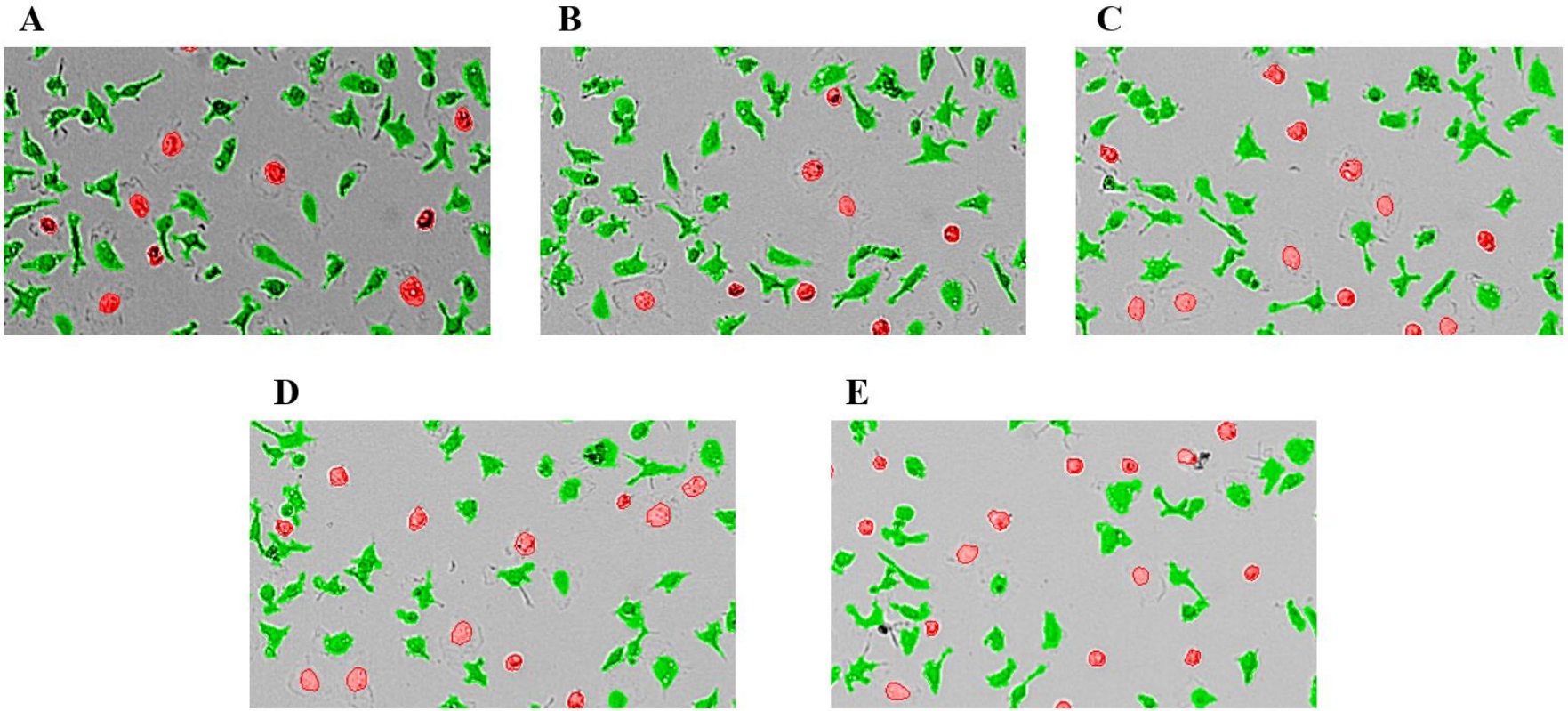

Supplementary Figure 3. Images acquired through the Operetta® CLS™ microscope with a 10× air objective over an 18-hours RSC migration assay and posteriorly used for morphological analysis of the BMDMs. Round BMDMs were defined as those with roundness > 0.92, represented in red, while non-round/motile macrophages were associated with roundness ≤ 0.92, represented in green. These images were acquired from the same frame show that the BMDMs marked in red tend to remain in the same place at **A)** 0 hours p.i,, **B)** 1 hour 30 minutes p.i., **C)** 3 hours p.i., **D)** 4 hours 30 minutes p.i., **E)** 6 hours p.i..

Supplementary Material 1. Woundhealing_TimeSegmentation macro developed by the i3S Scientific Platform Advanced Light Microscopy, member of the national infrastructure PPBI-Portuguese Platform of BioImaging (supported by POCI-01-0145-FEDER-022122). Analysis of sequence data – the protocol has been tested on the Fiji software. It requires the input of tiff files with time stack. For each time frame, it is suggested to perform gaussian blur, divide by the original, apply variance filter with radius = 5, apply default threshold default with upperthreslhold*0.1, analyse particles with minimum size = 8000, and measure area of each ROI;

Date: June/2019

Author: Mafalda Sousa, mafsousa@ibmc.up.pt

Advanced Ligth Microscopy, I3S

PPBI-Portuguese Platform of BioImaging

```
run("Scale...", "x=0.5 y=0.5 z=1.0 width=512 height=512 depth="+ nSlices + " interpolation=Bilinear average process create");
run("Select All");
w = getWidth;
h = getHeight;
//run("Specify...", "width=500 height=" + h + " x=" + round(w/2) + " y=" + round(h/2) + " slice=1 centered");
//run("Duplicate...", "duplicate");
img=getTitle();
run("Duplicate...", "duplicate");
run("Subtract Background...", "rolling=10 light stack");
run("Gaussian Blur...", "sigma=1 stack");
resetMinAndMax();
run("8-bit");
//run("Gray Morphology", "radius=1 type=circle operator=dilate");
run("Variance...", "radius=3 stack");
imgP=getTitle();
setAutoThreshold("Default");
getThreshold(lower, upper)
```

```
setThreshold(lower, upper*0.1);
run("Options...", "iterations=1 count=1 do=Open stack");
run("Analyze Particles...", "size=8000.00-Infinity show=Masks display clear include add stack");
//setAutoThreshold("Default dark");
//close();
selectWindow(imgP);
close();
selectWindow(img);
roiManager("Select", 0);
```